ELECTROKINETIC MEASUREMENTS ON FIBROUS MATERIALS

A Thesis

by

Gregory J. Biefer

Submitted to the Faculty of Graduate Studies and Research of McGill University in partial fulfilment of the requirements for the degree of Doctor of Philosophy

McGill University
Montreal, Canada.

October 1952

ACKNOWLEDGEMENTS

Thanks are due to

Dr. Stanley G. Mason, under whose direction this research was carried out;

the National Research Council, for a bursary, two studentships and three summer grants;

the Department of Veterans' Affairs for their financial assistance.

TABLE OF CONTENTS

Page

Page

LIST OF FIGURES

LIST OF SYMBOLS

Symbol	Meaning	Units
a	Area of cross section of channel	$cm.^2$
A	Area of cross section of pad	$cm.^2$
α	Specific volume	$cm.^3\ gm.^{-1}$
α_c	Specific volume from conductance measurements	$cm.^3\ gm.^{-1}$
α_k	Specific volume from permeability measurements	$cm.^3\ gm.^{-1}$
α_ζ	Specific volume from electrokinetic measurements	$cm.^3\ gm.^{-1}$
c	Pad solid concentration	$gm.\ cm.^{-3}$
C	Pad cell constant	$cm.^{-1}$
D	Dielectric constant	...
δ	Equivalent thickness of electrical double layer	$\mathring{A}$
E	Applied electro-osmotic potential	volts
e_o	Charge on an electron	e.s.u.
ϵ	Void fraction of pad	...
f	Electro-osmotic flow rate through a single channel	$cm.^3\ sec.^{-1}$
F	Electro-osmotic flow rate through a porous diaphragm	$cm.^3\ sec.^{-1}$
i	Stream current in single channel	microamps.
I	Stream current in porous diaphragm	microamps.
I_E	Electrical current in porous diaphragm	microamps.
I_o	Electro-osmotic current	ma.

Symbol	Meaning	Units
k	Specific conductivity of liquid	ohm^{-1} $cm.^{-1}$
k_p	Specific conductivity of liquid in pores of a diaphragm	ohm^{-1} $cm.^{-1}$
k_o	Boltzmann constant	ergs $deg.^{-1}$
k_j	Kozeny constant	...
k_s	Specific surface conductivity	ohm^{-1}
K	Permeability co-efficient	$cm.^2$
l_c	Length of a single channel	cm.
L	Length of pad	cm.
n	Concentration of ions in electrolyte	ions $cm.^{-3}$
η	Viscosity of liquid	centipoises
p	Applied pressure	cm. H_2O
p_E	Electro-osmotic pressure across single channels	cm. H_2O
P_E	Electro-osmotic pressure across diaphragm	cm. H_2O
q	Charge per unit area	e.s.u. $cm.^{-2}$
Q	Rate of liquid flow	$cm.^3$ $sec.^{-1}$
$\overline{r}$	Mean hydraulic radius	microns
R_c	Radius of circular capillary	cm.
R	Electrical resistance	ohms
ρ	Charge density in liquid	e.s.u. $cm.^{-3}$
s	Scale deflection	cm.
σ	Specific surface	$cm.^2$ $gm.^{-1}$
T	Temperature	°C.
u	Velocity	cm. $sec.^{-1}$
v	Stream potential across single channel	mv.

Symbol	Meaning	Units
V	Stream potential across diaphragm	mv.
ζ	The electrokinetic or ζ-potential	mv.
ζ_E	ζ-potential from electro-osmotic data	mv.
ζ_s	ζ-potential from stream data	mv.
ψ	Potential of liquid in diffuse layer	mv.
ψ_o	Potential at solid surface	mv.
Φ	Permeability, $Q\eta/p$	$cm.^3$

LIST OF TABLES

SUMMARY

Stream current, electro-osmotic flow, conductance, and permeability measurements were carried out on cylindrical pads composed of different fibrous materials over a range of solid concentrations.

The ζ-potentials calculated from stream current and electro-osmotic measurements on the same pad were shown to be identical. Some deficiencies of the bubble flowmeter used to measure the electro-osmotic flow were investigated and explained theoretically; a new type of flowmeter, free from these defects, was proposed.

Empirical equations relating the stream current and the conductance of a pad of fibers to its void fraction were demonstrated. These equations constituted a new means of determining the swollen specific volume of the fiber in the pad; the results obtained showed excellent agreement with independent permeability determinations of the same quantity.

Exploratory measurements of a low-frequency resistance dispersion effect were carried out on pads of a number of different fibers.

PREFACE

There is generally an electrical charge at a liquid-solid interface. Because of the existence of this charge, a number of electrokinetic effects may be observed when there is motion of one phase relative to the other; for example, a movement of the liquid with respect to the solid may constitute an electro-osmotic flow, or give rise to a stream current.

The quantitative measurement of the electrokinetic effects has led to the concept of the electrokinetic or ζ-potential at the liquid-solid interface. For the case where the movement of liquid takes place through a capillary of circular cross section, equations relating the electro-osmotic flow and the stream current to the ζ-potential at the interface have been deduced. These equations are consistent with the available experimental data, and have found general acceptance.

A number of equations have been proposed relating the electro-osmotic flow or stream current to the ζ-potential for the case where the movement of liquid takes place through a porous diaphragm of complex internal structure, such as that existing in beds of fibers. These equations show no general agreement and all are open to serious criticism; the chief difficulty is in the evaluation of the terms descriptive of the complex internal geometry of the diaphragm.

The main object of the present investigation is the development of a method for evaluating the terms descriptive of the complex internal structure of a cylindrical pad of fibers.

A secondary object is the comparison of stream current and electro-osmotic measurements on the same pad of fibers. While the calculation of the ζ-potential from stream current and electro-osmotic measurements should lead to the same result, according to conventional electrokinetic theory, the available experimental data indicate that there may be a discrepancy between the two methods for pads of cellulose fibers.

INTRODUCTION

In the introduction which follows, material relevant to the present investigation is reviewed. The subject matter can be roughly grouped under five headings:

1) Description of the electrokinetic effects, and the experimental methods used in stream and electro-osmotic measurements.

2) Discussion of theories of the structure of the electrical double layer.

3) Derivation of stream current and electro-osmotic equations for the case of a circular capillary.

4) Review of the various stream equations which have been deduced for porous diaphragms of complex internal structure.

5) Review of the comparisons between electro-osmotic and stream measurements on the same system appearing in the literature.

A brief note on the equation used in the liquid permeability measurements also appears.

Electrokinetic Effects

At a liquid-solid interface an electrical charge usually appears on the solid. The charge may arise from an orientation of polar molecules at the interface, or ionization of some of the surface molecules of the solid. If the

liquid is an electrolyte, there may be a preferential adsorption of one ionic species. The charge on the solid is neutralized by a diffuse layer of counter-ions of opposite electrical sign in the liquid; this charge distribution as a whole, consisting of a negatively charged layer and a positively charged layer, is called the electrical double layer.

When the equilibrium of the electrical double layer is disturbed by the application of external forces, the counter-ions of the diffuse layer are readily mobile with respect to the charged solid surface, and a number of electrokinetic effects may be observed. These are primarily distinguished by the nature of the disturbing force, which may be mechanical or electrical. The effects may be summarized as follows:

A) Effects produced by an applied electromotive force

1) Electrophoresis (cataphoresis), the movement of charged solid particles through a resting liquid under the influence of an electrical field;

2) Electro-osmosis, the movement of liquid through a capillary or porous diaphragm when an electrical field is applied;

B) Effects produced by an applied mechanical force

1) Sedimentation potential (Dorn effect), the potential gradient produced by charged solid particles moving through a resting liquid under the influence of gravity;

2) Stream current, the electrical current produced when liquid is streamed through a capillary or porous diaphragm.

In addition to these primary electrokinetic effects there is the electro-viscous effect, the change of viscosity in a sol with altered charge density on the solid particles.

The quantitative study of the electrokinetic effects led to the concept of the electrokinetic, or ζ-potential. This quantity is defined as the potential at the surface of shear between a charged solid and a liquid, relative to a point in the liquid beyond the influence of the electrical double layer. For simplicity, the surface of shear is generally considered to coincide with the solid surface when equations relating the ζ-potential to the electrokinetic effects are derived.

The present investigation consisted for the most part of measurements of stream current and electro-osmotic flow. A brief survey of the experimental methods employed in measuring each of these electrokinetic effects follows.

Stream Current

If a constant pressure is exerted so that electrolyte is streamed through a capillary or porous diaphragm held between perforated electrodes which are reversible with respect to the electrolyte, the stream current, resulting from the motion of the mobile counter-ions in the liquid portion of the electrical double layer, may be recorded by a low resistance galvanometer connected across the electrodes.

A number of workers have recently used stream cur-

rent measurements to determine the ζ-potential (6, 8, 23, 24). Silver electrodes coated with silver chloride have generally been employed, with the stream electrolytes containing the chloride ion.

The stream current may also manifest itself as a potential; if the galvanometer is replaced by a high resistance vacuum tube voltmeter, there is no external circuit for the stream current, which must leak back through the diaphragm. The product of the leak-back stream current and the electrical resistance of the diaphragm gives the stream potential, which may be measured on the vacuum tube voltmeter.

Many workers have carried out measurements of stream potential (7, 9, 22, 19, 21, 42). The method possesses one outstanding advantage compared to the stream current method: there is no necessity for the stream solution to be reversible with respect to the electrodes, and stream potential measurements can therefore be carried out in distilled water or pure organic liquids.

However, the stream current method also possesses a striking advantage; the measurements can be carried out in much more concentrated electrolytic solutions than possible with stream potential measurements. With the apparatus used in the present investigation, stream potentials were too low for accurate measurement at electrolytic concentrations greater than 10^{-4} M KCl; stream current measurements, on the other

hand, were successfully carried out in 2 x 10^{-2} M KCl.

Electro-osmosis

If a potential gradient is applied across a porous diaphragm or capillary held between electrodes, there will be a unidirectional movement of the counter-ions of the diffuse liquid layer, under the action of the electrical field. As a result of this movement there is a plug-type electro-osmotic flow of liquid through the capillary or porous diaphragm. In electro-osmotic measurements the electrodes need not be reversible with respect to the solution; however, if irreversible electrodes are used, difficulties may be encountered with polarization and evolution of gas at the electrodes (20, 21).

A number of workers have used electro-osmotic measurements to determine the ζ-potential. The electro-osmotic flow rate is usually measured by a bubble flowmeter, the liquid on opposite sides of the porous diaphragm being connected by means of a capillary tube containing an air bubble (29, 30, 31, 21, 52). The electro-osmotic flow follows a cyclic path, the rate of flow being indicated by the speed of the moving bubble in the capillary.

The electro-osmotic flow can also manifest itself as a pressure. If the opposite sides of the capillary or porous diaphragm are connected to the open vertical arms of a differential manometer, the electro-osmotic flow causes a pressure to build up, in opposition to the flow. As the pressure in-

creases it causes an increasing leak-back flow, until an equilibrium electro-osmotic pressure value is finally attained, at which leak-back and electro-osmotic flow are equal and opposite.

The only quantitative measurements of the electro-osmotic equilibrium pressure appearing in the literature are those of Quincke (36) and Coehn and Raydt (37).

Theories of Electrical Double Layer Structure

The earliest theoretical treatment of the electrical double layer was that of Helmholtz (1), who assumed that the mobile counter-ions in the liquid phase of the electrical double layer were all separated from the charged solid surface by a distance δ (Fig. 1(a)). Where the charge density of the solid is -q per unit area, that of the liquid layer is +q. Thus the two charged layers resemble an infinite parallel-plate capacitor, the potential difference between the two layers being the ζ-potential. From elementary electrostatics

$$\zeta = \frac{4\pi q \delta}{D} \qquad \ldots (1)$$

where D = dielectric constant of the liquid.

Gouy (2) pointed out that the Helmholtz picture was oversimplified. The mobile ions in the liquid phase of the double layer cound not be concentrated at a definite distance from the charged surface, as their position results

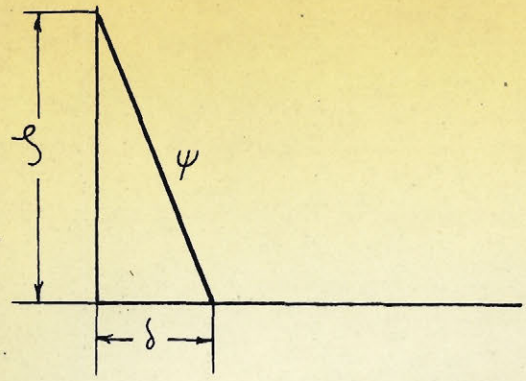

(a) Helmholtz

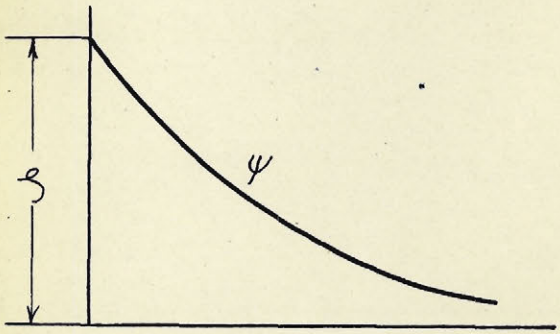

(b) Gouy-Chapman

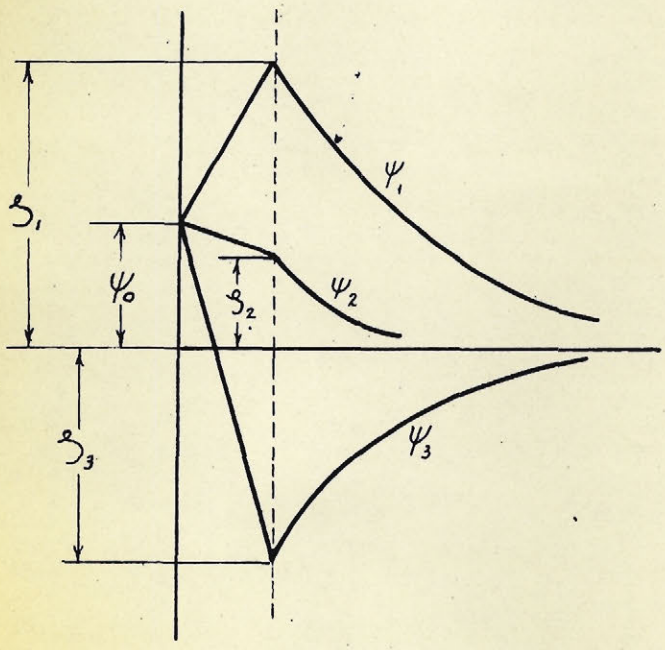

(c) Stern

FIG. 1 Electrical double layer theories

from an interaction of the electrical forces responsible for the existence of the double layer, and osmotic forces that tend to restore ionic homogeneity throughout the solution. According to the treatment of Gouy and Chapman (3), the charged solid surface is surrounded by an ionic atmosphere of considerable thickness, in which the liquid potential, ψ , equal to ζ at the solid surface, decreases exponentially with increasing distance from the surface (Fig. 1 (b)).

Stern (4) modified the Gouy-Chapman (2, 3) interpretation by dividing the liquid portion of the electrical double layer into two parts. There is a fixed layer of adsorbed ions at the solid surface; across this layer, there is a linear change of the liquid potential ψ . At the outer boundary of the fixed layer is the surface of shear; at this point ψ is equal to the ζ-potential. With increasing distance from the surface of shear, ψ falls off exponentially in a conventional Gouy-Chapman (2, 3) diffuse layer.

In the Stern (4) treatment the ζ-potential may be greater than the potential at the solid surface ψ_o when the adsorbed ions are of the same sign as the charge on the solid. If ions of opposite sign are adsorbed, the ζ-potential may be of opposite sign to ψ_o . In addition to these extreme cases there may be intermediate ζ-potential values equal or less than ψ_o , and of the same sign. Each of these three cases is illustrated in Fig. 1(c).

Gouy-Chapman Diffuse Electrical Double Layer

A derivation of the equations relating the charge distribution in the diffuse liquid layer to the charge at the solid surface follows; the treatment is after Neale (5). It is assumed that ions in the diffuse layer behave according to the ideal gas law, and that the charge is uniformly distributed over the solid surface; the potential at the solid surface is assumed equal to the ζ-potential. For simplicity, the case of a uni-univalent electrolyte is considered. The following symbols are employed:

ζ = the normal ζ-potential at the solid surface;

ψ = the liquid potential at a distance x from the solid surface;

q = electrical charge density per $cm.^2$ at the solid surface;

ρ = electrical charge density per $cm.^3$ at a distance x from the solid surface;

n = number of anions or cations per $cm.^3$ of the bulk liquid;

n^-, n^+ = number of anions and cations respectively per $cm.^3$ at a distance x from the solid surface;

e_o = charge on an electron;

k_o = Boltzmann constant R/N_A;

T = absolute temperature.

The concentration of both ionic species in the diffuse layer is given by the Boltzmann distribution law as

$$n^+ = n \exp. \frac{-e_o\psi}{k_oT}$$

$$n^- = n \exp. \frac{e_o\psi}{k_oT} \qquad \ldots \quad (2)$$

The effective charge density ρ at a point removed from the solid surface is given by

$$\rho = e_o(n^+ - n^-) = -2 ne_o \sinh \frac{e_o\psi}{k_oT} \qquad \ldots \quad (3)$$

ρ and ψ are related to the distance from the solid surface x by the Poisson equation. For the case of a one-dimensional field normal to the surface,

$$\frac{d^2\psi}{dx^2} = -\frac{4\pi\rho}{D} = \frac{8\pi e_o n}{D} \sinh \frac{e_o\psi}{k_oT} \qquad \ldots \quad (4)$$

Assuming the boundary conditions $\psi = 0$ and $d\psi/dx = 0$ at $x = \infty$, equation 4 can be integrated to give

$$\frac{1}{2}\left(\frac{d\psi}{dx}\right)^2 = \frac{16\,\pi n k_oT}{D} \sinh^2 \frac{e_o\psi}{2\,k_oT} \qquad \ldots \quad (5)$$

At the solid surface, the potential gradient is given by Gauss' theorem as

$$\left(\frac{d\psi}{dx}\right)_{x=o} = \frac{4\,\pi q}{D} \qquad \ldots \quad (6)$$

Combining equations 5 and 6 leads to the exact relationship between the potential at the solid surface ζ and the

charge density at the solid surface q as

$$\sinh \frac{e_o \zeta}{2 k_o T} = q \sqrt{\frac{\pi}{2 n k_o T D}} \qquad \ldots \quad (7)$$

According to this equation the ζ-potential should decrease with increasing electrolytic concentration, providing q remained constant. However, a number of workers have carried out stream measurements on porous diaphragms in which maximum ζ-potentials were obtained at low electrolytic concentrations (6, 7, 8, 42). Some controversy exists as to the reality of these maxima; discussion of this point is deferred.

The equation further states that the ζ-potential is of the same sign as the charge on the surface, and is inversely proportional to the square root of the absolute temperature. If q were assumed constant, the variation of ζ with slight changes of the ordinary room temperature would be negligible. This observation has been experimentally confirmed by several workers (13, 16, 6); in the present investigation the measurements were carried out in the temperature range 20-30°C., and the variation of ζ with temperature was assumed to be negligible.

Where $e_o \zeta << k_o T$, i.e. at ζ-potentials less than 20 mv., the Debye-Huckel approximation $\sinh \frac{e_o \zeta}{k_o T} \doteq \frac{e_o \zeta}{k_o T}$ gives a result that is accurate within 2.5%. Using the approximation, equation 7 becomes

$$\zeta = \frac{q}{e_o}\sqrt{\frac{2\pi k_o T}{nD}} \qquad \ldots \quad (8)$$

Equation 8 may be combined with equation 1 to eliminate ζ, and give the thickness of the equivalent Helmholtz electrical double layer as

$$\delta = \sqrt{\frac{k_o TD}{8\pi e_o{}^2 n}} \qquad \ldots \quad (9)$$

Electrokinetic Equations
for Circular Capillaries

Stream Current

Stream currents were first observed by Quincke (17) in 1859, who showed that the stream potential produced by the current was directly proportional to the applied liquid pressure. The first theoretical treatment of the effect was that of Helmholtz (1), in 1879, who derived the equation for the stream current i produced by viscous flow of liquid through a capillary as

$$i = \frac{pD\zeta R_c{}^2}{4\eta l_c} \qquad \ldots \quad (10)$$

where p = liquid pressure across the capillary,

R_c = internal radius of the capillary,

η = specific viscosity of liquid

and l_c = length of the capillary.

This equation was derived for a capillary in which $R_c >> \delta$, the thickness of the Helmholtz electrical double layer. If it is assumed that the thickness of the diffuse liquid layer is negligible, compared to R_c, i.e., that the wall of the capillary is effectively planar, the same stream current equation can be derived on the basis of the Gouy-Chapman (2,3) diffuse layer as follows.

Where the electrical charge density at a distance x from the wall is ρ, and the laminar velocity of the liquid layer at a distance x from the wall is u_x, then the stream current generated by viscous flow through a capillary of radius R_c is

$$i = \int_0^{R_c} 2\pi x u_x \rho dx \qquad \ldots \quad (11)$$

assuming that the surface of shear coincides with the solid surface, i.e. $\zeta = \psi_o$.

The term u_x may be derived from Poiseuille's Law as

$$u_x = \frac{pR_c x}{2\eta l_c} \qquad \ldots \quad (12)$$

and ρ may be represented by Poisson's equation, for the case of a one-dimensional field normal to the capillary wall (equation 4).

Making these substitutions in equation 11 and integrating, subject to the boundary conditions $\psi = 0$ and $d\psi/dx = 0$ for $x \ll R_c$, there results

$$i = - \frac{pD\zeta R_c^2}{4 \eta l_c} \quad .$$

This equation is the same as Helmholtz (1) equation 10 except for the negative sign which is generally omitted.

Stream Potential

The stream potential equation for a cylindrical capillary is easily deduced from the stream current equation. If there is no external connection between the ends of the capillary, then the stream current leaks back along the capillary, opposed by the electrical resistance of the capillary. At equilibrium, the leak-back current is equal to the stream current, and there is a potential difference between the ends of the capillary given by

$$v = i R$$

where v = the stream potential,

i = the stream current

and R = the electrical resistance of the capillary.

The stream potential produced by viscous flow through a capillary is therefore

$$v = \frac{pD\zeta R\ R_c^2}{4\ \eta l_c} \qquad \ldots \quad (13)$$

neglecting the negative sign.

Electro-osmotic Flow

Electro-osmotic flow was first observed by Reuss (34) in 1808. Wiedemann (35), in 1852, showed that the flow through a porous diaphragm was directly proportional to the applied potential. The first theoretical treatment of the effect was that of Helmholtz (1), in 1879. The classical Helmholtz equation for the electro-osmotic flow rate f, in volume per unit time, through a capillary of radius R_c and length l_c is

$$f = \frac{ED\zeta R_c^2}{4\ \eta l_c} \qquad \ldots \quad (14)$$

where E is the potential difference between the ends of the capillary. As in the derivation of the stream current equation, the thickness δ of the Helmholtz electrical double layer was assumed to be negligible compared to R_c.

It is important to note that electro-osmotic flow assumes a plug-flow character; the velocity of the moving liquid is constant throughout the capillary except within the electrical double layer, where the liquid velocity decreases until the layer of zero velocity is reached.

Assuming, as in the derivation of the stream cur-

rent equation, that the thickness of the diffuse liquid layer is negligible compared to the capillary radius, so that the capillary wall is effectively planar, an expression of the same form as the Helmholtz (1) electro-osmotic equation 14 may be derived on the basis of the Gouy-Chapman (2, 3) diffuse layer as follows.

If electro-osmotic flow occurs through a capillary under the action of a potential gradient E/l_c, then the electrical force per unit length F_{el} operative at a normal distance x from the wall is

$$F_{el} = \int_x^\infty 2\,\pi R_c \frac{E}{l_c}\,\rho dx \quad . \quad \ldots \quad (15)$$

This force is opposed by the equal and opposite viscous force F_{fr}.

$$F_{fr} = 2\,\pi R_c \eta \frac{du_x}{dx} \quad . \quad \ldots \quad (16)$$

Combination of equations 15 and 16 leads to

$$\frac{du_x}{dx} = \frac{E}{l_c \eta} \int_x^\infty \rho dx \quad \ldots \quad (17)$$

Differentiating with respect to x and substituting for ρ from Poisson's equation (equation 4) there results

$$\frac{d^2u_x}{dx^2} = -\frac{E\rho}{\eta l_c} = \frac{ED}{4\,\pi\eta l_c}\frac{d^2\psi}{dx^2} \quad . \quad \ldots \quad (18)$$

Integration of equation 18 leads to

$$u_x = -\frac{ED}{4\pi\eta l_c}(\zeta - \psi) \quad . \qquad \ldots \quad (19)$$

At $x = \infty$, $\psi = 0$; the velocity of the electro-osmotic flow at the center of the capillary is therefore

$$u = -\frac{ED\zeta}{4\pi\eta l_c} \qquad \ldots \quad (20)$$

Thus the electro-osmotic flow rate in volume per unit time is

$$f = u\pi R_c^2 = -\frac{ED\zeta R_c^2}{4\eta l_c} \quad ,$$

which is the same as the Helmholtz (1) electro-osmotic flow equation, except for the negative sign which is generally omitted.

Electro-osmotic Pressure

The electro-osmotic pressure equation is easily derived from the above expression. Representing the permeability of the capillary to liquid flow by $(Q\eta/p)_c = \Phi_c$, where Q is the flow rate of liquid of viscosity η produced by a pressure p across the capillary, then when the electro-osmotic equilibrium pressure p_E is attained, the leak-back flow rate Q is equal to the electro-osmotic flow rate f, i.e.

$$f = Q$$

$$\frac{f\eta}{p_E} = \left(\frac{Q\eta}{p}\right)_c = \Phi_c \quad .$$

Substituting the above expression into the Helmholtz electro-osmotic flow equation,

$$p_E = \frac{ED\zeta R_c^2}{4\,\Phi_c l_c} \qquad \ldots \quad (21)$$

This expression gives the equilibrium electro-osmotic pressure produced by electro-osmotic flow in a capillary of permeability Φ_c .

Electrokinetic Equations
for Porous Diaphragms

Stream and electro-osmotic equations have been derived for capillaries of circular cross section. However, relatively few materials can be formed into such capillaries; with fibrous substances such as cellulose, the stream or electro-osmotic measurements must be carried out on a porous bed composed of the tightly packed fibers. The correct electrokinetic equations for such a porous bed must include terms descriptive of the complex internal structure of the bed. Several methods of evaluating these terms have been proposed but all are open to serious criticism.

In the following pages a number of these methods are reviewed, and their validity tested by reference to the relevant experimental data. As a simplification, only stream

equations are discussed. However, any of the methods can be applied equally well to the derivation of electro-osmotic equations.

Helmholtz-Smoluchowski Equation

The stream potential equation for viscous flow through a circular capillary is

$$v = \frac{pD\zeta R\ R_c^2}{4\ \eta l_c}$$

which can be written as

$$v = \frac{pD\zeta Ra}{4\ \pi\eta l_c} \qquad \ldots \quad (22)$$

where $a = \pi R_c^2$ is the cross sectional area of the capillary.

In measurement of stream potential there is no effective external conducting circuit between the electrodes, and the counter-ions of the diffuse liquid layer must leak back along the capillary. Assuming that this movement takes place in the bulk of the liquid, the terms a and l_c can be evaluated conductometrically as

$$\frac{l_c}{a} = kR = C \qquad \ldots \quad (23)$$

where C = the cell constant of the capillary,

R = the electrical resistance of the capillary

and k = the specific conductivity of the bulk liquid being streamed through the capillary.

Putting $l_c/a = kR$ in equation 22, the stream potential produced by flow through the capillary is

$$v = V = \frac{pD\zeta}{4\pi\eta k} \qquad \ldots (24)$$

which is the classical Helmholtz-Smoluchowski stream potential equation.

This equation contains no terms descriptive of the capillary geometry; Smoluchowski (18) considered it to be applicable to a porous diaphragm having pores of arbitrary shape, as long as the pore radii were large compared to the thickness of the electrical double layer.

This is indicated by the inclusion of the V in equation 24. The convention is followed hereafter that the quantities previously designated v, i, f and p_E for circular capillaries become V, I, F and P_E for porous diaphragms.

However, the assumption of Smoluchowski that the internal geometry of a porous diaphragm could be evaluated conductometrically took no account of surface conductance, the additional conductance occurring in the electrical double layer. Because of surface conductance, the specific conductivity k_p of the liquid within the pores of a diaphragm is greater than the specific conductivity k of the bulk electrolyte. Thus the ζ-potentials given by equation 24 were too low, the error increasing as the surface conductance be-

came more important.

Briggs Equation

Briggs (19) devised a method of measuring the ζ-potential in which k_p was evaluated by means of conductance measurements. For cylindrical pads of cellulose fiber, Briggs observed that the pad cell constant C = kR, obtained by measuring the electrical resistance R of the pad and the specific conductivity k of the bulk electrolyte, rose in value as the concentration of the electrolyte was increased. A limiting value of C was attained when the electrolyte was 0.1 M KCl solution.

Briggs interpreted these measurements as showing that the contribution of surface conductance relative to bulk electrolyte conductance decreases with increasing electrolytic concentration, and becomes negligible at a concentration of 0.1 M KCl.

Briggs (19) determined the ζ-potential for a number of pads of cellulose by measuring V/p and the pad resistance R at a low electrolytic concentration, then determining the pad cell constant in 0.1 M KCl solution. The specific conductivity k_p of the liquid in the pores of the pad during the stream measurements, which included the contributions of surface and bulk electrolyte conductance, was evaluated as

$$k_p = \frac{C}{R} \qquad \ldots \quad (25)$$

and substituted in the Helmholtz-Smoluchowski equation, which became

$$V = \frac{pD\zeta R}{4\pi\eta C} \quad . \qquad \ldots \quad (26)$$

Briggs reported that the ζ-potentials calculated by this equation agreed within experimental error for different pads of cellulose, independent of the tightness of packing of the pad.

However, in these measurements the weight of material packed into a cell of fixed dimensions was only varied over a range of about 20%. Due to the inevitable difference in mode of packing for each pad, there was a considerable scatter in the ζ-potential value for pads of similar weight, which tended to obscure any trend in the results. More recent applications of the method have shown clearly that the ζ-potential given by the Briggs stream potential equation decreases steadily as the pad is more tightly packed (20, 21, 7).

Goring and Mason (21) carried out stream potential measurements on a number of pads of cotton fiber packed into a cylindrical cell of fixed dimensions over the solid concentration range 0.162 to 0.215 gm. cm.$^{-3}$. The ζ-potential as calculated by the Briggs (19) method showed a definite decrease with increasing pad concentration, falling from - 19.1 mv. at the lowest concentration to -12.1 mv. at the highest

concentration.

Rabinov and Heymann (7) obtained a similar result in stream potential measurements on cylindrical pads of cellulosic materials; the Briggs ζ-potential was always observed to decrease with increasing pad concentration. They remarked that the equivalent pore radius might have fallen below a certain limit approaching the thickness of the electrical double layer, so that the solid surface was not effectively planar, as assumed in the derivation of the stream potential equation.

From these experimental data it is clear that the Briggs method fails for pads of cellulose, as a unique ζ-potential for the cellulose-liquid interface is not provided.

Bikerman (14) has explained the failure of the Briggs method for pads of such highly swelling fibers as cellulose by pointing out that ionic migration through the fiber structure is possible, so that the cross section of the pad available for ionic migration S_2 is greater than that available for fluid flow S_1. He suggested that the cell constant in the Briggs method (equation 26) should be multiplied by S_2/S_1, which would give real ζ-potentials greater than the Briggs value by the factor S_2/S_1. Values of S_2/S_1 around 1.2 were proposed.

The factor S_2/S_1 would be expected to increase with the pad concentration as the cross sectional area of fiber

increases with respect to the void cross sectional area with increasing pad concentration. Thus the correction of Bikerman would tend to neutralize the decrease shown by the Briggs (19) ζ-potential with increasing pad concentration. However, it is difficult to test this hypothesis, as the problem of assigning correct values to S_2 and S_1 must first be solved.

Surface Conductance Equations

Rutgers (9) derived the stream potential equation for a cylindrical capillary containing electrolyte of bulk specific conductivity k, and having a specific surface conductivity k_s at the wall. The electrical resistance of the capillary was taken to be

$$R = \frac{l_c}{\pi R_c^2 k + 2 \pi R_c k_s} \qquad \ldots\ (27)$$

Substituting for R in equation 13 led to the stream potential equation

$$v = \frac{pD\zeta}{4 \pi \eta k} \cdot \frac{1}{1 + \frac{2 k_s}{R_c k}} \qquad \ldots\ (28)$$

This equation has the drawback of containing the uncertain quantity k_s. Experimental determinations of k_s for the same liquid-solid interface differ widely; Rutgers and de Smet (33) even obtained absurdly negative values for the quantity.

Overbeek and Wijga (22) discussed the possibility of extending equation 28 to the case of a porous diaphragm of complex structure. In a preliminary study, they considered the individual pores within a diaphragm in terms of their electrical and hydrodynamic resistance, and capacity of conductance. They treated the cases of pores of different equivalent radius in series, and in parallel, and concluded that the value of the cell constant C used in the Briggs (19) method was too low, the error increasing as surface conductance became more important. Thus the Briggs ζ-potential values determined from stream potential measurements on porous diaphragms at low electrolytic concentrations were erroneously low.

As experimental confirmation of this theory, Overbeek and Wijga reported the ζ-potential of a glass capillary in conductivity water as -140 mv., calculated according to equation 28. The capillary was then crumbled to a powder, and formed into a porous diaphragm. The ζ-potential as determined from stream potential measurements on the diaphragm, using the Briggs method, was -70 mv.

This experimental evidence is open to serious criticism; the ζ-potential value for the capillary contains the uncertain quantity k_s, and the considerable alteration of the surface on powdering the capillary might be expected to alter the ζ-potential at the glass-water interface.

Stream Current Equations

The stream current equation for viscous flow through a capillary of circular cross section has been derived as

$$i = \frac{pD\zeta R_c^2}{4 \eta l_c} \quad \ldots \quad (10)$$

which can be written equally well as

$$i = \frac{pD\zeta a}{4 \pi \eta l_c} \quad \ldots \quad (29)$$

where $a = \pi R_c^2$ = the cross sectional area of the capillary.

The Helmholtz-Smoluchowski (1, 18) stream current equation for flow through a porous diaphragm is therefore

$$I = \frac{pD\zeta}{4 \pi \eta k R} \quad \ldots \quad (30)$$

and the Briggs (19) stream current equation is

$$I = \frac{pD\zeta}{4 \pi \eta C} \quad \ldots \quad (31)$$

Neale Equation

Neale (5) employed diffuse layer theory in deducing an expression for the stream current produced by a flow of liquid through a cylindrical pad of complex structure in terms of the internal geometry of the pad. Neale's stream current equation for dilute aqueous solutions at 18°C. is

$$I = -0.742 \times 10^{-8} \frac{pA\epsilon\zeta}{L} \quad \ldots \quad (32)$$

where p = pressure across pad in cm. of Hg,
I = stream current in amps.,
ζ = ζ-potential in mv.,
L = length of the pad in cm.,
A = cross sectional area of the pad in $cm.^2$,
ϵ = fraction of the pad volume containing liquid, i.e., the void fraction.

Neale and Peters (6) carried out stream current measurements using a cylindrical compression cell, in which a pad of fibrous material was held between perforated Ag-AgCl electrodes. The electrodes were movable, so that the pad could be compressed <u>in situ</u> over a considerable range of solid concentrations. It was found that the ζ-potential, as calculated from equation 32, decreased as the pad concentration was increased.

This decrease of the ζ-potential was attributed to a "wall curvature" effect, i.e., the decrease of the mean pore radius within the pad to a value of the same order of magnitude as the thickness of the electrical double layer. The highest ζ-potential value, determined at the lowest pad concentration, was taken to be the correct value.

Thus the Neale (5) stream current equation is open to the same criticism as the Briggs (19) equation. Instead of providing a unique ζ-potential for the solid-liquid interface, the equation gives a series of values for ζ. Neale's

choice of the value obtained at the lowest concentration is arbitrary; the lower limit of concentration attainable would vary according to the nature of the pad material and the experimental conditions employed.

Goring-Mason Equation

Goring and Mason (20, 21, 8) carried out stream current measurements on cylindrical pads of fibrous materials over a range of pad concentrations, using a compression cell and reversible electrodes similar to those of Neale and Peters (5, 6). An expression for the stream current produced by flow of liquid through a cylindrical pad was deduced, in which the stream current function $I\eta L/pD$ was linearly related to the pad concentration. A derivation of this expression follows.

In the laminar flow of liquid through a cylindrical pad of tightly packed fibers, it is recognized that the individual fibers within the pad vary widely as to shape and size, and have axes inclined at a variety of different angles to the direction of normal flow through the pad. Considering a single pore of arbitrary shape and cross sectional area a, where

θ = inclination of pore axis to direction of normal flow,

w = wetted perimeter of pore,

$\bar{r}$ = a/w = mean hydraulic radius of pore,

and in which the pressure gradient along the direction of normal flow is dp/dl_c, then the pressure gradient along the pore axis is $dp/dl_c \cos \theta$.

When liquid is moving through the pore, the hydraulic force causing the motion is opposed by a viscous drag of equal magnitude at the walls of the pore, so that

$$a \frac{dp}{dl_c} \cos \theta = \left(\frac{du'}{dx}\right)_{x = o} \eta w \qquad \ldots \quad (33)$$

where u' is the velocity of the liquid along the pore axis and $\left(\frac{du'}{dx}\right)_{x = o}$ is the velocity gradient at the wall, assumed to be constant over the perimeter of the pore. For small values of x, the distance normal to the wall, the equation may be written

$$u' = \frac{ax}{w\eta} \frac{dp}{dl_c} \cos \theta \qquad \ldots \quad (34)$$

To obtain the velocity component u_x in the direction of the pad axis, the right hand side of the above equation must be multiplied by cos θ which gives

$$u_x = \frac{ax}{w\eta} \frac{dp}{dl_c} \cos^2 \theta \quad . \qquad \ldots \quad (35)$$

Using equation 35, the stream current component i_x in the direction of the pore axis may be written

$$i_x = \int_o^{\bar{r}} w\rho u_x dx = - \frac{aD}{4 \pi\eta} \frac{dp}{dl_c} \cos^2 \theta \int_o^{\bar{r}} x \frac{d^2 \psi}{dx^2} dx \qquad \ldots \quad (36)$$

substituting for ρ from equation 4, and for u_x from equation 35.

Assuming that the surface of the pore is effectively planar, so that $\psi = 0$ and $d\psi/dx = 0$ for $x \ll \bar{r}$, then the integration of equation 36 leads to

$$i_x = - \frac{aD\zeta}{4\pi\eta} \frac{dp}{dl_c} \cos^2\theta \quad . \qquad \ldots (37)$$

Equation 37 gives the component of the stream current in the normal direction of flow for one pore of cross-sectional area a, inclined at an angle θ to the axis of the pad.

In evaluating the total stream current produced by flow through a complex porous pad, the contributions of a large number of pores having different a and $\cos^2\theta$ values must be taken into consideration. Assuming that the pore structure of the pad is statistically homogeneous, there is a value $\overline{\cos^2\theta}$ representing the average axis inclination of all pores in the pad. Where A is the cross sectional area of the pad, and ϵ the fraction of that area void of solid material, i.e. available for liquid flow, then the total stream current I generated upon flow of liquid through all the pores of the pad is

$$I = - \frac{A \epsilon D\zeta p}{4\pi\eta L} \overline{\cos^2\theta} \qquad \ldots (38)$$

where p = the pressure drop across the pad,
and L = the length of the pad.

In equation 38 the void fraction ϵ may be replaced by $(1 - \alpha_\zeta c)$, where α_ζ is the swollen specific volume in $cm.^3$ per gm. of the dry material, and c is the concentration in gm. $cm.^{-3}$ of the dry material in the pad. Making this substitution in equation 38 and rearranging the terms,

$$\frac{I\eta L}{pD} = \frac{A\zeta}{4\pi}\left(1 - \alpha_\zeta c\right)\overline{\cos^2\theta} \qquad \ldots (39)$$

neglecting the negative sign.

Sullivan and Hertel (25) showed that $\overline{\cos^2\theta} = 0.5$ for flow measurements through a porous bed consisting of randomly oriented cylindrical particles. Assuming this value was applicable for a cylindrical pad of randomly oriented fibers, Goring and Mason (20, 21) obtained the stream current equation

$$\frac{I\eta L}{pD} = \frac{A\zeta}{8\pi}\left(1 - \alpha_\zeta c\right) \qquad \ldots (40)$$

Employing Ohm's law, the corresponding stream potential equation was

$$\frac{V\eta L}{pDR} = \frac{A\zeta}{8\pi}\left(1 - \alpha_\zeta c\right) \qquad \ldots (41)$$

Employing this equation in the analysis of stream current data obtained over a range of pad concentrations

with the compression cell, Goring and Mason (8) plotted $I\eta L/pD$ versus c, and extrapolated the resulting straight line to the co-ordinate axes. The intercepts gave values for the ζ-potential and for α_ζ from

$$\left(\frac{I\eta L}{pD}\right)_{c = o} = \frac{A\zeta}{8\pi}$$

and

$$\left(1 - \alpha_\zeta c\right)_{\frac{I\eta L}{pD} = 0} = 0$$

It must be emphasized that α_ζ is the "hydrodynamic" specific volume of the material in the pad, i.e., the specific volume per unit mass of the dry material which excludes flow. Goring and Mason (8) carried out their stream current measurements on cylindrical pads of cotton and sulphite pulp; each of these fibers imbibes a considerable quantity of water, so that the "hydrodynamic" specific volume may be two to nine times the "true" specific volume of cellulose, 0.62 $cm.^3\ gm.^{-1}$ (26). Thus the correctness of the α_ζ values could only be judged if comparison were made with a value obtained by an alternative method.

The liquid permeability method proved a convenient alternative method for determining the "hydrodynamic" specific volumes of the cellulose fibers. Goring and Mason (8) carried out determinations of liquid permeability at each pad concentration, concurrently with the stream current measurements. The permeability data were interpreted by the

Robertson-Mason (26) modification of the Kozeny (27) permeability equation; Carroll and Mason (49, 50) have offered convincing experimental evidence that the specific volume α_k given by this equation is correct.

Goring and Mason observed that the α_ζ values were consistently higher than the corresponding α_k for both sulphite pulp and cotton pads, the discrepancy ranging from 25-50%. The α_ζ values obtained from measurements on a series of pads of sulphite pulp showed no significant change when the concentration of the electrolyte was varied over the range 10^{-4} to 2×10^{-2} M KCl. Since the thickness of the equivalent Helmholtz electrical double layer varied from 300 - 20Å over this range of electrolytic concentrations, it was considered unlikely that the discrepancy between α_ζ and α_k was due to an electrical layer thickness effect.

In order to explain this discrepancy, Goring and Mason (8) proposed an alternative model of the ionic distribution at the cellulose-liquid interface. Cellulose is believed to consist of an assembly of flexible linear chain molecules whose length may be as great as several microns, held together by lateral hydrogen bonding and Van der Waals' forces in amorphous and crystalline regions (53). In the theory of swelling of cellulose in water originally proposed by Campbell (54), surface molecules of amorphous cellulose are considered to be anchored to the body of the structure,

with a portion of the molecule or a group of molecules "dissolved" and free to move as a unit in the water in a restricted Brownian movement.

With this concept in mind, Goring and Mason (8) suggested that each water-swollen cellulose fiber was surrounded by a diffuse layer of considerable thickness, called the β-layer, in which partially dissolved molecules and groups of molecules, bearing an electrical charge, extended into the liquid. Each such unit was surrounded by its own Gouy-Chapman diffuse electrical layer, having an equivalent thickness, δ, small compared to the length of the chain.

In terms of this model, a semi-quantitative explanation for the discrepancy between α_ζ and α_k was offered. The model could also be used to account for the anomalous resistance dispersion effect observed in impedance measurements on pads of sulphite pulp (28, 8). This effect was first noticed when stream potential and stream current measurements were carried out on the same pad of sulphite pulp. It was found that the stream potential function $V\eta L/pDR$ was only equal to the corresponding stream current function $I\eta L/pD$ when the d.-c. resistance of the pad R_o was used; the 1000 c.p.s. a.-c. resistance R_{1000} was 25-30% less than R_o.

Goring and Mason restricted their measurements to pads of cellulose; thus there was no experimental evidence that the stream current equation was valid for measurements

on pads of fibers, such as glass, which possessed no β-layer. Further verification of the equation was therefore required.

Comparison of Stream and Electro-Osmotic Measurements

A survey is next made of the few cases appearing in the literature where stream and electro-osmotic measurements were carried out on the same system.

According to the classical Helmholtz-Smoluchowski equations

$$\frac{V}{p} = \frac{F}{I_o} = \frac{D\zeta}{4\pi\eta k}$$

where I_o is the electro-osmotic current.

Saxen (38), in 1892, verified this relationship for electrolytic solutions in contact with a clay diaphragm held between reversible electrodes, showing that pF/VI_o was equal to unity with a mean deviation of less than 2%. He was unable to confirm the relationship for distilled water in contact with the diaphragm.

Saxen's observations have been confirmed for the glass-water system. Rutgers and de Smet (33) used the Briggs method in determining ζ_E from measurements of electro-osmotic flow and ζ_s from measurements of stream voltage on the same glass capillary. It was shown that ζ_E/ζ_s was equal to unity

within experimental error for capillaries of different diameter in contact with conductivity water and various electrolytic solutions. Wijga (39, 22) was able to show ζ_E/ζ_s was equal to unity for diaphragms of powdered glass as well as for glass capillaries.

It is interesting to note that available experimental evidence indicates that the two methods are not equivalent in the iso-electric region for the glass-electrolyte interface.

Monaghan, White, and Urban (40) determined the iso-electric concentration from stream potential measurements on a glass capillary as $\sim 4 \times 10^{-7}$ M $ThCl_4$. According to measurements of electro-osmotic flow, there was a negative charge on the glass wall until the concentration of the electrolyte had been increased to $\sim 3 \times 10^{-6}$ M $ThCl_4$. To explain this result, the authors suggested that an outer portion of the "fixed" layer might sometimes be moved by electrostatic, though not by hydrostatic forces.

Dubois and Roberts (41), attempting to show the equivalence of stream potential and electro-osmotic measurements with indifferent success, reported a result similar to that of Monaghan, White, and Urban. For a pyrex slit in 10^{-5} N $AlCl_3$ solution, ζ_s was + 32 mv. while ζ_E was - 46 mv.

Rutgers and de Smet (33) were apparently unable to report agreement between the two methods in the iso-electric

region. In a graph showing ζ_E and ζ_s plotted against the concentration of $AlCl_3$, in which a reversal in the sign of the ζ-potential occurred, ζ_E and ζ_s values were paired at the high negative and high positive ζ-potentials, showing agreement between the two methods. However, no ζ_E values appear in the iso-electric region, and the authors make no comment concerning the omission.

In the few cases where measurements of ζ_E and ζ_s have been carried out on the same pad of cellulose fibers, the electro-osmotic and stream measurements have failed to agree.

Kanamaru (42) carried out extensive measurements of stream potential and electro-osmotic flow on pads of cellulose and cellulose derivatives in contact with water and numerous electrolytic solutions, and reported that $\zeta_E/\zeta_s = \sim 0.38$.

Goring and Mason (20, 21) used the Briggs method in determining ζ_E and ζ_s from electro-osmotic flow and stream potential measurements on a series of cotton pads of the same external dimensions, but packed to different degrees of tightness. Over the pad concentration range 0.16 to 0.22 gm. $cm.^{-3}$, it was found that the ζ_E/ζ_s ratio varied from 1.2 to 1.5. This discrepancy from the expected value of unity could not be accounted for on the basis of the model structure assumed to exist at the cellulose-water interface (8).

In making the electro-osmotic measurements, Goring and Mason observed a movement of the bubble in the capillary flowmeter upon application of a potential across the electrodes with no pad in the electro-osmotic cell. This was attributed to the action of a potential gradient upon the liquid at the walls of the capillary. The potential gradient was assumed to exist unchanged when a pad was in the cell, and a standard correction for "capillary electro-osmosis" was applied to all measurements of electro-osmotic flow carried out with pads of fibers in the cell.

However, if the experimental data of Goring and Mason are recalculated with the correction for capillary electro-osmosis omitted, the ζ_E/ζ_s values range from 0.97 - 1.12, with a much less marked tendency for the ratio to increase with increasing pad concentration (Table I). This result is close to the theoretical value of unity, and suggests that the correction for capillary electro-osmosis was spurious.

TABLE I

Comparison between ζ_E and ζ_s on A Series of Cotton Pads over A Range of Pad Concentrations from The Experimental Data of Goring and Mason (20, 21).

c. gm. cm.$^{-3}$	ζ_E/ζ_s Corrected for capillary electro-osmosis	ζ_E/ζ_s Neglecting the capillary electro-osmosis correction
0.162	1.22	1.03
0.174	1.14	0.97
0.183	1.29	1.01
0.195	1.36	1.10
0.197	1.36	1.07
0.207	1.45	1.12
0.215	1.55	1.09

Permeability Measurements

Throughout the investigation permeability measurements were carried out concurrently with the electrokinetic measurements. A brief description of the method of analysis of the experimental data follows.

According to an empirical relationship known as Darcy's Law (51) the permeability co-efficient K can be expressed

$$K = \frac{Q\eta L}{pA} \qquad \ldots \quad (42)$$

where the flow occurs through a cylindrical pad of length L and cross sectional area A, and the other symbols are as previously defined.

Robertson, Carroll and Mason (49, 50, 26) have carried out liquid permeability measurements on cylindrical pads of fibers in swelling and non-swelling media, using a compression cell which enabled the measurements to be carried out over a range of pad concentrations.

The rectilinear form of the Kozeny (27) permeability equation

$$(Kc^2)^{1/3} = \frac{1}{(5.55\ \sigma^2)^{1/3}} (1 - \alpha_k c) \qquad \ldots \quad (43)$$

was employed for analysis of the experimental data; σ is the specific surface per unit mass of dry fiber, and α_k is the "hydrodynamic" specific volume per unit mass of the dry fiber.

When the flow data are plotted as $(Kc^2)^{1/3}$ versus c curves, extrapolation of the linear part of the curve to the co-ordinate axes gives values for α_k and σ, from

$$\left(Kc^2\right)^{1/3}_{c = o} \qquad \frac{1}{(5.55\ \sigma^2)^{1/3}}$$

and $$\left(1 - \alpha_k c\right)_{(Kc^2)^{1/3} = o} = 0$$

Carroll and Mason (49, 50) have presented convincing evidence that the α_k values obtained with this method are correct; in the present investigation, the method was used to calculate an α_k value for each pad measured, which provided an invaluable check on the α_ζ value obtained in the electrokinetic measurements.

EXPERIMENTAL PART

Scope of the Investigation

The experimental work which follows is divided into two sections. In the first, the apparatus, preparation of materials, and general experimental procedures are described; and the calculation of the stream current, electro-osmotic and permeability functions for a specimen pad are presented in detail. In the second section, some of the improvements in experimental technique are described; the results obtained in the measurements are listed, and their significance discussed briefly.

Two compression cells were used in the investigation; the measurements carried out with each cell are briefly outlined in the following paragraphs.

The cell used in the earlier work was that of Goring and Mason (20, 21, 8), which will subsequently be referred to as the low-compression cell. The following measurements were carried out with this cell:

1) Stream current and permeability measurements on pads of glass, nylon, cotton, acetate rayon, viscose rayon, and sulphite pulp over a range of solid concentrations. ζ and a_ζ were calculated from equation 40.

2) Investigation into the effect of the space between pad and electrode.

3) Exploratory measurements of the low frequency resistance dispersion effect, first observed by Goring and Mason (see Appendix A).

For the later stages of the work, a second compression cell was constructed, similar to the first but designed to compress materials between the electrodes to a much greater extent than previously possible. With this cell, which will subsequently be referred to as the high-compression cell, the following measurements were carried out:

1) Stream current and permeability measurements on pads of acetate rayon, Dacron, nylon, surgical cotton, and viscose rayon over a range of pad solid concentrations. With acetate rayon and Dacron, the measurements were carried out at a number of different concentrations of electrolyte. α_k and σ were calculated from permeability equation 43 for each pad.

2) Measurements of the variation of the stream current with continued flow of electrolyte through the pad for acetate rayon, viscose rayon, nylon, and surgical cotton.

3) Measurement of the variation of electro-osmotic flow F with change of the applied potential E for pads of 2.5 micron dia. glass, surgical cotton, acetate rayon, and sulphite pulp.

4) Measurements of stream current, electro-osmotic flow, and permeability on the same pad over a range of solid

concentrations for pads of 0.5 micron dia. glass, surgical cotton, sulphite pulp, and acetate rayon. α_k and σ were calculated from permeability equation 43 for each pad.

5) Investigation into the deviations from conventional electrokinetic theory observed in the electro-osmotic measurements (see Appendix B).

6) Comparison of stream current and electro-osmotic flow measurements near the iso-electric point (see Appendix C).

Earlier experimental procedures were those of Goring and Mason (20, 21, 8) but modifications were made as the work progressed. Standard procedures were finally adopted, which were used in the measurements with the high-compression cell; these are described in detail. To avoid repetition, the experimental procedures with the low-compression cell are not described fully; only the more significant differences from the procedures used with the high-compression cell are mentioned.

Apparatus and Materials

High-Compression Cell

A half-section of the high-compression cell and electrodes is shown in Fig. 2.

The cell was of pyrex tubing having an internal cross sectional area of 5.00 $cm.^2$, a wall thickness of 0.4 cm., and a length of 60 cm. The cell was provided with four sidearms, two being fitted with ground-glass taper joints to permit the connection of a differential water manometer. The other two

sidearms served as inlet and outlet for liquids being streamed through the cell.

The silver electrodes were chloridized, so they would be reversible with respect to chloride solutions, and fitted snugly into the cell. Each electrode was 1/2 in. thick and tapered toward the back side, which was provided with a socket 1/4 in. deep. Into the socket was inserted a thick-walled pyrex capillary of 1/2 in. outer diameter and 35 cm. length, which was fastened to the electrode with de Khotinsky cement. The external junction between the electrode and the capillary was sealed with Tygon paint. Thirty holes of 1/16 in. diameter, drilled through the electrode in the space between the socket and the edge, permitted liquid to flow freely through the electrode. Electrical connection was provided by a silver bus bar, which was fused to the back of the electrode and ran through the capillary upon which the electrode was mounted. At the end of the capillary, the bus bar ran through a bakelite insert. In the assembled apparatus, each capillary was inserted through a rubber stopper which held it concentric with the cell walls and provided a liquid-tight seal at the end of the cell.

The silver electrodes were chloridized by anodizing at 3 ma. $cm.^{-2}$ for 2 1/2 hr. in 0.1 M hydrochloric acid, using a platinum cathode. This followed the procedure of other workers (6, 8).

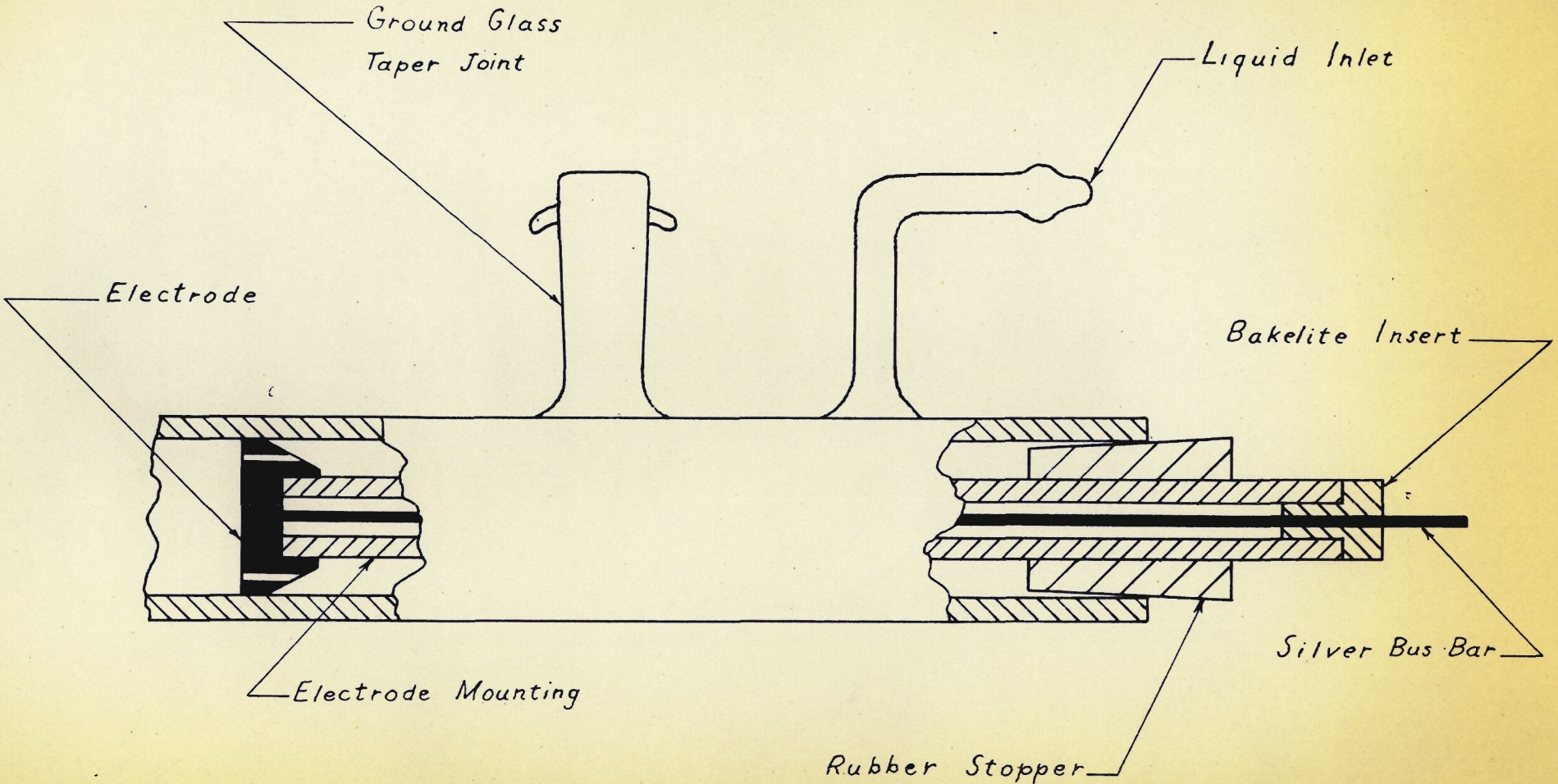

FIG. 2. Half section of the high-compression cell

Fig. 3 shows a top view of the arrangement used to apply high compression to pads of fibrous materials.

The cell was clamped in a wooden frame between two threaded 1/4 in. steel tie rods of 95 cm. length, which were held to the frame by means of wing nuts. At each end of the cell a brass plate, drilled to fit over the tie rods and the capillary mounting the electrode, could be tightened against the rubber stopper with wing nuts. This held each rubber stopper securely in place.

A second pair of brass plates were drilled to fit over the tie rods and the silver bus bar. Ample clearance was allowed in the latter case, so that the brass plate could be brought against the bakelite insert at the end of the capillary without touching the bus bar. When wing nuts were tightened against the brass plates, pressure was exerted along the axes of the capillaries mounting the electrodes, compressing the material held between the electrodes. The danger of breakage was minimized by the rugged construction of cell and electrodes.

Low-Compression Cell

The low-compression cell, which was similar to the high-compression cell, has been described by Goring and Mason (20, 21, 8).

The chief difference between the two cells was the relatively fragile construction of the low-compression cell

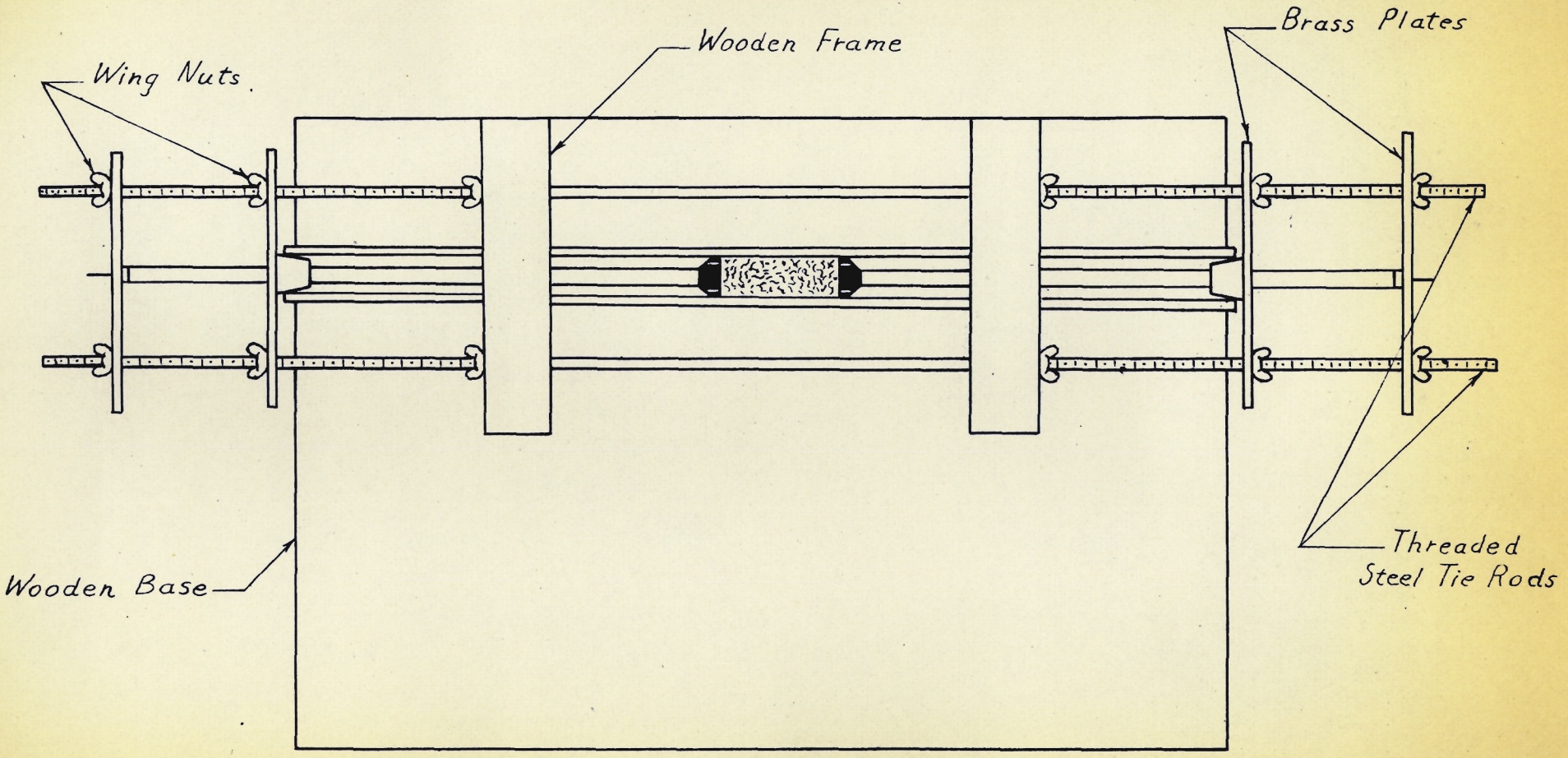

FIG. 3 High-compression cell showing arrangement for compression of pads.

and its electrodes. Pads were compressed by hand pressure, an awkward procedure involving considerable danger of breakage. The compression obtainable was much less than with the high-compression cell.

Materials

The fibrous materials used in the course of the investigation are described briefly in Table II.

TABLE II

Fibrous Materials Used in Electrokinetic and Permeability Measurements

Material	Description	Source
Glass fiber	0.5 micron dia. staple	Glass Fibers, Inc.
Glass fiber	2.5 micron dia. staple	Owens-Corning Fiberglas Corporation
Dacron	1.5 denier staple	E.I. du Pont de Nemours
Nylon	3 denier delustered	Canadian Industries Limited
Acetate rayon	3 denier staple, acetyl value 54	Canadian Celanese Ltd.
Cotton	Surgical batting	Parke Davis and Co. Ltd.
Viscose rayon	Continuous filament	Courtaulds(Canada) Ltd.
Sulphite pulp	Air dry bleached lap	Pulp and Paper Research Institute of Canada

The 0.5 micron dia. glass fiber was used in the form supplied by the manufacturer. Cotton, viscose rayon and

the 2.5 micron dia. glass fiber were chopped into short lengths in the Wiley mill. With acetate rayon, nylon, and Dacron, the fibers were chopped in the Wiley mill, and the "fines" removed by wet-screening over the 150 mesh screen of a Bauer-McNett classifier. The fibers were then oven dried at 90°C., and stored ready for use. The sulphite pulp was supplied as air dry bleached lap. It was made into a suspension of fibers by a thorough soaking in distilled water, followed by dispersion in a British Standard disintegrator. When the sulphite pulp was wet-screened it was stored as an aqueous suspension.

Upon completion of measurements on a pad of fibers, the pad was dried for 24 hr. at 105°C. and cooled in a desiccator. The dry weight of the pad thus obtained was used in calculating the pad concentration in gm. $cm.^{-3}$.

Pad Formation

High-Compression Cell

Prior to pad formation, the fibrous material was washed by allowing it to soak in 2 1/2 litres of distilled water for about one hour followed by filtration on a nichrome screen. This procedure was repeated 4 or 5 times in all, the pad material thus being washed in 10 to 12 litres of water. The fiber was then soaked for 12 hr. in 4 litres of electrolyte having the same concentration as that to be used in measurements.

Samples of fiber weighing 9 gm. were generally used,

except for 0.5 micron dia. glass and sulphite pulp. With these fibers the slow draining properties of the pads made it impractical to use more than 1.2 gm. for the glass, and 3 gm. for the sulphite pulp.

To form the pad, the high-compression cell was clamped vertically, with the lower electrode in position (Fig. 4). The manometer openings were sealed with ground-glass taper plugs, and the liquid inlet with a rubber cap. A piece of rubber tubing provided with an adjustable clamp was fastened to the liquid outlet. The cell was filled with electrolyte through the open end, and the clamp adjusted to give slow draining. The suspension of fiber in 4 litres of electrolyte was then formed into a pad by filtration through the electrode. During this process the settling suspension was repeatedly stirred in the cell to reduce flocculation, and to free any air bubbles adhering to the fibers or to the sides of the cell. The filtrate was collected in a 4 litre florence flask.

When the pad was completely formed, the second electrode was inserted into the cell, care being taken to compress the pad as little as possible. The cell was then clamped in the wooden frame. The innermost brass plates were tightened against the rubber stoppers, ensuring that no leakage could occur at the ends of the cell. The flask containing the filtrate was connected to the liquid inlet of the cell, as shown in Fig. 5. Any visible air bubbles were removed through the manometer sidearms, being displaced by electrolyte. The

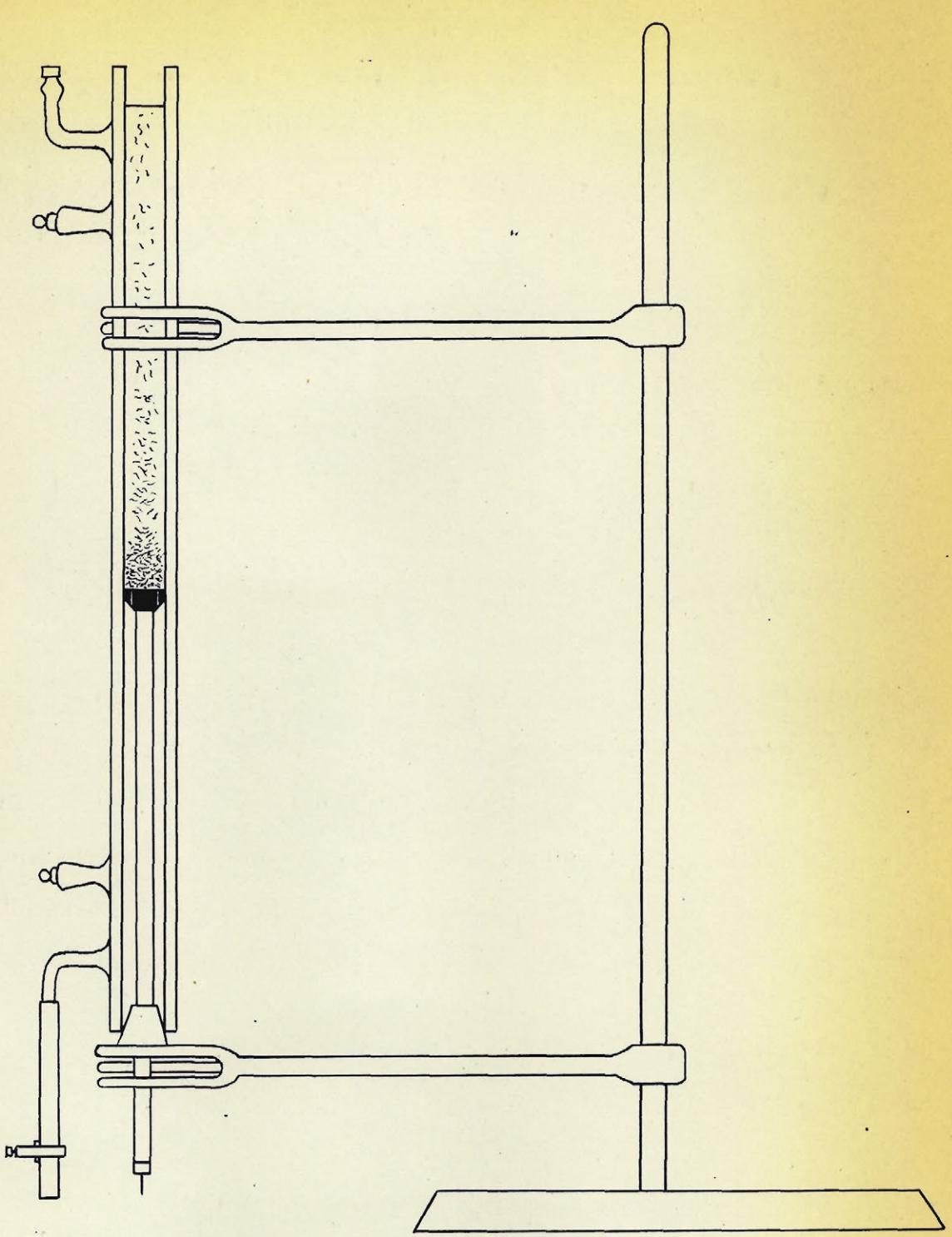

FIG. 4 High-compression cell during pad formation

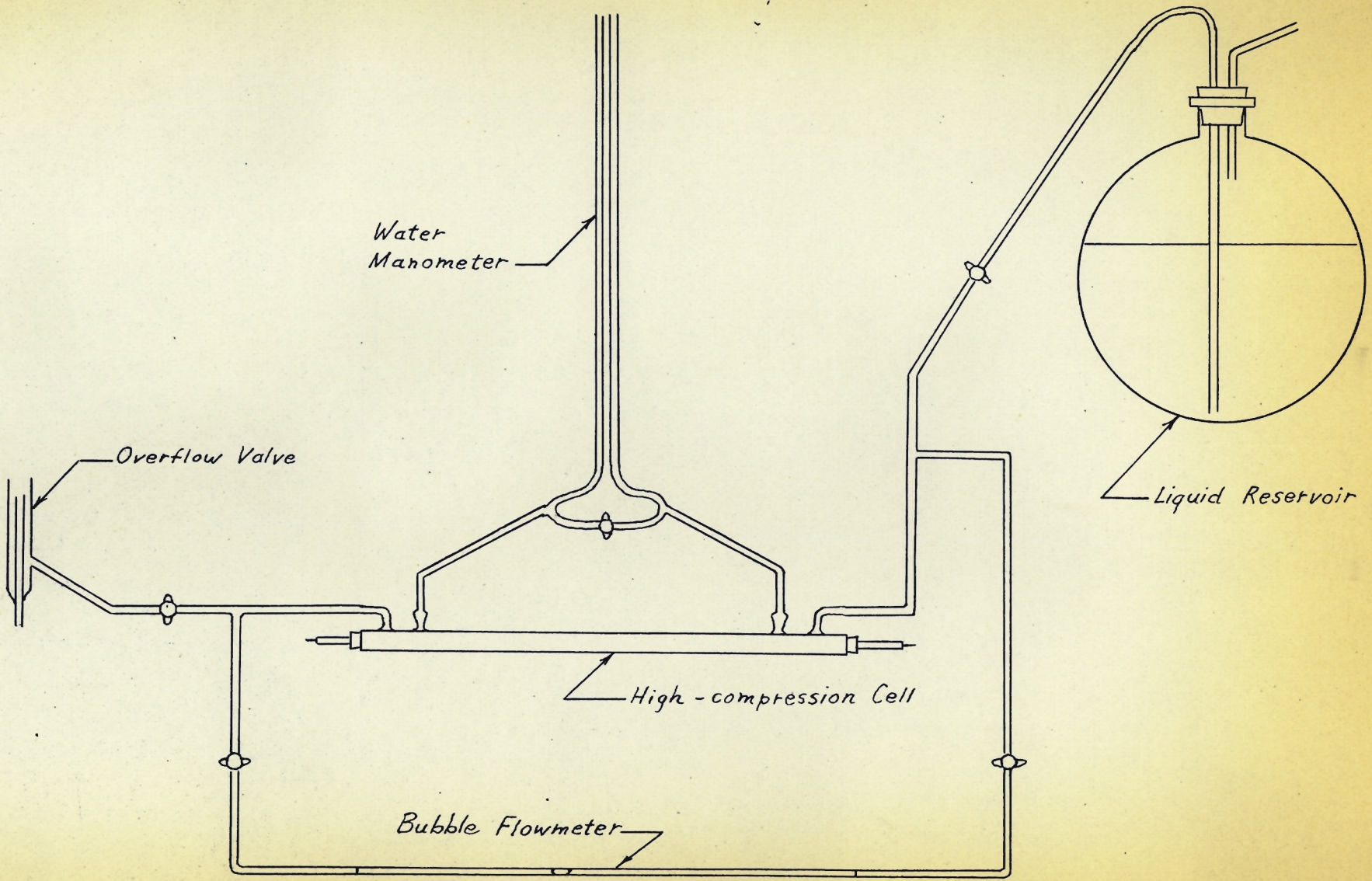

FIG. 5 Assembly of the apparatus for stream current, electro-osmosis and permeability measurements.

water manometer and liquid outlet were then connected as shown in Fig. 5.

Complete de-aeration was achieved by boiling the filtrate at room temperature, and allowing it to cool to about 70°C. The liquid in the cell was then displaced by about 400 ml. of the warm electrolyte, connection in parallel with the pad being established by opening the manometer stop-cock. This stop-cock was then closed, and 100 ml. of the warm electrolyte passed through the loosely-packed pad. This procedure was repeated 3 times at 30-minute intervals, after which the pad was allowed to stand 12 hr.

The solution used in an experimental run was a 10 litre batch of the same electrolytic concentration as that used for de-aeration, freshly prepared from de-aerated distilled water. Immediately prior to the experimental run, electrolyte sorption equilibrium between pad and solution was established by a repetition of the de-aeration procedure, carried out with the fresh electrolyte at room temperature.

Low-Compression Cell

The treatment of the fibrous material prior to pad formation was similar to that with the high-compression cell. In pad formation and de-aeration, the procedures used were those described by Goring and Mason (20, 21, 8), which differed from the methods used with the high-compression cell in several respects.

Pads were formed by filtration on a disc of 80-mesh copper gauze, which was removed after pad formation was complete. Before inserting the electrodes into the cell, a few layers of plastic mesh were placed at the ends of the pad. This procedure was awkward, as the pad dried partially, and sometimes collapsed after the gauze disc had been removed.

In the de-aeration procedure a few litres of the filtrate electrolyte were heated to about 50°C., and boiled under reduced pressure. The pad and cell were flushed out with warm electrolyte, as with the high-compression cell. Care was taken not to warm the pad too much, as this would destroy the sorption equilibrium between pad and electrolyte. The pad was then allowed to stand 12 hr. after which measurements were carried out with the remaining filtrate electrolyte, now cooled to room temperature.

This de-aeration procedure was milder than that used with the high-compression cell, and there was a greater possibility of incomplete de-aeration. In spite of all precautions, the electrolyte sorption equilibrium was sometimes destroyed, as evidenced by initial stream current readings having a rising or falling trend.

Stream Current and Permeability Measurements

High-Compression Cell

The arrangement of the apparatus for measurements

of stream current and permeability is shown in Fig. 5, the by-pass used to measure electro-osmotic flow being cut off during these measurements.

Pressure was maintained across the pad by gravity feed, and held constant at the liquid outlet by means of an overflow valve. The use of a 12 litre round-bottomed flask as solution reservoir helped to control the pressure on the liquid inlet side, the change of liquid level during a determination of the stream current being within experimental error. Using a 10 litre batch of liquid as reservoir also gave a measure of temperature control, the large volume of liquid being relatively unresponsive to small fluctuations of room temperature.

Before measuring the stream current it was necessary to determine the residual electrode current with no pressure across the pad. This was generally less than 0.02 microamp. A steady pressure of 20-60 cm. of liquid was then placed across the pad. The recorded stream current was the deflection immediately after the damping motion of the galvanometer had ceased, and ranged from 0.20 to 0.70 microamp. Pressure on opposite sides of the pad was then equalized by means of the manometer stop-cock. The residual current, which had generally changed less than 0.003 microamp., was measured again. The observed stream current I_{obs} was the difference between the average of the two residual values, and the value recorded

during streaming. The ratio I_{obs}/p, the observed stream current per unit liquid pressure, was experimentally reproducible within 1/2%.

The observed stream current was corrected for leakback through the pad, according to the equation

$$I = I_{obs}\left(1 + \frac{Rg}{R}\right) \quad \ldots \quad (44)$$

where Rg = the electrical resistance of the galvanometer circuit

and R = the resistance of the pad.

Current was measured with a calibrated d'Arsonval galvanometer of 0.03 microamp $cm.^{-1}$ sensitivity, in parallel with a 3000 ohm shunt. The combined resistance of galvanometer and shunt gave Rg = 412 ohms.

The pad resistance R was measured with an Industrial Instruments Inc. Model RC16 60 c.p.s. conductivity bridge, which was also used to check the conductivity of the effluent liquid, by measuring the resistance of a conductivity cell in the liquid outlet line.

In a typical stream current run, a pad was compressed in stages, I_{obs}/p and R being measured at each stage. The pad concentration at each stage was calculated from the known cross sectional area of cell, the dry pad weight, and the length of the pad, measured with a travelling microscope.

For all runs, temperature was recorded for each reading by means of a thermometer immersed in the outlet overflow valve. The values of η and D used in the permeability and electrokinetic equations were those of pure water at the same temperature.

The permeability measurements were carried out using the experimental methods of Robertson, Carroll, and Mason (26, 49, 50). The flow rate at constant pressure across the pad was determined by collecting the effluent liquid in a calibrated graduate over a measured time interval. The high-compression cell provided sufficient compression for α_k and σ to be determined for all fibers except glass wool.

Low-Compression Cell

The experimental procedures in measurements of stream current and permeability with the low-compression cell, which have been described by Goring and Mason (20, 21, 8), were similar to those used with the high-compression cell.

An important difference in measurements with the two cells was the arrangement used to control the liquid pressure across the pad. With the low-compression cell, the liquid reservoir was a 4 litre suction flask, so that the variation of the liquid level with flow was greater than that occurring with the high-compression cell arrangement. On the other side of the pad, the liquid outlet was immersed in a 100 ml. calibrated graduate, which was moved manually during a run to main-

tain a constant pressure difference across the pad. In the permeability measurements, the rate of liquid flow was determined in the graduate. Except with sulphite pulp, the hand pressure used with the low-compression cell did not provide sufficient compression for the permeability measurement of α_k and σ.

This crude method of pressure control gave acceptable results for such fibers as sulphite pulp and cotton with which the slow-draining properties of the pads provided a measure of pressure control. However, the method failed for fibers such as nylon and acetate rayon, which formed fast-draining pads, and was modified as described previously in measurements with the high-compression cell.

Goring and Mason (20, 21) observed that both the stream current and the permeability of a pad decreased on prolonged flow of solution through the pad. This "decay" effect was eliminated by placing a few layers of plastic mesh between the electrodes and the ends of the pad. In measuring the pad length, the total thickness of the mesh was subtracted from the measured distance between the electrodes. No correction was made for the mesh space resistance when the measured pad resistance was used in the calculation of the leak-back current.

Electro-Osmotic Flow Measurements

The experimental arrangement used to measure elec-

tro-osmotic flow in the high-compression cell is shown in Fig. 5. A calibrated capillary of 33 cm. length and 0.246 cm. internal radius was connected in parallel with the pad by means of Tygon tubing, an air bubble being left at one end of the capillary during the assembly.

When measurements of electro-osmotic flow were being carried out, the stop-cocks in the manometer and those in the liquid inlet and outlet lines were closed, and the stop-cocks in the capillary by-pass were opened. A potential difference was then applied across the electrodes from a battery of 45 volt dry cells; the use of reversible electrodes directly in contact with the pad made it possible to measure the potential drop across the pad with a high-resistance calibrated voltmeter.

The electro-osmotic flow rate F_{obs} was calculated from the speed of the bubble. It was observed that a clean capillary was essential for an accurate measurement of F_{obs}, otherwise the bubble speed was irregular, and the bubble tended to stick at the lower speeds. The capillary was cleaned satisfactorily with a sulphuric acid - potassium dichromate solution, followed by a thorough rinsing with the electrolyte used in the electro-osmotic run.

During a typical determination of electro-osmotic flow rate, 0.2 to 0.7 ml. of liquid flowed through the pad in 30 to 120 seconds at an electro-osmotic current of about 0.5

ma. Once the inertia had been overcome, the bubble moved along the capillary at a constant rate, within the accuracy of the experimental determination.

Immediately after a measurement of F_{obs} was concluded, and the potential drop across the pad was removed, a considerable deflection was observed when the d'Arsonval galvanometer was connected across the electrodes. This residual current could be wiped out by running 100-200 ml. of liquid through the pad, but it was found more convenient to reverse the potential across the electrodes, driving the air bubble back to its starting point. After this had been done, and 25 ml. of solution had been streamed through the pad, the residual current was generally close to zero.

The "depolarizing" electro-osmotic flow rates, with the flow through the pad in the opposite direction, were recorded as a check on the result obtained in the initial determination. Agreement between the two runs was generally within 2%, indicating that polarization was negligible during the initial run. However, in a few cases the discrepancy between the two runs exceeded 2%; this suggested that a significant polarization might have taken place during the initial run. The largest discrepancies were exhibited by the slow-draining pads; a pad of 0.5 micron dia. glass, the least permeable pad measured, showed reverse flow rates as much as 8% lower than the initial rate. A pad of sulphite pulp showed the opposite tendency; reverse flow rates were recorded as much as 5%

higher than the initial rate.

If these discrepancies are due to polarization, the mechanism of the effect is difficult to envisage. The 0.5 micron dia. glass and sulphite pulp both showed a low negative charge in 2 x 10^{-5} M KCl solution, which was the permeant in the runs described above; there is no apparent reason for polarization to occur in the opposite sense for the two fibers.

It is perhaps more probable that the discrepancies shown between the initial and reverse runs derived from directional properties of the pad. Carroll, Goring and Mason (20, 49) have observed marked changes of stream potential and permeability upon reversal of the direction of flow through the pad.

In the present investigation, no systematic examination of the effect of direction of flow through the pad was undertaken. All the electro-osmotic flow rates quoted in the experimental results were the initial runs on a pad with zero residual current, with the induced flow in the direction of pad formation. This conformed to the measurements of stream current and permeability, which were also carried out with the flow in this same direction.

Tests were made for "capillary electro-osmosis", the bubble movement observed by Goring and Mason (20, 21) upon application of a potential across the electrodes when no pad was in the cell. No such movement could be detected; the de-

sign of the cell used in the present investigation made it impossible for a pressure difference to exist between the ends of the capillary when no pad was in the cell.

Due to the appreciable resistance to flow in the capillary, the observed electro-osmotic flow rate F_{obs} required correction for leak-back flow through the pad. Using the quantity $Q\eta/p = \Phi$ as a measure of liquid permeability, where Q is the flow in $cm.^3$ $sec.^{-1}$ at a pressure p of a liquid of viscosity η, the true electro-osmotic flow F was calculated from

$$F = F_{obs}\left(1 + \frac{\Phi_p}{\Phi_c}\right) \qquad \ldots \quad (45)$$

where Φ_p = the permeability of the pad
and
Φ_c = the permeability of the capillary.

Φ_p was easily determined from flow measurements, but this method proved less practical for determining Φ_c, as the capillary was sufficiently permeable for turbulent flow to occur at pressures greater than 2 cm. of water. In the initial treatment of the experimental data, Φ_c was therefore calculated by the Poiseuille equation as

$$\Phi_c = \frac{\pi R_c^4}{8\, l_c} \qquad \ldots \quad (46)$$

Electro-Osmotic Pressure Measurements

For these measurements the capillary by-pass was cut off. Upon the application of a potential across the electrodes, the electro-osmotic flow was manifested as a pressure across the pad; this pressure increased until the equilibrium value p_E was reached, at which the leak-back flow was equal and opposite to the electro-osmotic flow. In order to reduce the duration of flow necessary for the attainment of p_E, and thus to reduce polarization, a differential water manometer of 1 mm. i.d. was used in the measurements of p_E.

The lack of temperature control in the apparatus led to difficulties in measuring p_E. Shifting temperatures in different parts of the apparatus were reflected in the water manometer, which usually indicated a slow rising or falling trend. Thus, after the application of voltage to the electrodes, p_E had to be determined by reading the value indicated on one manometer arm and then the other, as rapidly as possible, until two successive $p_E$values were obtained which were within 0.2 mm. of each other. This usually occurred after the potential had been applied for over 90 sec. In a few cases a steady rise of p_E persisted after 90 sec.; when this occurred, the value pf p_E shown after 120 sec. was recorded, as it was feared polarization was taking place.

As with the electro-osmosis, the initial measurement of p_E was carried out under conditions of zero residual current,

with the induced flow in the direction of pad formation. When comparing the electro-osmotic pressure results with those obtained in concurrent stream current and electro-osmotic flow measurements, the values quoted were those with flow in this direction.

Specimen Calculations

The present investigation consisted for the most part of measurements of stream current, electro-osmotic flow, and permeability. The experimental data were usually analysed as the functions of pad concentration $I\eta L/pD$, $F\eta L/ED$ and $(Kc^2)^{1/3}$.

A specimen set of experimental data, obtained in concurrent measurements of stream current, electro-osmotic flow, and permeability on cotton pad 30 in 2×10^{-5} M KCl solution at a single pad concentration, is presented in Table III. Each quantity determined directly from the measurements is shown, and also the various quantities calculated from the experimental data. On the following pages these calculations are described in detail.

The values of η and D were taken to be those of pure water at the measured temperature of the electrolyte. The pad length L was used in the electrokinetic and permeability functions, and also in calculating the pad concentration c from

$$c = \frac{\text{Pad Weight}}{LA} = \frac{8.476}{5.715 \times 5.00} = 0.296 \text{ gm. cm.}^{-3}$$

TABLE III

Stream Current, Electro-Osmotic Flow and Permeability for Cotton Pad 30 in 2 x 10^{-5} M KCl solution at a Single Pad Concentration in the High Compression Cell

A: 5.00 $cm.^2$; Galvanometer calibration: 31.00 cm./microamp.; Pad weight: 8.476 gm.; Φ_c: 274 x 10^{-8} $cm.^3$.

Experimentally Determined			Calculated from the Experimental Data		
Quantity	Units	Value	Quantity	Units	Value
T	°C.	28.1	η	poises x 10^2	0.834
L	cm.	5.715	D	D	76.75
S_r	cm.	(-0.30 (-0.34	c	gm. $cm.^{-3}$	0.296
S_s	cm.	+7.80	$I\eta L/pD$	mv. $cm.^2$	3.38
S_{obs}	cm.	+8.12	$F\eta L/ED$	mv. $cm.^2$	3.32
p	cm. H_2O	44.15	Φ_p	$cm.^3$ x 10^8	4.00
F_{obs}	$cm.^3$ $sec.^{-1}$ x 10^3	5.37	K	$cm.^2$ x 10^8	4.58
E	volts	92	$(K_c^2)^{1/3}$	$gm.^{2/3}cm.^{-4/3}$ x 10^3	1.59
Q	$cm.^3$ $sec.^{-1}$	0.209			
p_k	cm. H_2O	44.3			
R	ohms x 10^{-4}	30.0			

Stream Current

The quantity S_r was the residual galvanometer deflection, with no pressure across the pad. The two values shown are those measured before and after the measurement of S_s, the galvanometer deflection when liquid was being streamed through the pad at a steady pressure p. The average of the S_r values was used in calculating S_{obs}, the galvanometer deflection due to the stream current, from

$$S_{obs} = (S_s - S_r) = (7.80 - (-0.32)) = +8.12$$

The galvanometer deflection S_{obs} required correction for leak-back current through the pad. For this correction, the a.-c. resistance of the pad R and the known resistance of the external galvanometer circuit R_g were employed in equation 44, to give the stream current S as

$$S = S_{obs} \left(1 + \frac{R_g}{R}\right)$$

$$S = 8.12 \left(1 + \frac{412}{300,000}\right)$$

$$S = 8.12 \times 1.0014 = 8.13$$

It should be noted that a correction this small is usually ignored, as it lies within the experimental error in determining S_{obs}.

S was then transformed into microamps., using the galvanometer calibration obtained prior to the run by noting

the galvanometer deflection caused by a known current. In this case, a deflection of 31.00 cm. was caused by 1 microamp., so that the stream current I was 8.13/31.00 = 0.262 microamp.

The dimensions of the stream current function are

$$\frac{I\eta L}{pD} = \frac{(\epsilon^{1/2}\ m^{1/2}\ l^{3/2}\ t^{-2})\ (ml^{-1}\ t^{-1})\ (l)}{(ml^{-1}\ t^{-2})\ (\epsilon)}$$

i.e.

$$\frac{I\eta L}{pD} = \epsilon^{-1/2}\ m^{1/2}\ t^{-1}\ l^{5/2}$$

However, the dimensions of potential are $\epsilon^{-1/2}\ m^{1/2}\ t^{-1}\ l^{1/2}$, so that $I\eta L/pD$ is statvolts x $cm.^2$ in the c.g.s. system of units. In the present investigation, $I\eta L/pD$ values were more conveniently quoted in mv. $cm.^2$; however, the functions were first evaluated in c.g.s. units, then the transformation was made.

Thus, in calculating $I\eta L/pD$, the L, η and D values of Table III could be employed directly; however, it was necessary to change I to statamperes and p to dynes $cm.^{-2}$ as follows:

I = 0.262 microamp. = $0.262 \times 10^{-6} \times 2.9979 \times 10^{9}$ statamp

= 0.786×10^{3} statamperes.

p = 44.15 cm. H_2O = 44.15 x 981 dynes cm^{-2}.

= 4.34×10^{4} dynes $cm.^{-2}$

The stream current function was thus

$$\frac{I\eta L}{pD} = \frac{0.786 \times 10^{3} \times 0.834 \times 10^{-2} \times 5.715}{4.34 \times 10^{4} \times 76.75} = 1.127 \times 10^{-5}$$

Statamperes cm.^{2}.

or

$$\frac{I\eta L}{pD} = 1.127 \times 10^{-5} \times 299.79 \times 10^{3} = 3.38 \text{ mv. cm.}^{2}.$$

Permeability

The rate of flow through the pad Q was measured at a steady pressure p_k. These two quantities were combined with the viscosity η of Table III to give the pad permeability $\Phi_p = Q\eta/p_k$. The dimensions of Φ_p are

$$\frac{Q\eta}{p_k} = \frac{(l^3t^{-1})\ (ml^{-1}t^{-1})}{(ml^{-1}t^{-2})} = l^3$$

To obtain Φ_p in c.g.s. units as cm.^{3}, it was necessary to change p_k from cm. H_2O to dynes cm.$^{-2}$ as follows:

$$p_k = 44.3 \times 981 = 4.35 \times 10^{4} \text{ dynes cm.}^{-2}.$$

The Q and η values of Table III were in c.g.s. units, so that

$$\Phi_p = \frac{Q\eta}{p_k} = \frac{0.209 \times 0.834 \times 10^{-2}}{4.35 \times 10^{4}} \text{ cm.}^3$$

$$\Phi_p = 4.00 \times 10^{-8} \text{ cm.}^3$$

The permeability coefficient K was determined from

$$K = \frac{Q\eta}{p_k}\frac{L}{A} = \Phi_p\frac{L}{A} \text{ cm.}^2 \qquad \ldots \quad (42)$$

$$K = \frac{4.00 \times 5.715 \times 10^{-8}}{5.00} \text{ cm.}^2$$

$$K = 4.58 \times 10^{-8} \text{ cm.}^2.$$

The permeability function $(Kc^2)^{1/3}$ was then evaluated. The dimensions of this function are $\left(l^2 \ (ml^{-3})^2\right)^{1/3}$, i.e. $m^{2/3}l^{4/3}$. Combining K in cm.^{2}, and c in gm. cm.$^{-3}$, $(Kc^2)^{1/3}$ is therefore gm.$^{2/3}$ cm.$^{-4/3}$ in c.g.s. units. In the present case,

$$(Kc^2)^{1/3} = (4.58 \times 10^{-8} \times 0.296^2)^{1/3} \text{ gm.}^{2/3}\text{cm.}^{-4/3}$$

$$(Kc^2)^{1/3} = 1.59 \times 10^{-3} \text{ gm.}^{2/3} \text{ cm.}^{-4/3}$$

Electro-Osmotic Flow

The observed electro-osmotic flow rate first required correction for leak-back through the pad by equation 45 as follows:

$$F = F_{obs}\left(1 + \frac{\Phi_p}{\Phi_c}\right) = F_{obs}\ 1 + \left(\frac{4.00 \times 10^{-8}}{274 \times 10^{-8}}\right)$$

$$F = 5.37\ (1.0146) \times 10^{-3} = 5.45 \times 10^{-3} \text{ cm.}^3 \text{ sec.}^{-1}$$

The value of Φ_c in the above equation was obtained by the Poiseuille equation, and Φ_p from the permeability measurements previously described.

The dimensions of the electro-osmotic function are:

$$\frac{F\eta L}{ED} = \frac{(l^3t^{-1})\,(ml^{-1}t^{-1})\,(l)}{(\epsilon^{-1/2}\, m^{1/2} t^{-1} l^{1/2})\,\epsilon} = \epsilon^{-1/2}\, m^{1/2}\, t^{-1}\, l^{5/2}$$

This is the same as $I\eta L/pD$, and $F\eta L/ED$ is therefore statvolts cm.^{2} in c.g.s. units. In calculating $F\eta L/ED$, all the quantities of Table III are in the correct units except the applied voltage E, which must be changed to statvolts. i.e.

$$E = 92 \times 3.3335 \times 10^{-3} = 0.307 \text{ statvolts.}$$

The electro-osmotic function was thus

$$\frac{F\eta L}{ED} = \frac{5.45 \times 10^{-3} \times 0.834 \times 10^{-2} \times 5.715}{0.307 \times 76.75}$$

$$= 1.102 \times 10^{-5} \text{ statvolts cm.}^2$$

$$\frac{F\eta L}{ED} = 1.102 \times 10^{-5} \times 299.79 \times 10^{3} = 3.31 \text{ mv. cm.}^2.$$

RESULTS

Stream Current and Permeability Measurements in the Low-Compression Cell

Attention was first directed to the discrepancy between α_ζ and α_k, observed by Goring and Mason (20, 21, 8) in combined stream and permeability measurements on cylindrical pads of sulphite pulp and cotton over a range of pad concentrations. For both fibers, the specific volume α_ζ obtained from the stream current measurements using

$$\frac{I\eta L}{pD} = \frac{A\zeta}{8\pi}(1 - \alpha_\zeta c) \qquad \ldots \quad (40)$$

was 25-50% higher than the specific volume α_k obtained from the permeability measurements using the relation

$$(Kc^2)^{1/3} = \frac{1}{(5.55\,\sigma^2)^{1/3}}(1 - \alpha_k c) \qquad \ldots \quad (43)$$

Carroll and Mason (49, 50) have offered convincing evidence that the α_k values given by equation 43 are correct; Goring and Mason (8) explained the erroneously high α_ζ values given by equation 40 by postulating a model structure at the cellulose-water interface, which they termed the β-layer. No evidence was offered for the validity of the equation for pads of fibers, such as glass, obviously not possessing a β-layer at the fiber-liquid interface.

In the present investigation it was decided to repeat the measurements of Goring and Mason on cellulose, and also carry out stream current determinations of α_ζ for other fibrous materials. These included non-swelling glass and slightly-swelling nylon and acetate rayon; for these fibers, there was no evidence for the existence of a β-layer such as that postulated for the cellulose-water interface. Thus it might be expected that the α_ζ value obtained from stream current measurements on these fibers would be equal to the α_k value determined in concurrent permeability measurements.

Stream Current Results

The experimental results obtained in the stream current measurements with the low-compression cell appear in Figs. 6-11 as plots of the stream current function $I\eta L/pD$ versus the pad concentration c. Duplicate runs were carried out for glass, nylon, surgical cotton, viscose rayon, and sulphite pulp; for all these fibers except nylon, the electrolyte was either 10^{-4}M or 2×10^{-4} M KCl solution. With nylon, the ζ-potential in KCl solution was too small to be measured accurately; it was therefore necessary to use $ThCl_4$ solution as electrolyte, which gave a high positive charge on the fiber. Acetate rayon was measured in 10^{-4} M KCl and in 4×10^{-5} M $ThCl_4$; the sign of the charge on the fiber in these two electrolytes was respectively negative and positive.

It is seen that the curves were generally linear. In the duplicate runs, reproducibility varied from fair to good.

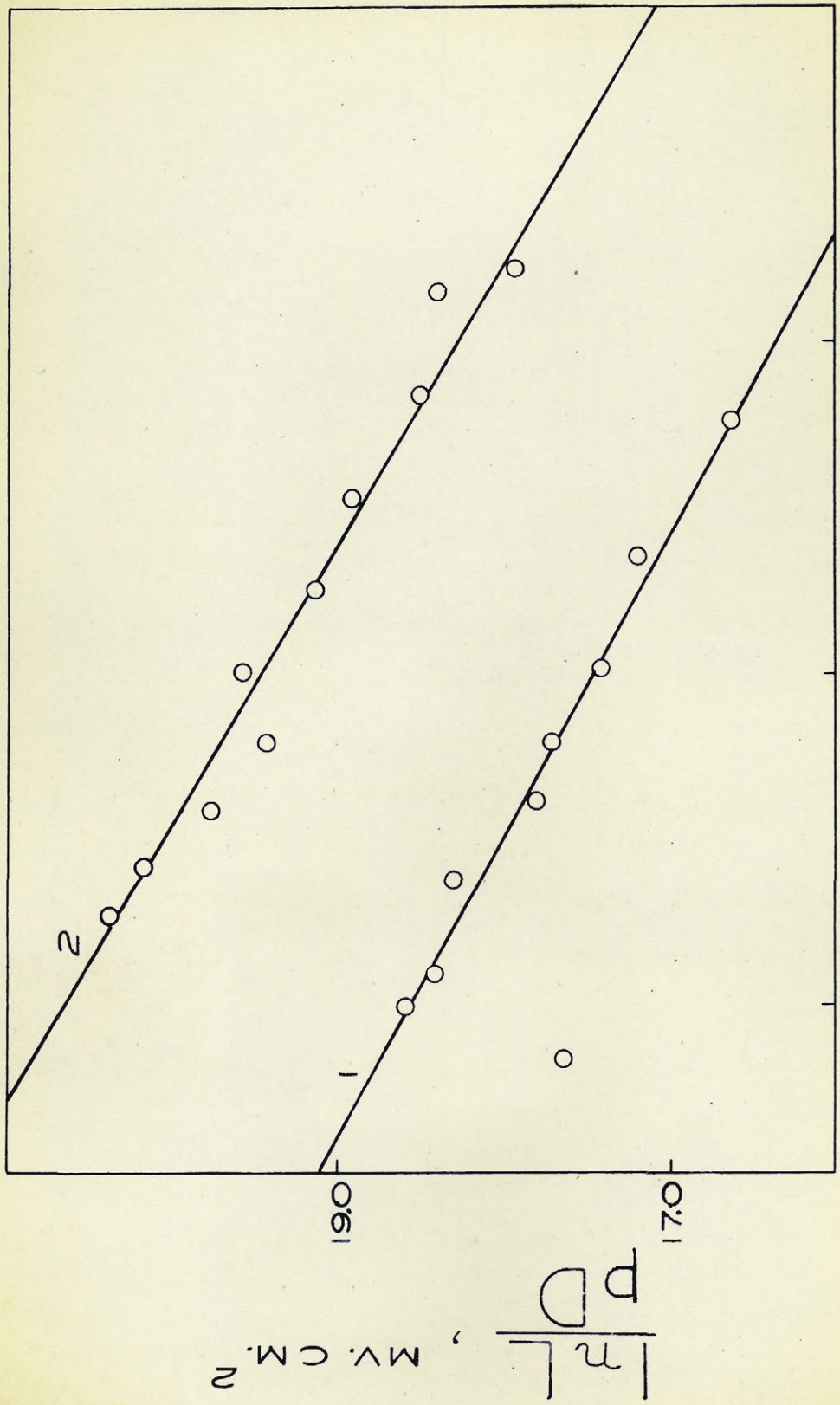

FIG. 6 $\eta L/pD$ versus c plots for pads 1 and 2

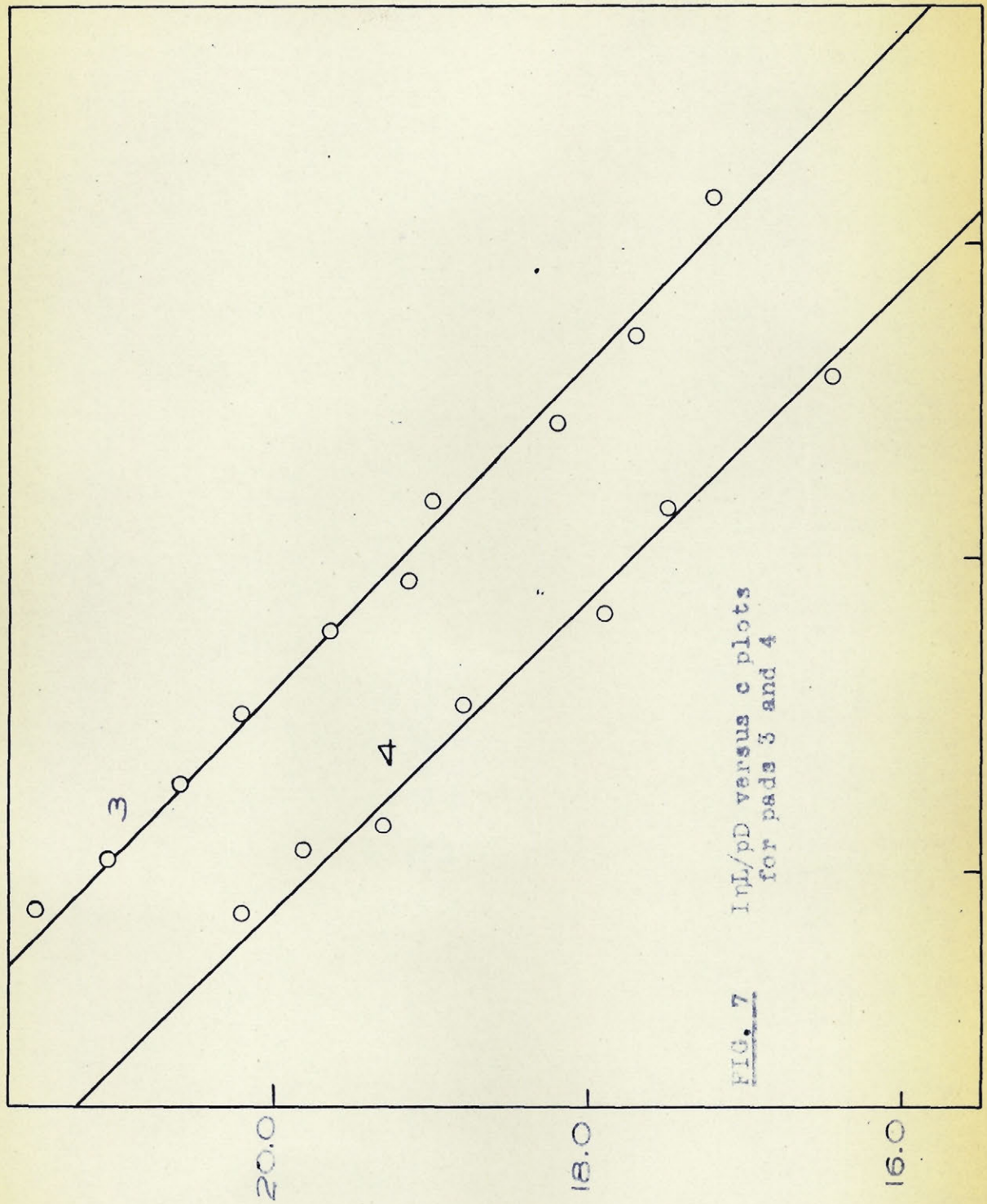

FIG. 7 $\ln L/pD$ versus c plots for pads 3 and 4

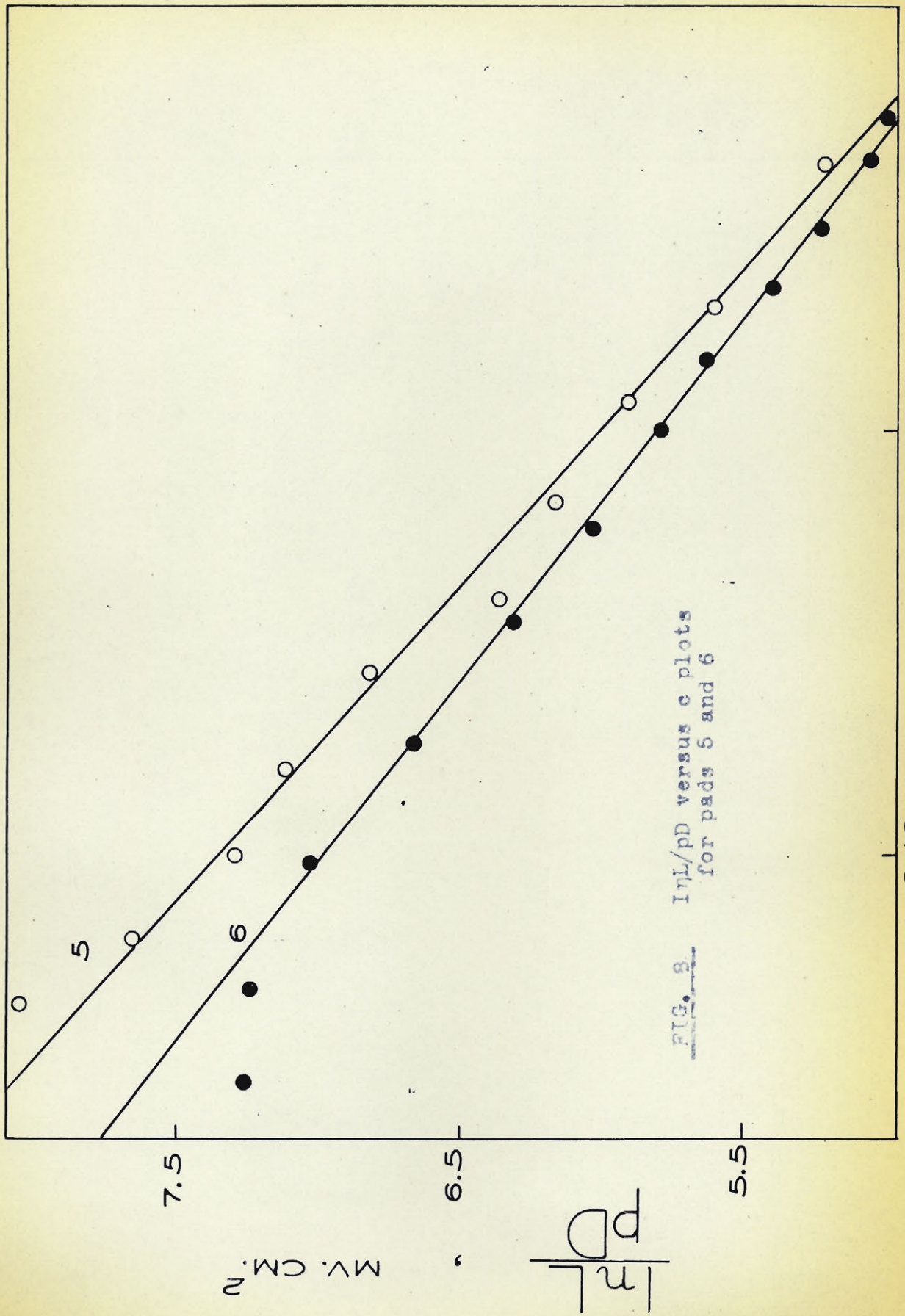

FIG. 8. $\eta L/pD$ versus c plots for pads 5 and 6

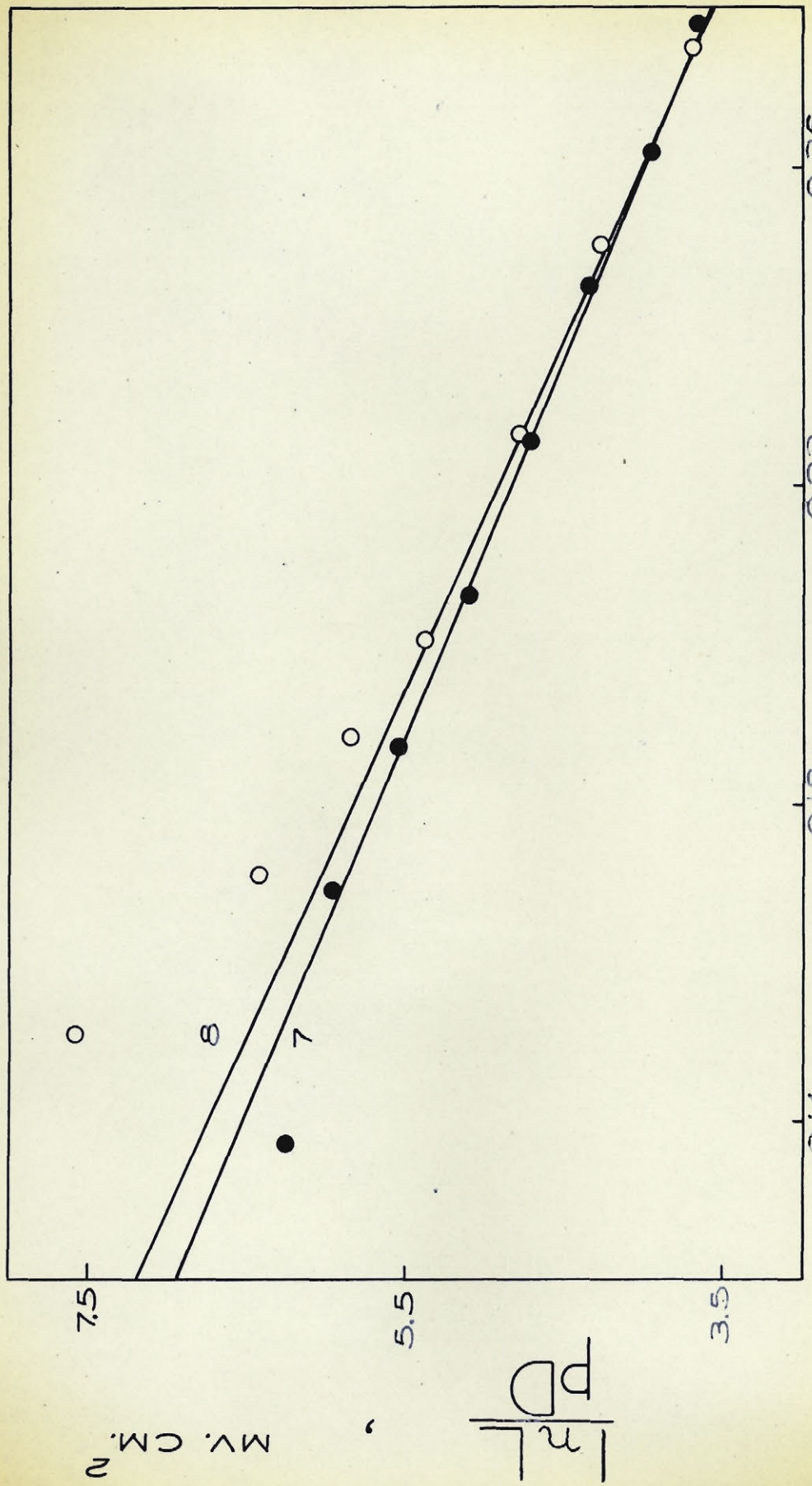

FIG. 9 $\ln L/pD$ versus c plots for pads 7 and 8

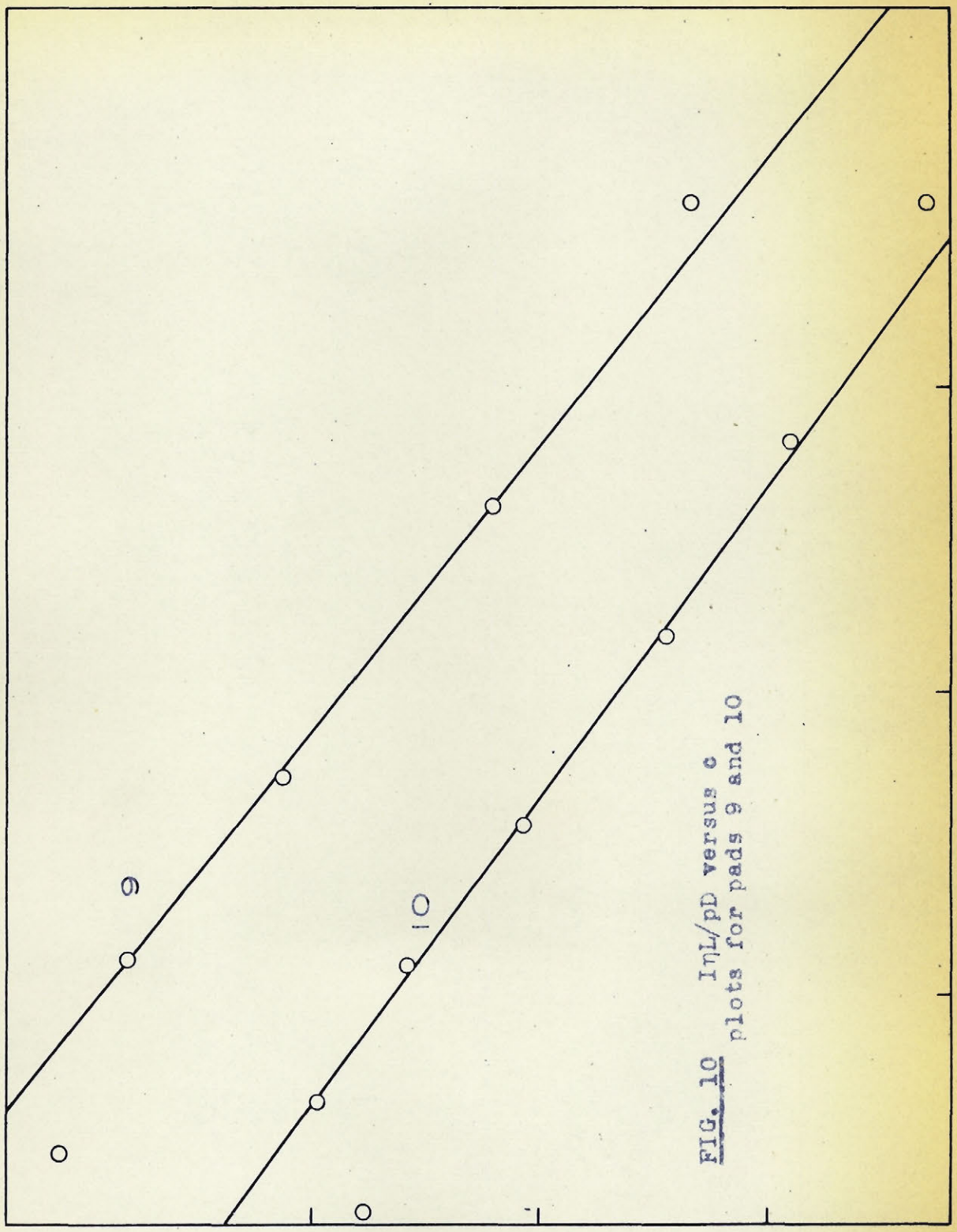

FIG. 10 $\eta L/pD$ versus c plots for pads 9 and 10

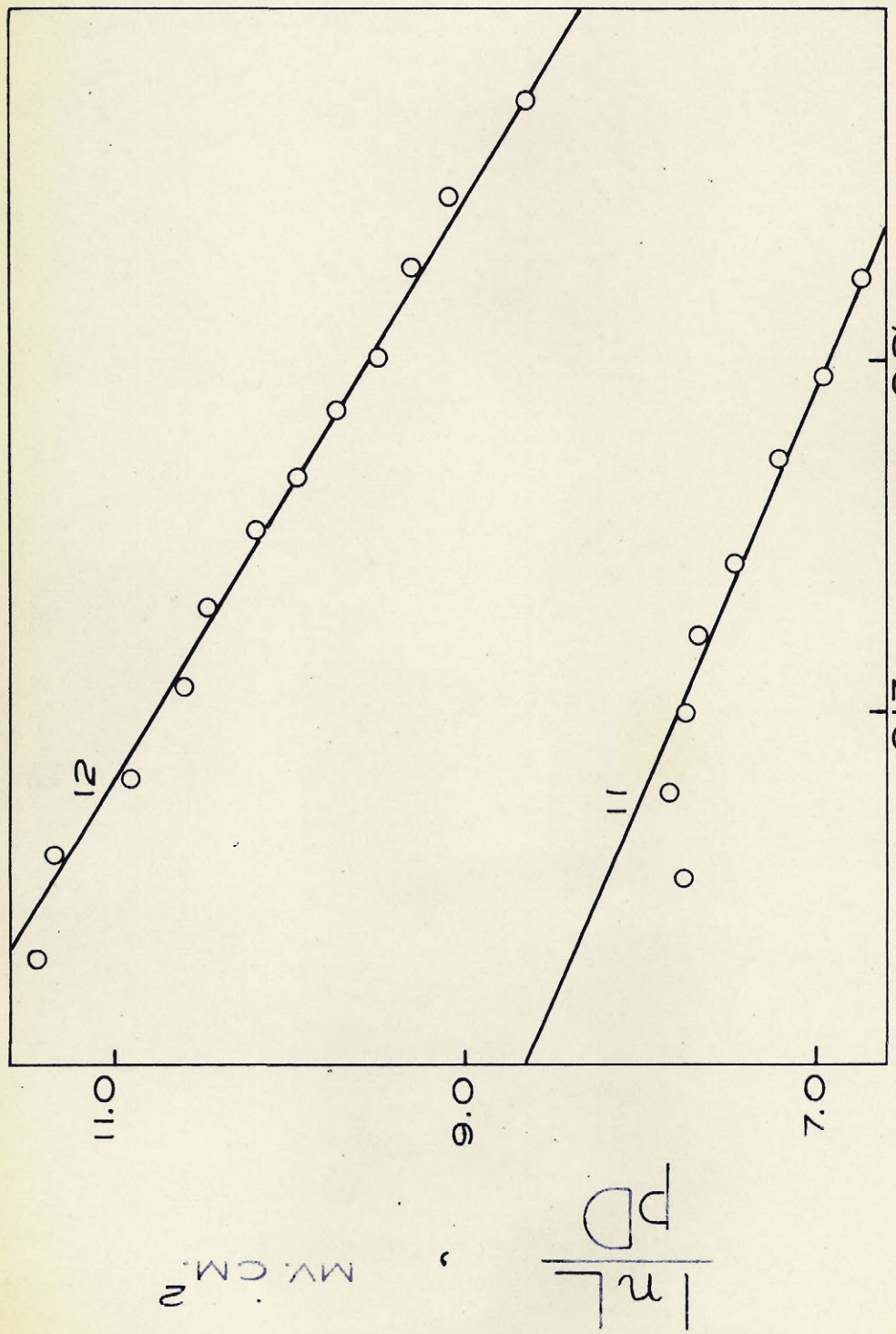

FIG. 11 $\ln L/pD$ versus c plots for pads 11 and 12

Random scatter was greatest for the fast-draining pads of nylon and glass wool, due to the ineffective system of pressure control used with the low-compression cell. With the other fibers the slow-draining properties of the pad helped to control the pressure, and much less random scatter occurred.

Significant deviations from linearity nearly always occurred at the lowest pad concentrations, the effect being most noticeable with the slow-draining pads. These deviations were due to an initial lack of sorption equilibrium between the pad and electrolyte, resulting from the inadequate de-aeration procedure used with the low-compression cell. Equilibrium was usually attained after electrolyte sufficient to measure permeability and stream current for one or two points had been streamed through the pad.

With the pads of sulphite pulp, deviations from linearity occurred at pad concentrations greater than 0.15 gm. $cm.^{-3}$, as previously observed by Goring and Mason (20, 21, 8). In their permeability measurements, Carroll and Mason (49, 50) observed that this effect generally occurred for pads of swollen fibers at a solid fraction $\alpha_k c > 0.5$, and attributed it to a de-swelling of the fiber wall under pressure.

The effect of the $ThCl_4$ solution on the flocculating properties of the acetate rayon was of particular interest. In comparison with the suspension of acetate rayon in 10^{-4} M KCl solution much larger flocs were formed, and sedimentation was more rapid. The sedimented fiber was fluffy in appearance

and had twice the volume of the same weight of fiber sedimented from 10^{-4} M KCl solution.

Table IV shows the values of ζ-potential and α_ζ, determined from the data of Figs. 6 - 11 by extrapolating the linear part of the curve to the co-ordinate axes of the graph. No α_k values appear in this table; the permeability method failed for all fibers except sulphite pulp. For the other fibers, the hand pressure employed for compressing pads in the low-compression cell was insufficient; the range of pad concentrations obtainable within the valid range of the Kozeny (27) permeability equation was too small for an accurate determination of α_k.

The data of Table IV show that the ζ-potential and α_ζ values for the duplicate runs agreed well. The observation of Goring and Mason (8) that α_ζ is unaffected by a reversal of the sign of the charge on the fiber was confirmed by the results obtained with acetate rayon.

Significance of Stream Current Results

As far as the discrepancy between α_ζ and α_k is concerned, the significance of the results of Table IV becomes clearer upon examination of Table V, which lists the average α_ζ value for each fiber, and α_k as obtained from permeability measurements on the same water-swollen fiber. For sulphite pulp, the α_ζ value was that determined in the low-compression cell, while for acetate rayon, nylon, viscose rayon, and sur-

TABLE IV

Stream Current Measurements on Pads of Miscellaneous Fibrous Materials in The Low-Compression Cell

Pad Number	Pad Material	Range of c (gm. cm.$^{-3}$)	Electrolyte	ζ (mv.)	a_ζ (cm.^{3} gm.$^{-1}$)
1	Glass wool,	0.134 - 0.211	1×10^{-4} M KCl	-110	1.23
2	2.5 micron dia.	0.151 - 0.229		-122	1.19
3	Nylon	0.202 - 0.286	3.3×10^{-5} M $ThCl_4$	+152	1.56
4		0.195 - 0.285		+156	1.70
5	Surgical cotton	0.139 - 0.257	2×10^{-4} M KCl	- 53.5	2.06
6		0.128 - 0.264		- 49.5	1.95
7	Viscose rayon	0.137 - 0.278	1×10^{-4} M KCl	- 46.5	2.23
8		0.151 - 0.275		- 48.5	2.28
9	Sulphite pulp	0.099 - 0.1620	1×10^{-4} M KCl	- 21.0	3.78
10		0.096 - 0.1620		- 18.2	3.96
11	Acetate rayon	0.151 - 0.219	1×10^{-4} M KCl	- 58.4	1.92
12		0.142 - 0.240	4×10^{-5} M $ThCl_4$	+ 80.0	1.91

gical cotton, the α_k was the average value obtained in subsequent permeability measurements in the high-compression cell. For glass, the value listed was the specific volume of the dry fiber.

Another significant physical quantity appears in Table V: the ratio R_o/R_{1000} is listed for each fiber. R_o is the d.-c. resistance of a pad of the fiber in 10^{-4} M KCl solution, and R_{1000} is the 1000 c.p.s. a.-c. resistance of the same pad. The ratio is taken as a rough measure of the magnitude of the resistance dispersion effect, first observed by Goring and Mason (8) for a pad of sulphite pulp. The R_o/R_{1000} values listed were obtained from Appendix A; this appendix consists of exploratory investigations of the resistance dispersion effect.

The experimental data of Table V show clearly that the discrepancy between α_ζ and α_k was general. For all fibers investigated the α_ζ values were considerably higher than α_k, $(\alpha_\zeta - \alpha_k) = \Delta\alpha$ ranging from 0.65 with nylon to 1.30 with sulphite pulp. The average value of $\Delta\alpha$ was 0.95.

Goring and Mason (8) indicated that the low frequency resistance dispersion effect, observed in impedance measurements on a pad of sulphite pulp, might be accounted for on the basis of the β-layer. This suggested that the dispersion effect and a discrepancy between α_ζ and α_k may occur together; however, the data of Table V show no significant relationship between R_o/R_{1000} and $\Delta\alpha$. Acetate rayon and viscose rayon had similar $\Delta\alpha$ values,

TABLE V

Average α_ζ Values Obtained in Stream Current Measurements with The Low-Compression Cell on Pads of a Number of Different Fibrous Materials

(Reference α_k values and the ratio R_o/R_{1000} in 10^{-4} M KCl are included for each fiber)

Fibrous Material	Average α_ζ $cm.^3gm.^{-1}$	Average α_k $cm.^3gm.^{-1}$	$\Delta\alpha$ $(\alpha_\zeta - \alpha_k)$ $cm.^3gm.^{-1}$	R_o/R_{1000}
Nylon	1.63	0.98	0.65	1.03
Acetate rayon	1.92	0.95	0.97	1.03
Surgical cotton	2.00	1.09	0.91	1.06
Glass wool, 2.5 micron dia.	1.21	0.40(a)	0.81	1.07
Viscose rayon	2.26	1.27	0.99	1.23
Sulphite pulp	3.87	2.57	1.30	1.26
Mean value	....	....	0.95	....

(a) specific volume

yet the highly swelling viscose rayon exhibited the resistance dispersion effect, while acetate rayon did not. Sulphite pulp, which exhibited a marked dispersion effect, showed the greatest value of $\Delta\alpha$. However, this may have been fortuitous; the $\Delta\alpha$ value for nylon showed a deviation of similar magnitude below the average $\Delta\alpha$ value of 0.95.

It was thus clear that the β-layer hypothesis of Goring and Mason (8) failed to account for the general discrepancy shown between α_ζ and α_k for non-swelling, slightly-

swelling and highly-swelling fibers, whether the dispersion effect was exhibited or not. However, in view of the faulty experimental techniques employed in measurements with the low-compression cell, the constancy of $\Delta\alpha$ was striking, and suggested that there was a general functional relationship between $I\eta L/pD$ and the pad concentration.

Effects at The Ends of The Pad

Effect of The Mesh

As the next step in the investigation it was decided to extend the measurements over a greater range of pad concentrations. This would increase the accuracy in the determination of α_ζ, and permit permeability determinations of α_k for most of the fibers. Accordingly, the high-compression cell was constructed, designed so that the pad could be compressed by tightening wing nuts against brass plates at the ends of the electrodes; this more than doubled the range of pad concentrations obtainable for the stream current and permeability measurements.

However, initial measurements with the high-compression cell disclosed a new source of error; at the higher pad concentrations the plastic mesh at the ends of the pad were compressed, and the pad pushed partly through the mesh. This made the mesh thickness, used as a correction in determining the true pad length, an extremely uncertain quantity. The error was greatest at the high pad compressions which the new cell had been designed

to attain.

The mesh was considered essential in avoiding decay, the decrease of permeability and stream current occurring with prolonged flow of solution through a pad (7, 20, 49). An alternative means of separating the ends of the pad from the electrodes was therefore sought, which would resist distortion at the higher pad compressions. In attempting to design such a mesh substitute, the question arose as to the validity of the experimental procedure with the low-compression cell, in which the electrical resistance of the mesh space was ignored.

In order to check this point, stream current and 1000 c.p.s. a.-c. resistance R_{1000} were measured on a fully expanded pad of surgical cotton in 2 x 10^{-4} M KCl solution, one electrode being drawn back about 10 cm. from the end of the pad. The electrode was then moved towards the pad in steps, and finally brought in contact with the mesh at the end of the pad. At each step, stream current and R_{1000} were measured. The electrical resistance $\triangle R_i$ of the space separating the pad and the electrode was calculated for each step by subtraction of the pad resistance with only the mesh separating the electrodes from the pad, obtained in the final measurement. The stream current measurements were then continued, different values of electrical resistance $\triangle R_e$ being inserted in series with the galvanometer circuit.

It can be seen from Fig. 12, in which $I\eta/pD$ is plotted against the added resistance $\triangle R$, that the effect was the same

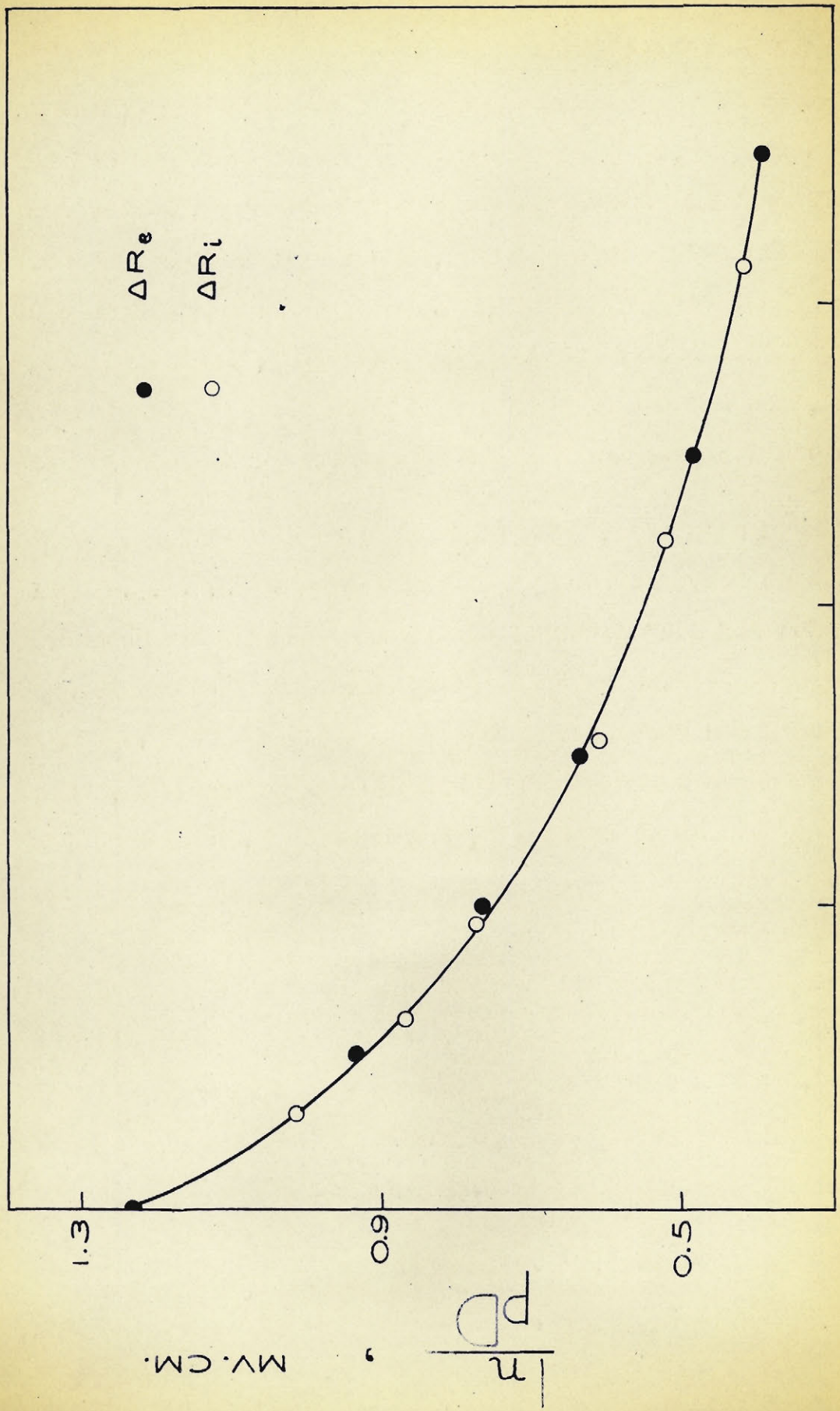

Fig. 12 Effect of added resistance on the stream current

for $\triangle R_i$ and $\triangle R_e$. This meant that any electrical resistance between the electrode face and the end of the pad should be considered as an external resistance in series with the galvanometer when the stream current was corrected for leak-back according to equation 44.

The resistance of the mesh space in 10^{-4} M KCl solution, determined by direct measurement of the mesh held between the electrodes, was about 5000 ohms. The average pad resistance in this electrolyte was about 50,000 ohms; thus a correction to the observed stream current of about 10% had been overlooked in previous measurements.

It can be seen that such a large correction to the observed stream current would be a serious source of error, even if a mesh could be designed such that the mesh space would remain constant over a wide range of pad concentrations. The resistance of the mesh space would be temperature dependent, necessitating an indirect calculation from the mesh space cell constant and the specific conductivity of the electrolyte. The measured pad resistance would require correction for the mesh space resistance, and an accurate evaluation of both quantities would be essential to a determination of the true stream current.

On the other hand, if the mesh could be abandoned, the simple procedure of the earlier stream current measurements could be resumed, in which the leak-back current had been determined from the measured (uncorrected) pad resistance, and the

known resistance of the galvanometer circuit. It was therefore decided to carry out tests for decay on a pad without mesh, to see whether the error from this source was greater than that which would result from the uncertain mesh space corrections.

Decay

Measurements were therefore carried out on a pad of acetate rayon in 2 x 10^{-4} M KCl solution, with the electrodes in direct contact with the pad. Upon streaming as much as 2 1/2 litres of electrolyte through the pad, no decay of stream current or permeability occurred. From this result it was decided to omit the mesh provisionally in measurements with the high-compression cell, meanwhile carrying out tests for decay on pads of each fibrous material.

The results obtained in these tests are listed in Table VI, which shows $I\eta L/pD$, and then a repeat determination after a few hundred ml. of solution had been streamed through the pad. Bearing in mind that 100 ml. of solution are sufficient to measure both stream current and permeability at each pad concentration, it is clear that no appreciable decay occurred.

No decay tests were carried out with Dacron pads. However, four different permeability runs, carried out on the same re-expanded pad over the period of a week, gave the same result within experimental error. It could be assumed from this that no decay of stream current had occurred, as

TABLE VI

Tests for Decay of Stream Current on Flow of Electrolyte through A Pad without Mesh, Carried out in The High-Compression Cell

Pad Number	Pad Material	c (gm. $cm.^{-3}$)	Volume of Liquid Streamed (ml.)	$I\eta L/pD$ mv. $cm.^2$ (before)	$I\eta L/pD$ mv. $cm.^2$ (after)
14	Acetate Rayon	0.193	250	11.90	11.90
		0.302	250	8.00	8.10
		0.437	250	4.95	5.00
22	Surgical Cotton	0.391	250	2.06	2.07
21	Nylon	0.247	400	12.10	11.95
		0.369	400	8.25	8.25
23	Viscose Rayon	0.351	400	2.99	2.93

any significant decay of stream current is always accompanied by a decay of the permeability.(20).

Stream Current and Permeability Measurements in The High-Compression Cell

With the high-compression cell, stream current and permeability runs were carried out on pads of acetate rayon, Dacron, nylon, surgical cotton, and viscose rayon. For acetate rayon and Dacron, the measurements were made at a number of different concentrations of electrolyte. Measurements failed with the 2.5 micron dia. glass which fractured under compression and was washed from the pad as a fine powder.

Stream Current Results

The results obtained in the stream current measurements with the high-compression cell appear in Figs. 13 - 15 as graphical plots of $I\eta L/pD$ versus c. It is seen that the random scatter was much less than that occurring with the low-compression cell, due to the improved pressure control system.

Deviations at the lower pad concentrations, which were noticeable with the low-compression cell, were completely eliminated by the experimental methods employed with the high-compression cell, in which sorption equilibrium between pad and electrolyte was ensured before measurements were commenced.

The extended range of pad concentrations obtainable with the high-compression cell showed that the $I\eta L/pD$ versus c plot, previously regarded as linear, was in reality a curve. A rough numerical indication of the extent of the curvature was obtained by drawing tangents to the curve over the upper and lower concentration ranges, and extrapolating to the concentration co-ordinate axis. The α_ζ values thus obtained, and the range of pad concentration covered in measurements on the pad, appear in Table VII, which includes the average α_ζ values obtained for pads of the same fiber with the low-compression cell, and the average pad concentration range covered in these measurements.

An examination of the experimental data of Table VII explains the high α_ζ values obtained with the low-compression cell. The entire pad concentration range obtainable with this

TABLE VII

Stream Current and Permeability Measurements with The High-Compression Cell Compared to The Stream Current Results Obtained with The Low-Compression Cell

High-Compression Cell							Low-Compression Cell	
			Permeability		Stream Current		Stream Current	
Pad Number	Pad Material	Electrolyte Molarity	α_k $cm.^3 gm.^{-1}$	σ $cm.^2 gm.^{-1}$	Concentration Range $gm.\ cm.^{-3}$	α_ζ Range $cm.^3 gm.^{-1}$	Average Concentration Range $gm.\ cm.^{-3}$	Average α_ζ Value $cm.^3 gm.^{-1}$
13	Acetate rayon	2×10^{-5} KCl	1.00	2360	0.145 - 0.428	2.14 - 1.37	0.140 - 0.230	1.92
14		2×10^{-4} KCl	0.95	2460	0.193 - 0.437	1.95 - 1.45		
15		10^{-3} KCl	0.93	2400	0.184 - 0.415	1.91 - 1.51		
16		10^{-2} KCl	0.97	2500	0.193 - 0.434	1.91 - 1.46		
17	Dacron	2×10^{-5} KCl	0.74	2860	0.203 - 0.405	1.61 - 1.38	...	...
18		2×10^{-4} KCl	0.79	2780	0.209 - 0.417	1.62 - 1.41		
19		10^{-3} KCl	0.74	2860	0.168 - 0.418	1.53 - 1.28		
20		2×10^{-3} KCl	0.75	2860	0.184 - 0.405	1.66 - 1.34		
21	Nylon	3×10^{-5} $ThCl_4$	0.98	2030	0.219 - 0.435	1.80 - 1.44	0.195 - 0.285	1.63
22	Surgical cotton	2×10^{-4} KCl	1.08	4500	0.145 - 0.450	2.07 - 1.64	0.135 - 0.260	2.00
23	Viscose rayon	2×10^{-4} KCl	1.27	2580	0.158 - 0.429	2.22 - 1.72	0.140 - 0.280	2.26

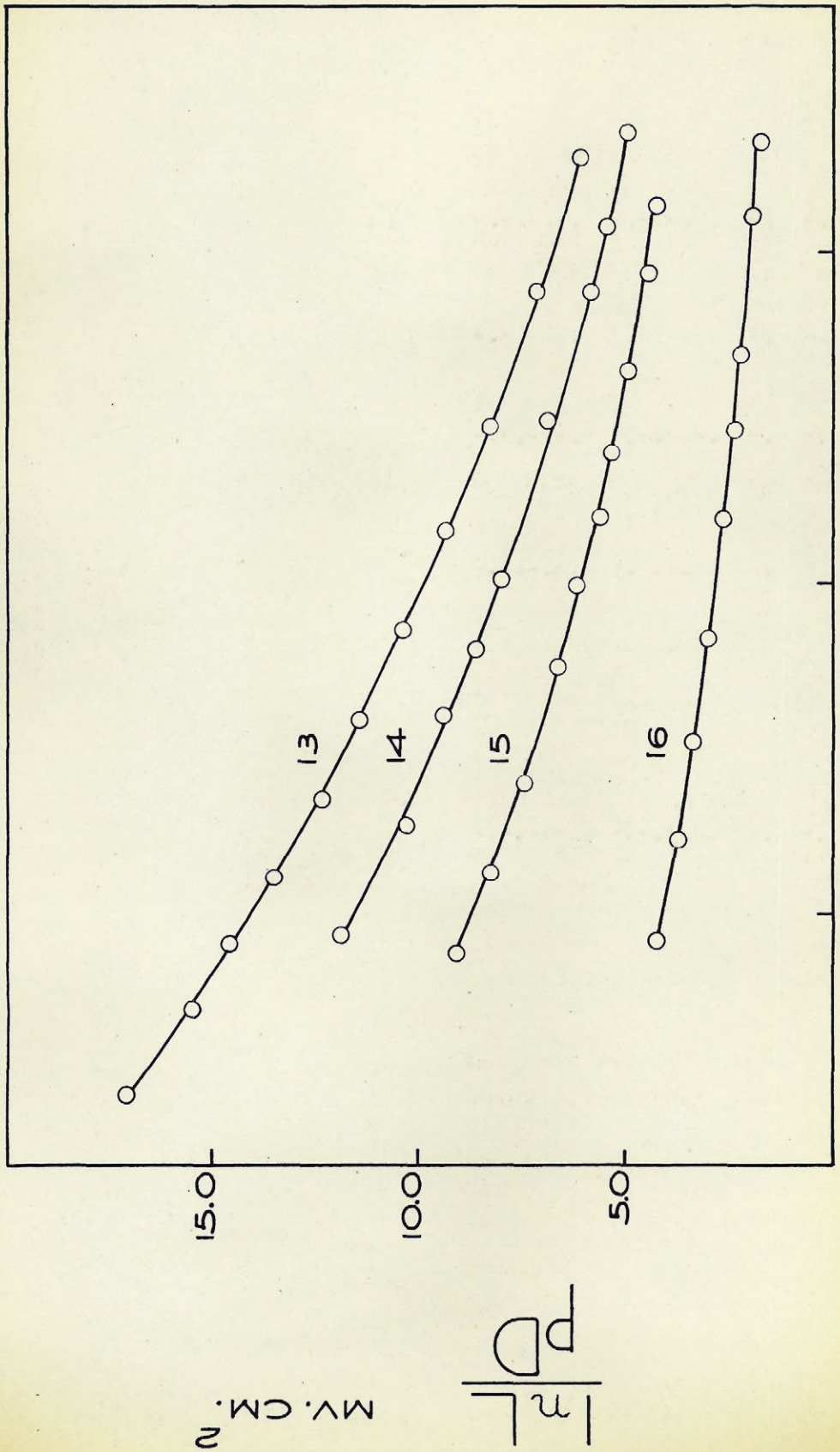

FIG. 13 ln L/pD versus c plots for pads 13, 14, 15 and 16.

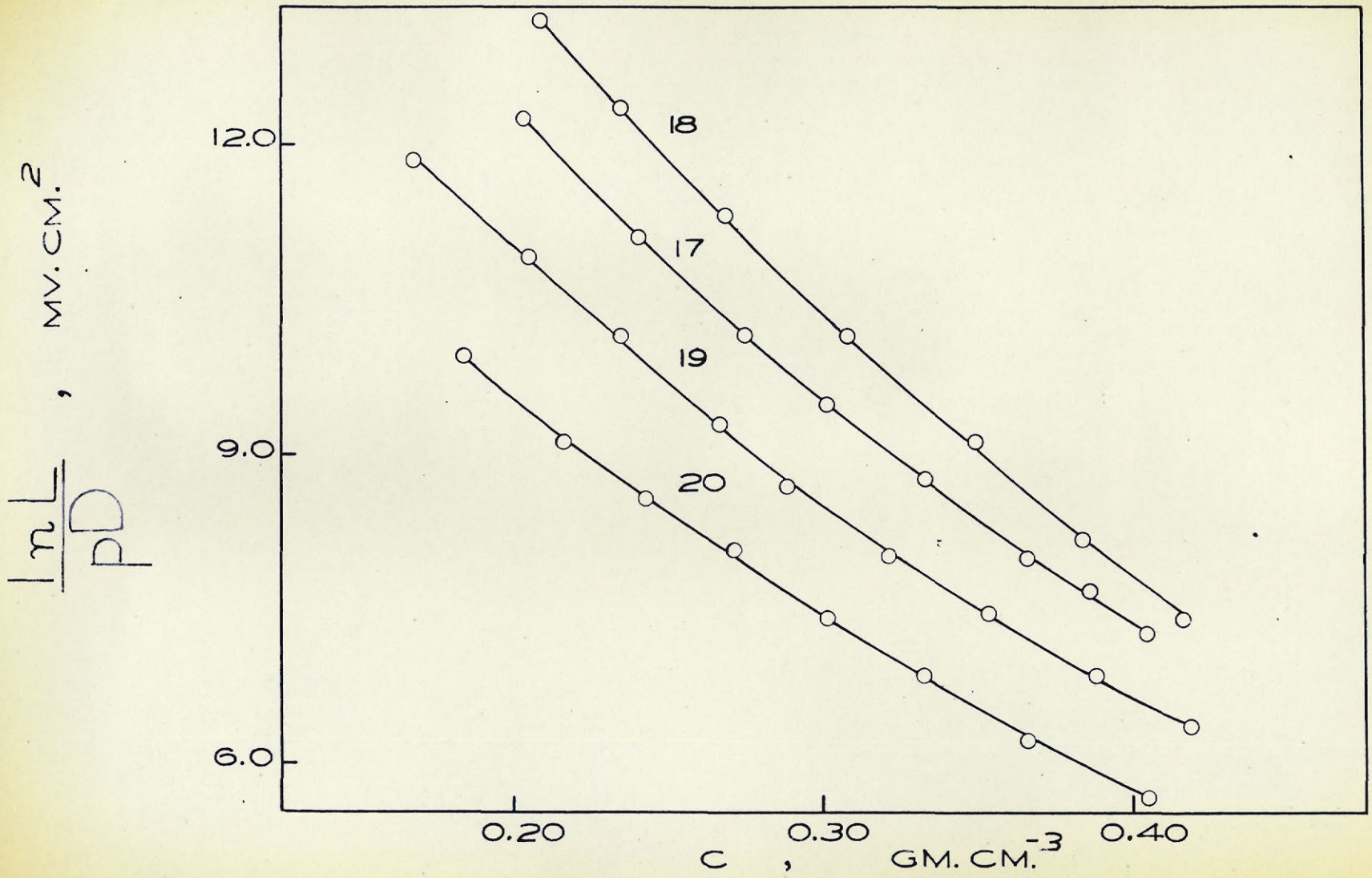

FIG. 14 IηL/pD versus c plots for pads 17, 18, 19, and 20.

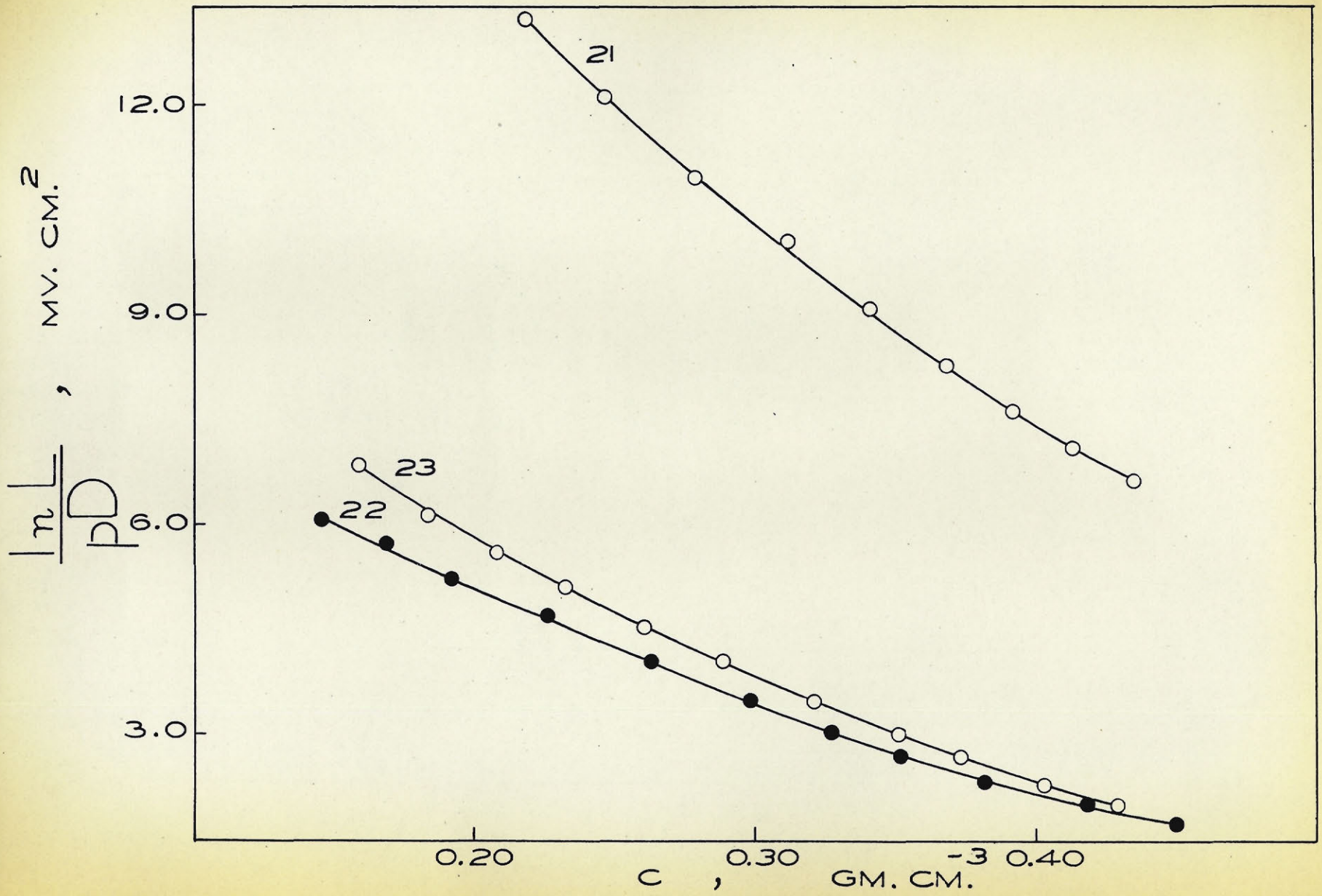

FIG. 15 IηL/pD versus c plots for pads 21, 22, and 23.

apparatus corresponded roughly to the lower concentration range in which the tangent was drawn to the stream current curve obtained with the high-compression cell. The average α_ζ value obtained with the low-compression cell was therefore equivalent to the low concentration α_ζ of the high-compression cell, both α_ζ values deriving from tangents to the curve in the same concentration range. Table VII shows good agreement between these two sets of α_ζ values.

Permeability Results

In contrast to the low-compression apparatus, with which α_k and σ could only be determined from the flow measurements on sulphite pulp, the range of pad concentrations obtainable in the high-compression cell was sufficient for determination of these values for each of the fibrous materials investigated. Flow measurements were carried out during each stream current run, and α_k and σ were determined from the permeability equation 43 of Robertson and Mason (26). These data appear in Table VII.

As an indication of the accuracy of the permeability method, sample plots of $(Kc^2)^{1/3}$ versus c are shown in Figs. 16 - 17 for each of the fibrous materials of Table VII. With the exception of nylon, which was in contact with 3×10^{-5} M $ThCl_4$ solution, the electrolyte was 2×10^{-4} M KCl. It is seen that the linearity of the curves is in general excellent; the deviations from linearity shown for Dacron and nylon at the lower pad concentrations are typical of the method (26, 49, 50).

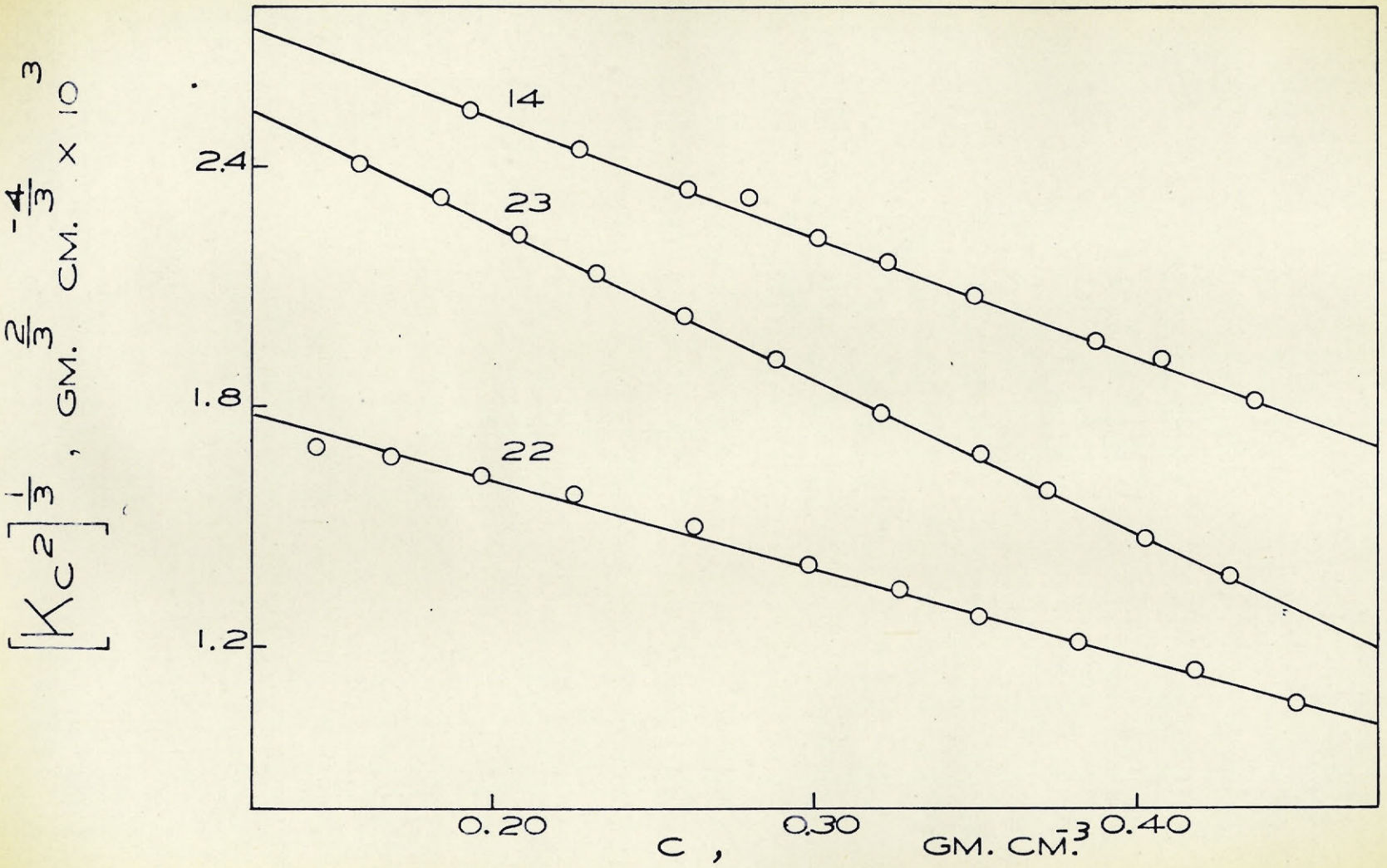

FIG. 16. Permeability plots for pads 14, 22, and 23.

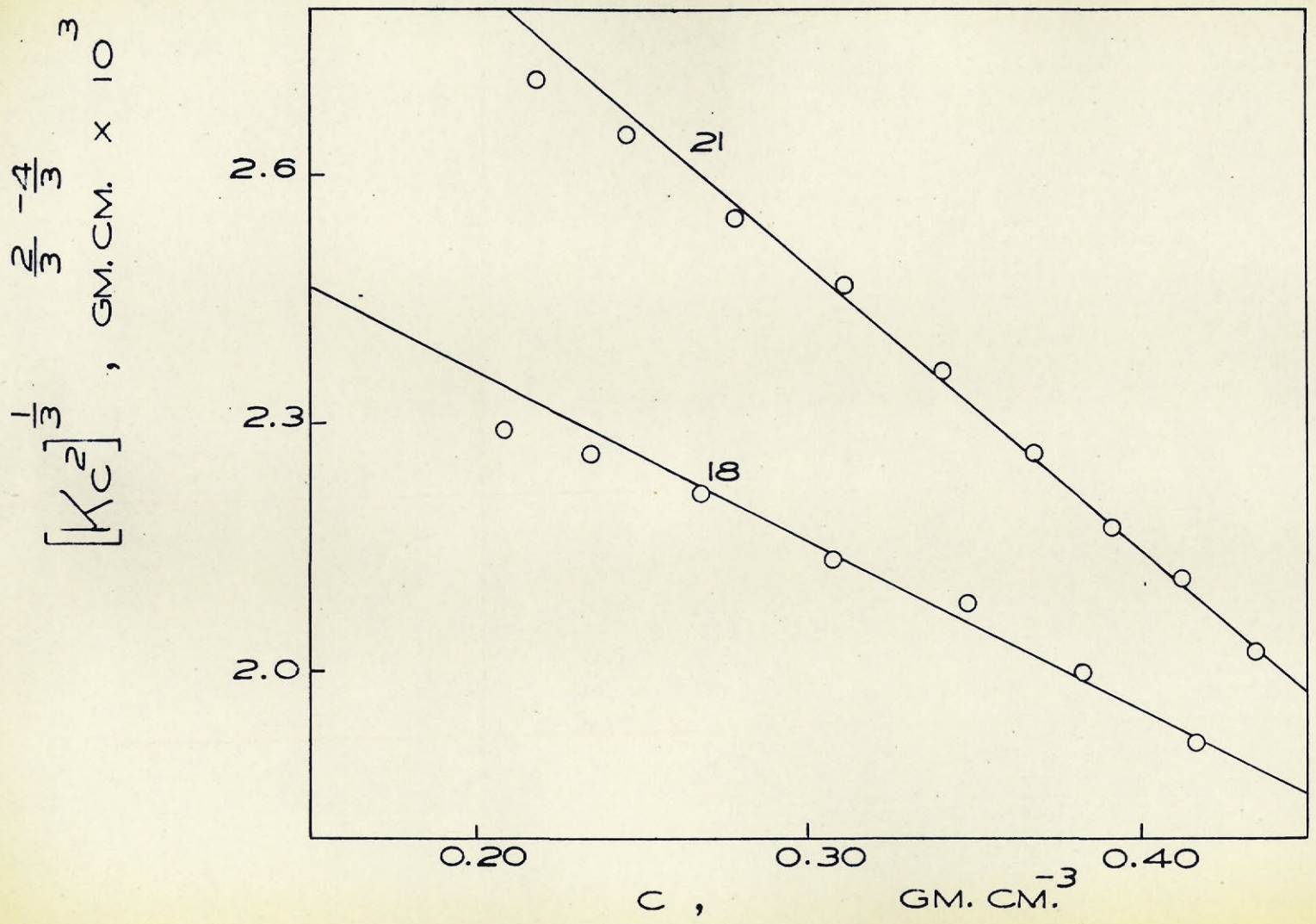

FIG. 17 Permeability plots for pads 18 and 21

The α_k and σ values obtained from the permeability measurements in the high-compression cell agreed well with those obtained by Carroll and Mason (49, 50) for the same fibers, using a similar apparatus and technique. These values are listed in the discussion section of the present work, for purposes of comparison.

Significance of Stream Current Results

The discrepancy between α_ζ and α_k, clearly shown in the results of Table VII, could now be accounted for; there was evidently some defect in the Goring-Mason stream current equation

$$\frac{I\eta L}{pD} = \frac{A\zeta}{8\pi}(1 - \alpha_\zeta c) \qquad \ldots \quad (40)$$

The linear relationship between $I\eta L/pD$ and c predicted by this equation was in every case contradicted by the experimental evidence. Thus the α_ζ values quoted in earlier work (20, 21, 8) were without theoretical significance, and the extent of their discrepancy from α_k was equally without significance.

Attention was henceforth directed towards ascertaining the theoretical significance of the $I\eta L/pD$ versus c curves of Figs. 13 - 15. It was suggested previously that there might be a general functional relationship between $I\eta L/pD$ and the pad solid fraction $\alpha_k c$; if the existence of such a relationship is assumed, the following consequences ensue:

1) $\frac{I\eta L}{pD} = k_1 \zeta f(\alpha_k c)$ where k_1 = constant

2) $\left(\frac{I\eta L}{pD}\right)_{\alpha_k c = 0.25} = k_2 \zeta$ where k_2 = constant

3) $\frac{I\eta L}{pD} \Big/ \left(\frac{I\eta L}{pD}\right)_{\alpha_k c = 0.25} = k_3 f(\alpha_k c)$

where $k_3 = k_1/k_2$ = constant.

The quantity ζ is thus eliminated; if $f(\alpha_k c)$ were the same for pads of all fibers, the graphical plot of $\frac{I\eta L}{pD} \Big/ \left(\frac{I\eta L}{pD}\right)_{\alpha_k c = 0.25}$ versus $\alpha_k c$ would give the same curve in every case.

In Fig. 18 this plot is made for pads of each of the fibers investigated with the high-compression cell. A result obtained with the low-compression cell, sulphite pulp pad 10 in 10^{-4} M KCl solution, is also included, as no stream current measurements of the fiber were carried out in the high-compression cell. With the exception of the sulphite pulp and nylon, which was measured in 3 x 10^{-5} M $ThCl_4$, the pads of Fig. 18 were in contact with 2 x 10^{-4} M KCl solution.

It is seen that the curves coincide, showing that the same functional relationship exists between $I\eta L/pD$ and the pad solid fraction for pads of all the fibrous materials investigated.

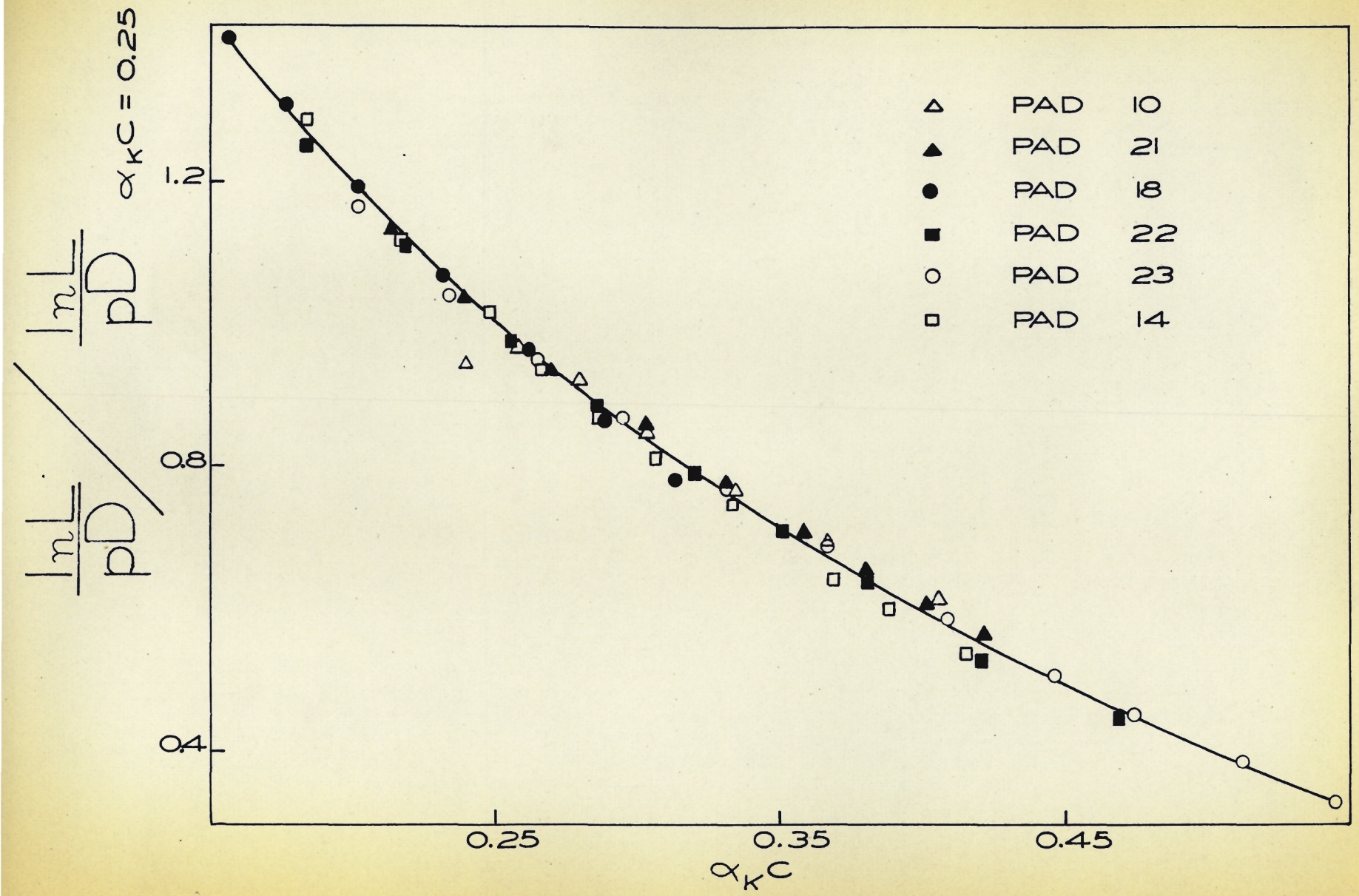

FIG. 18 $\frac{\ln L}{pD} \Big/ \frac{\ln L}{pD}$ versus $\alpha_k c$ plots $\alpha_k c = 0.25$ for pads 10, 14, 18, 21, 22, and 23.

In Fig. 19 the same graphical plot is carried out for the four pads of acetate rayon measured in the high-compression cell at different electrolytic concentrations. The curves for all the pads coincide, though the thickness δ of the equivalent Helmholtz double layer varied from 30Å with the 10^{-2} M KCl to 680Å with the 2×10^{-5} M KCl solution. From this result, the general curve shown in Figs. 18 - 19 cannot be explained by a "wall curvature" effect; it must be concluded that δ is negligible compared to the mean pore radius for all electrolytic concentrations investigated, as previously observed by Goring and Mason (8).

There is further support for this conclusion in the data of Table VIII, in which the mean pore radius $\bar{r}$ was calculated after Goring and Mason (8) by the simplified form of the Kozeny (27) equation

$$\bar{r} = \frac{2\,(1 - \alpha_k c)}{\sigma c} \qquad \ldots \quad (47)$$

The values of α_k and σ used to calculate $\bar{r}$ at a pad concentration of 0.40 gm. cm.$^{-3}$ were the average values obtained in the permeability measurements. This concentration is near the upper limit of pad concentrations obtainable for acetate rayon pads in the high-compression cell, thus the $\bar{r}$ value of Table VIII is near the lower limit for pads of acetate rayon. The thickness of the equivalent Helmholtz electrical double layer δ was calculated from equation 9.

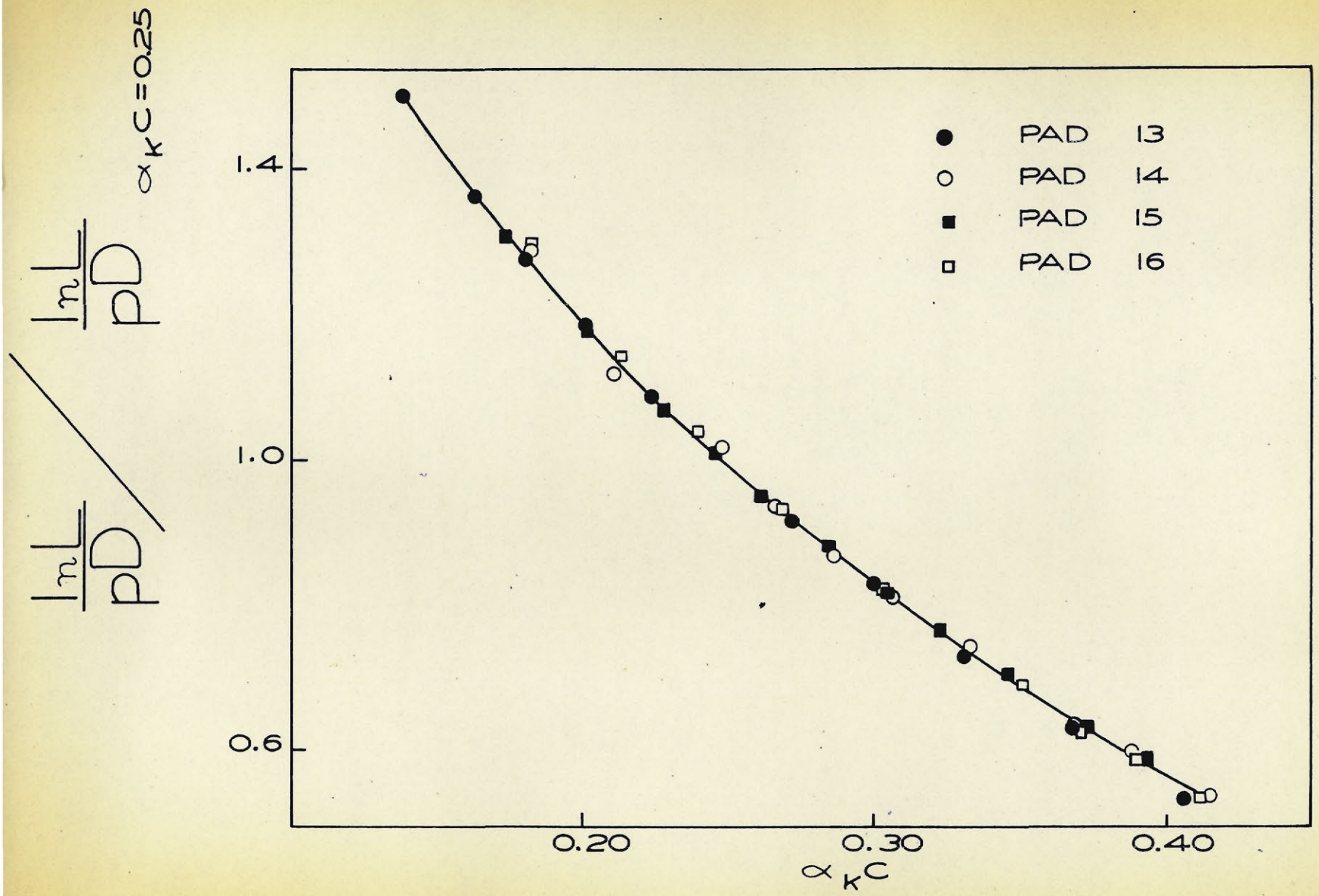

FIG. 19 $\frac{\ln L}{pD} \Big/ \frac{\ln L}{pD}_{\alpha_k c = 0.25}$ versus $\alpha_k c$ plots for pads 13, 14, 15, and 16.

TABLE VIII

Approximate Thickness of The Electrical Double Layer δ Compared to The Mean Pore Radius $\bar{r}$ at c = 0.40 gm. $cm.^{-3}$ for Acetate Rayon in The KCl Solutions Measured in The High-Compression Cell

Permeant	δ (Å)	$\bar{r}_{0.40}/\delta$
2×10^{-5} M KCl	680	190
2×10^{-4} M KCl	220	590
10^{-3} M KCl	100	1290
10^{-2} M KCl	30	4300

From the foregoing experimental evidence it was clear that there was a general functional relationship between $I\eta L/pD$ and the solid fraction $\alpha_k c$ for all the fibrous materials investigated, independent of the swelling properties of the fiber, the occurrence of the low-frequency resistance dispersion effect, or the thickness of the equivalent Helmholtz electrical double layer.

However, the precise nature of this functional relationship remained obscure; further investigations into the theoretical significance of the stream current data were carried out, which are more conveniently described in the general discussion of results.

Electro-Osmotic Flow Measurements

Attention was next directed to the second main subject of the investigation, the discrepancy between ζ_E as calculated from electro-osmotic measurements and ζ_s as calculated from stream measurements on the same cylindrical pad of cellulose, observed by Goring and Mason (20, 21) and Kanamaru (42).

Effect of Bubble Length

Goring and Mason reported that the observed electro-osmotic flow rate F_{obs} was a function of the length of the air bubble used in the capillary flow-meter, maximum F_{obs} being obtained with a bubble length slightly greater than the internal diameter of the capillary. F_{obs} decreased with bubble lengths greater or smaller than this optimum value.

In the present investigation this observation was confirmed in measurements of F_{obs} on a loosely packed pad of 2.5 micron dia. glass fibers in which bubble lengths from 2.2 to 4.5 mm. were employed. The data of Table IX show that maximum F_{obs} occurred at a bubble length of 3 mm. This was slightly greater than the internal diameter of the capillary, which is 2.46 mm. Unless otherwise specified, a bubble length of 3 mm. was used in subsequent measurements of electro-osmotic flow rate.

Measurements of permeability and stream current were also carried out and Table IX lists the electrokinetic functions $F\eta L/ED$ and $I\eta L/pD$ for every bubble length. In calculating

TABLE IX

Stream Current, Electro-Osmotic Flow, and Permeability Measurements on Pad 24, 2.5 micron dia. Glass Fibers in 2×10^{-5} M KCl Solution

Bubble Length mm.	Φ_p $cm.^3 \times 10^8$	Poiseuille Leak-back Correction Factor	F_{obs} $cm.^3\ sec.^{-1} \times 10^3$	$F\eta L/ED$ mv. $cm.^2$	$I\eta L/pD$ mv. $cm.^2$	ζ_E/ζ_s
2.2	26.5	1.096	3.90	10.60	14.90	0.71
2.5	26.5	1.096	4.98	13.60	14.95	0.91
3.0	26.5	1.096	5.10	13.80	15.05	0.915
3.5	26.5	1.096	4.95	13.50	15.00	0.90
4.5	26.5	1.096	4.76	13.00	14.95	0.87

$F\eta L/ED$, the Poiseuile equation 46 was used to evaluate the capillary permeability $\Phi_c = \pi R_c^4/8\ l_c = 274 \times 10^{-8}\ cm.^3$ in the correction of F_{obs} for leak-back flow according to

$$F = F_{obs}\left(1 + \frac{\Phi_p}{\Phi_c}\right) . \qquad \ldots \quad (45)$$

The pad permeability Φ_p was evaluated from the flow measurements. The value of the Poiseuille leak-back correction factor $(1 + \Phi_p/\Phi_c)$ appears in Table IX and in subsequent tables, as an indication of the importance of the leak-back correction.

ζ_E and ζ_s are compared in Table IX as the ratio $\frac{F\eta L}{ED} \Big/ \frac{I\eta L}{pD} = \zeta_E/\zeta_s$. It is seen that ζ_E/ζ_s fell below the theoretical value of unity even at the optimum bubble length of 3 mm. However, the discrepancy between ζ_E and ζ_s was much less than that reported by Goring and Mason (21, 20) and Kanamaru (42) on pads of cellulose.

Effect of Applied Potential

According to conventional theory the electro-osmotic flow rate F should be directly proportional to the applied potential E. However, several workers (43, 52) have reported a non-linear relationship between F and E. In order to check this point, and at the same time test the functioning of the apparatus, measurements of F were carried out on a number of pads of different fibrous materials at a fixed pad concentration, varying E. These pads are listed in Table X, which includes the pad concentration c, the pad permeability Φ_p, and the Poiseuille leak-back correction to F_{obs}. Figs. 20 - 23 show the F and $F\eta L/ED$ values at different E for each of the pads of Table X. All the measurements were carried out in 2×10^{-5} M KCl solution.

It was observed that the bubble tended to stick at the lower speeds; an accurate determination of F_{obs} was found impossible at F_{obs} values approaching 10^{-3} cm.^{3} sec.$^{-1}$. This imposed a lower limit of 48 volts upon E for measurements with cotton and sulphite pulp pads, which showed low electro-osmotic

TABLE X

Pads in which Electro-Osmotic Flow Rate F at Different Applied Voltage E was Measured in 2 x 10^{-5}M KCl Solution

Pad Number	Pad Material	c gm. $cm.^{-3}$	Φ_p $cm.^3$ x 10^8	Poiseuille Leak-back Correction Factor
25	Glass wool 2.5 micron dia.	....	26.5	1.096
26	Sulphite pulp	0.119	1.07	1.004
27-A	Cotton	0.122	19.1	1.069
27-B		0.365	2.56	1.009
28-A	Acetate Rayon	0.135	41.8	1.153
28-B		0.214	23.2	1.085

flow rates indicative of their relatively low ζ-potentials in 2 x 10^{-5} M KCl. With glass and acetate rayon the ζ-potentials in this electrolyte were higher, permitting accurate measurement of F at lower E values than possible with the cellulose pads.

Examination of Figs. 20 - 23 shows that F was directly proportional to E at the higher voltages. However, with decreasing E, F fell increasingly below the straight line joining the higher F values to the origin. This tendency was most marked for acetate rayon and 2.5 micron dia. glass, which were the pads of highest permeability. The tendency was less no-

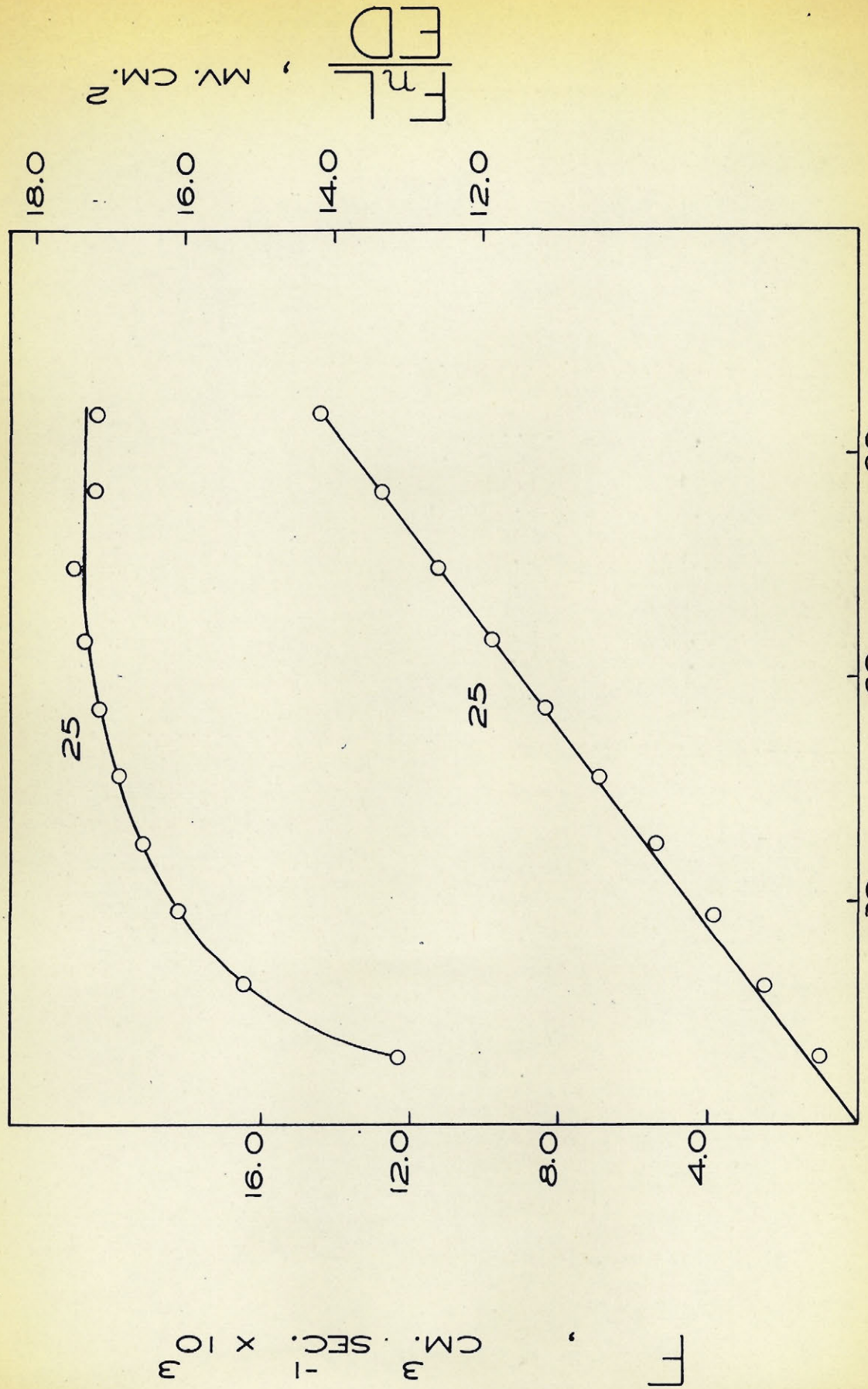

FIG. 20 Γ versus E and FηL/ED versus E plots for pad 25

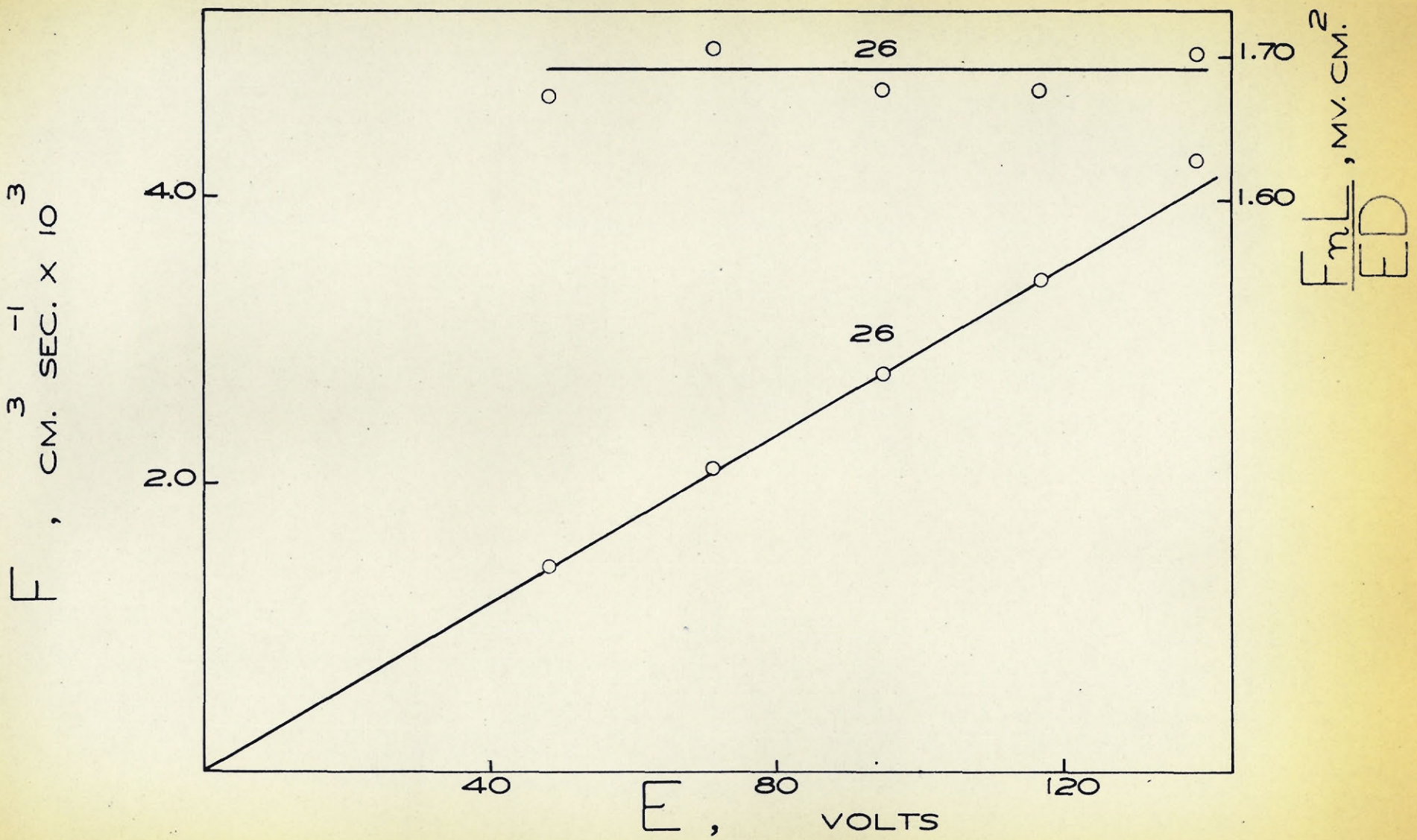

FIG. 21 F versus E and FηL/ED versus E plots for pad 26

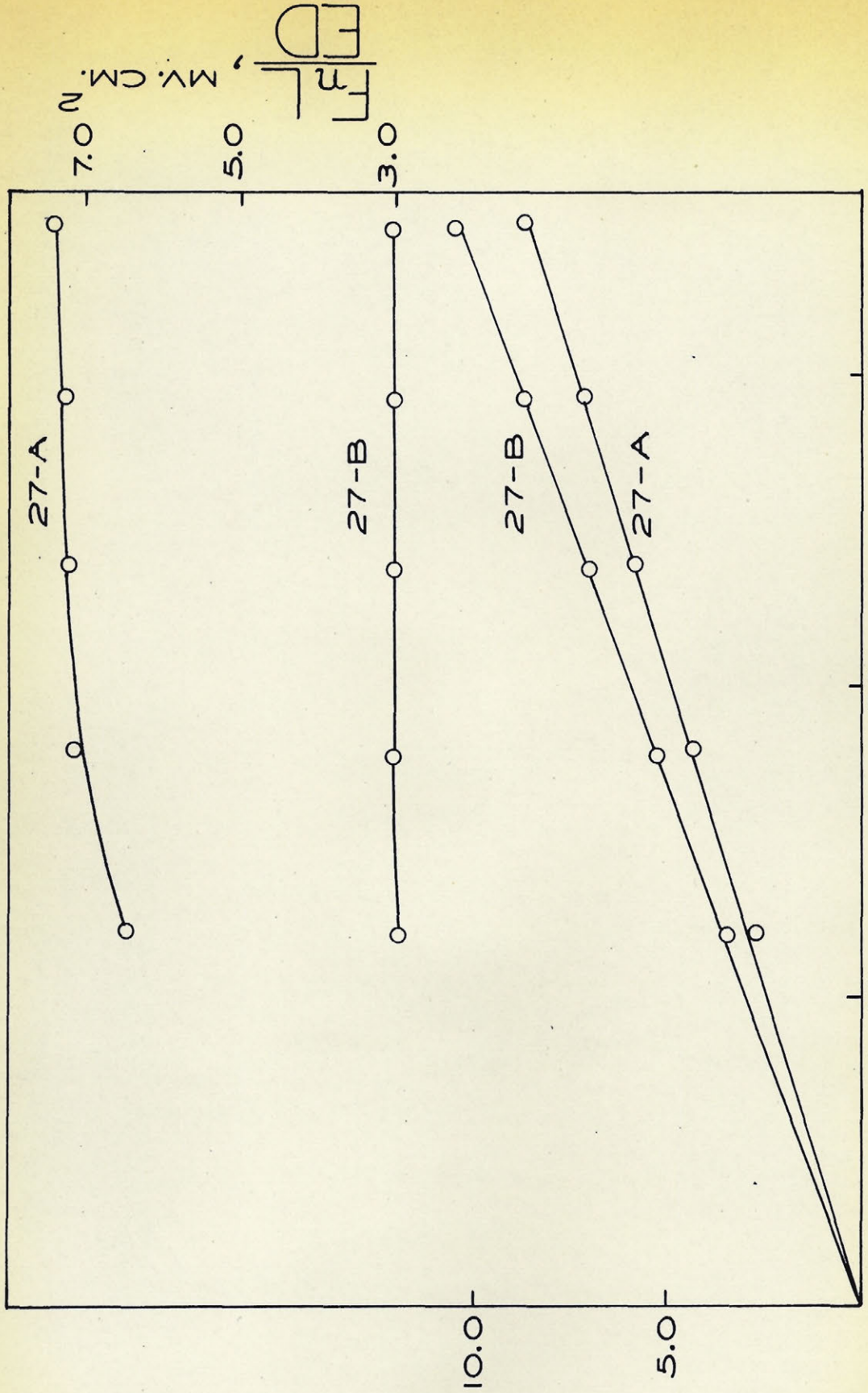

FIG. 22 F versus E and FμL/ED versus E plots for pad 27

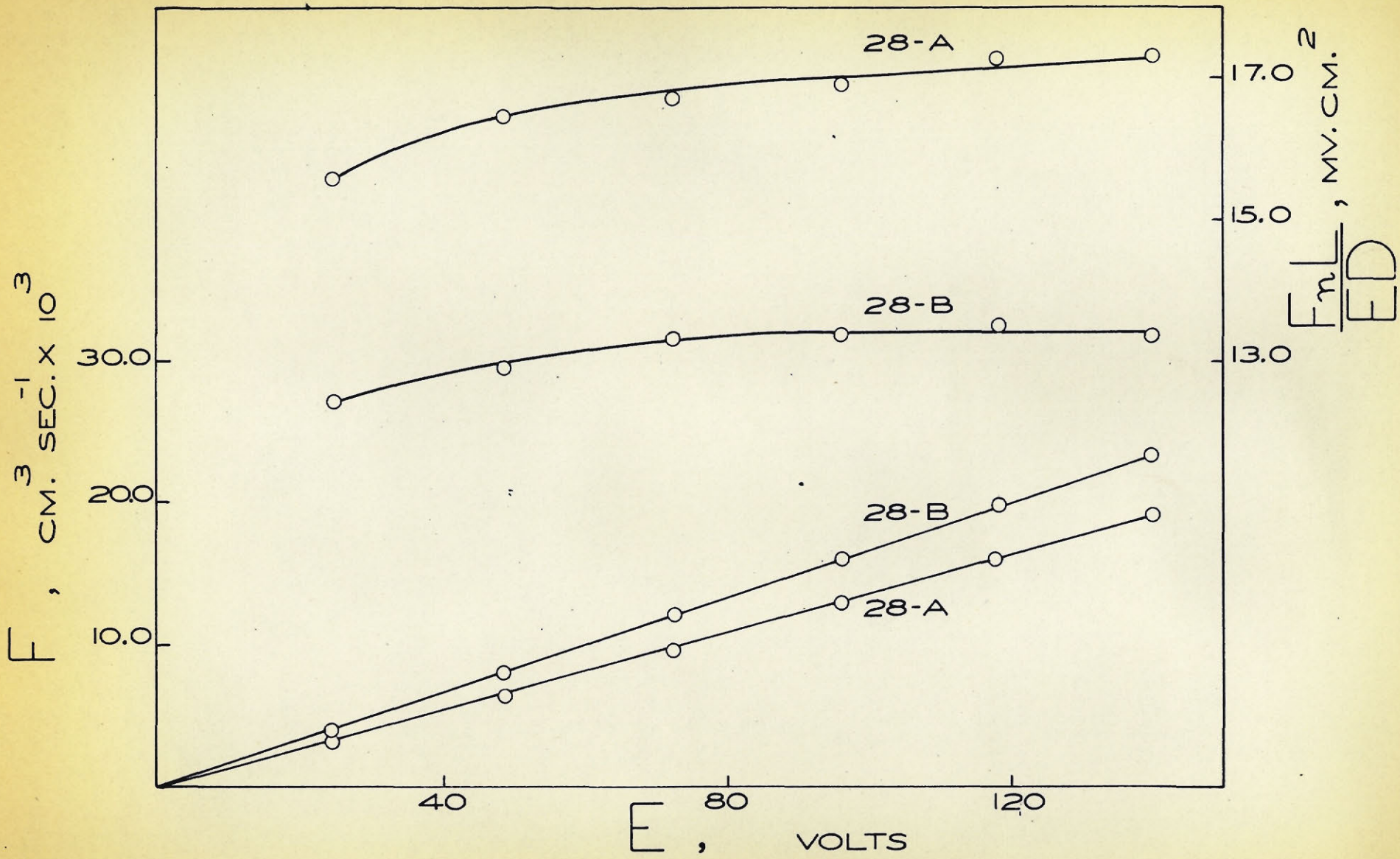

FIG. 23 F versus E and FηL/ED versus E plots for pad 28

ticeable with cotton and sulphite pulp.

As a result of this trend in the F versus E plot, the electro-osmotic function $F\eta L/ED$ exhibited decreasing values with decreasing E. However, $F\eta L/ED$ appeared to reach a limiting value at the higher E values.

Comparison of ζ_E and ζ_s

It was next decided to carry out measurements of electro-osmotic flow, stream current, and permeability over a range of solid concentrations on the same pad, using the data obtained in the F versus E measurements to choose an operating voltage sufficiently high for the variation of $F\eta L/ED$ with E to be negligible.

The results obtained in measurements on sulphite pulp, surgical cotton, 0.5 micron dia. glass, and acetate rayon appear in Tables XI - XIV, in which ζ_s and ζ_E are compared as the ratio $\frac{F\eta L}{ED} \Big/ \frac{I\eta L}{pD} = \zeta_E/\zeta_s$. The pad permeability Φ_p and the Poiseuille leak-back correction factor to F_{obs} are also shown.

Permeability determinations of α_k were carried out for the pads of sulphite pulp, acetate rayon, and surgical cotton; these data appear in Table XVIII of the general discussion.

TABLE XI

Measurements of Electro-Osmotic Flow, Stream Current and Permeability on Sulphite Pulp Pad 29 in 2×10^{-5}M KCl

c gm. cm.$^{-3}$	Φ_p cm.^{3} x 10^8	Poiseuille Leak-Back Correction Factor	$F\eta L/ED$ mv. cm.^{2}	$I\eta L/pD$ mv. cm.^{2}	ζ_E/ζ_s
0.096	3.72	1.014	3.80	3.84	0.99
0.106	2.95	1.011	3.54	3.45	1.03
0.116	2.37	1.009	3.34	3.29	1.01
0.126	1.88	1.007	3.04	3.01	1.01
0.137	1.51	1.005	2.86	2.80	1.02
0.145	1.26	1.005	2.60	2.56	1.01
0.156	1.01	1.004	2.38	2.37	1.00

TABLE XII

Measurements of Electro-Osmotic Flow, Stream Current, and Permeability on Surgical Cotton Pad 30 in 2 x 10-5M KCl

c gm. cm.-3	Φ_p cm.3 x 10^8	Poiseuille Leak-Back Correction Factor	$F\eta L/ED$ mv. cm.2	$I\eta L/pD$ mv. cm.2	ζ_E/ζ_s
0.170	10.45	1.038	4.91	5.34	0.92
0.202	8.55	1.031	4.55	4.75	0.96
0.236	6.62	1.024	4.03	4.17	0.97
0.265	5.01	1.018	3.63	3.78	0.96
0.296	4.00	1.015	3.31	3.38	0.98
0.325	3.16	1.012	2.95	3.03	0.97
0.353	2.47	1.009	2.52	2.72	0.92
0.389	1.78	1.006	2.24	2.28	0.98
0.433	1.29	1.005	1.90	1.92	0.99

TABLE XIII

Measurements of Electro-Osmotic Flow, Stream Current, and Permeability on 0.5 micron dia. Glass Pad 31 in 2×10^{-5} M KCl

c gm. cm.$^{-3}$	Φ_p cm.^{3} x 10^8	Poiseuille Leak-Back Correction Factor	$F\eta L/ED$ mv. cm.^{2}	$I\eta L/pD$ mv. cm.^{2}	ζ_E/ζ_s
0.0216	1.38	1.005	8.00	8.05	0.99
0.0285	1.22	1.004	7.40	8.00	0.93
0.0382	1.04	1.004	7.30	7.60	0.96
0.0485	0.94	1.003	7.20	7.55	0.95
0.0648	0.84	1.003	7.15	7.35	0.97
0.0903	0.72	1.003	6.80	6.90	0.98
0.130	0.56	1.002	5.90	6.05	0.97
0.197	0.37	1.001	4.85	4.90	0.99
0.263	0.26	1.001	4.00	3.95	1.01

TABLE XIV

Measurements of Electro-Osmotic Flow, Stream Current and Permeability on Acetate Rayon Pad 32 in 2 x 10^{-5}M KCl

c gm. cm.$^{-3}$	Φ_p cm.^{3} x 10^8	Poiseuille Leak-Back Correction Factor	$F\eta L/ED$ mv. cm.^{2}	$I\eta L/pD$ mv. cm.^{2}	ζ_E/ζ_s	ζ_E/ζ_s(a)
0.114	48	1.175	17.30	20.20	0.86	0.98
0.137	40.5	1.148	16.00	19.20	0.83	0.93
0.176	30.8	1.113	15.80	17.30	0.91	0.99
0.216	23.6	1.086	13.80	15.40	0.90	0.96
0.257	17.85	1.065	12.60	13.50	0.93	0.99
0.294	13.75	1.050	11.10	12.00	0.92	0.97
0.334	10.50	1.038	9.90	10.40	0.95	0.98
0.375	7.95	1.029	8.75	9.00	0.97	1.00
0.410	6.10	1.022	8.00	7.85	1.02	1.04
0.453	4.50	1.016	6.60	6.75	0.98	1.00

(a) corrected for bubble effect, see Appendix B.

Tables XI and XII, respectively showing the experimental data for sulphite pulp and cotton, clearly demonstrated the equivalence of stream current and electro-osmotic flow measurements on cylindrical pads of cellulose. ζ_E/ζ_S was close to unity for both pads, with an average deviation of less than 1.5% for the sulphite pulp, and less than 4.0% for the cotton. This result is in conformity with conventional electrokinetic theory, and indicates that the large discrepancies between ζ_E and ζ_S observed by Goring and Mason (20, 21) and Kanamaru (42) in their measurements on cellulose pads were spurious.

Table XIII shows the results obtained in measurements on a pad of 0.5 micron dia. glass wool, which formed an exceedingly slow-draining pad in contrast to the 2.5 micron dia. variety. ζ_E/ζ_S was close to the theoretical value of unity over the entire range of pad concentrations, the average deviation from unity being less than 3%. This result was in agreement with the observations of Wijga (39, 22) who showed the equality of ζ_E and ζ_S in measurements on a diaphragm of powdered glass.

Table XIV shows the results obtained in measurements on acetate rayon. This was the only pad in which significant deviations of ζ_E/ζ_S from unity were observed, ζ_E/ζ_S dropping as low as 0.83. The greatest deviations occurred at the lowest pad concentrations where the permeability--and consequently the Poiseuille leak-back correction factor--was largest.

At concentrations greater than 0.334 gm. cm.$^{-3}$, where the leak-back correction factor was less than 1.03, ζ_E/ζ_S was equal to unity within experimental error.

With the sulphite pulp, surgical cotton and 0.5 micron dia. pads, ζ_E/ζ_S had been equal to unity within experimental error at all solid concentrations; however, these pads were much less permeable than the acetate rayon. The leak-back correction was negligible for sulphite pulp and 0.5 micron dia. glass, and had a maximum value of 1.038 for the cotton.

Thus ζ_E/ζ_S was equal to unity within experimental error for pads of all the fibrous materials investigated, provided the leak-back correction to F_{obs} was less than 1.04. The decrease of ζ_E/ζ_S below unitywhen the leak-back correction exceeded 1.04, observed with 2.5 micron dia. glass and acetate rayon, seemed indicative of some error in the calculation of leak-back flow rather than a departure from conventional electrokinetic theory.

An investigation into this and other minor discrepancies observed in the electro-osmotic flow measurements was carried out in which it was demonstrated that the decrease of $F\eta L/ED$ below $I\eta L/pD$ for relatively permeable pads was due to the effect of the contained air bubble on Φ_C; the effect of the bubble length and applied potential upon the observed value of $F\eta L/ED$ could also be explained on this basis. This inves-

tigation is reported separately, in Appendix B.

With the measurements recorded in Tables XI - XIV, investigation into the second main subject of the research was completed; measurements of electro-osmotic flow and stream current on cylindrical pads of cellulose in 2 x 10^{-5} M KCl had clearly shown that there was no discrepancy between ζ_E and ζ_s, ζ_E/ζ_s being equal to unity within experimental error at all pad concentrations.

GENERAL DISCUSSION OF RESULTS

Briggs Method

An analysis of the stream current data obtained in the present investigation demonstrated the existence of a general functional relationship between $I\eta L/pD$ and the pad solid fraction $\alpha_k c$. However, the precise nature of this relationship remained obscure; in order to interpret the data it was first necessary to evaluate the terms descriptive of the complex pore geometry of the pad.

Several treatments of the internal pad geometry have been shown to be inadequate; from the experimental data appearing in the literature, the Briggs (19) method fails for pads of cellulose fiber, yielding ζ-potential values which decrease as the pad is more tightly packed (20, 21, 7). This decrease has been explained as a "wall curvature" effect (7, 6); Bikerman (14) suggested that electrical conduction takes place through the highly-swollen cellulose fiber during the cell constant determination, yielding spuriously low C values.

However, some of the experimental data obtained in the present investigation were much less open to criticism on these grounds. Consider, for example, acetate rayon pad 16 in 10^{-2} M KCl solution. It is reasonable to suppose that this electrolyte is sufficiently concentrated for the effect of surface conductance to be negligible; in their resistance measure-

ments on cylindrical pads of cotton, Goring and Mason (20) observed that the effect of surface conductance was negligible with 10^{-2} M KCl as electrolyte. It has been seen that the thickness of the electrical double layer is negligible compared to the mean pore radius for this pad (Table VIII); this would rule out the possibility of a "wall curvature" effect. Acetate rayon has a moisture pick-up of about 14% at 100% R.H.; thus the degree of swelling is slight, compared to cellulose. It may be assumed provisionally that electrical conduction through the solid fiber structure is unimportant, compared to the conduction taking place through the electrolyte in the pores of the pad.

It was decided to test the validity of the Briggs (19) method by calculating the ζ-potential for this pad over the entire range of solid concentrations using the Briggs stream current equation

$$I = \frac{pD\zeta}{4\pi\eta C} \quad . \qquad \ldots \quad (31)$$

The results obtained are listed in Table XV, which shows the ζ-potential at each pad concentration, and the corresponding pad void fraction ϵ and cell constant C. As before, acetate rayon was assigned a swollen specific volume of 0.95 $cm.^3\ gm.^{-1}$ in calculating the void fraction from $\epsilon = (1 - \alpha_k c)$; this was the average α_k value obtained in the permeability measurements.

TABLE XV

Briggs ζ-Potential over A Range of Pad Concentrations for Acetate Rayon Pad 16 in 10^{-2}M KCl Solution

c (gm. cm.$^{-3}$)	ϵ	C (cm.$^{-1}$)	ζ (mv.)
0.193	0.817	2.84	-17.00
0.224	0.788	2.615	-16.05
0.253	0.760	2.525	-15.90
0.284	0.731	2.44	-15.45
0.320	0.696	2.355	-14.70
0.347	0.670	2.355	-14.35
0.369	0.650	2.34	-14.40
0.392	0.628	2.39	-14.15
0.411	0.609	2.40	-13.90
0.434	0.588	2.44	-13.70

It is seen that there was a marked decrease of the ζ-potential with increasing pad concentration. This decrease could not be accounted for by a "wall curvature" effect; assuming that electrical conduction through the acetate rayon fiber was negligible, it could only be concluded that there was some basic theoretical defect in the Briggs (19) method. The defect was almost certainly in the assumption that the complex internal geometry of the pad was accurately described by the cell constant C.

Analysis of the Conductance Measurements

The cell constant values of Table XV showed an interesting trend; there was a distinct minimum C at a void fraction of $\sim$ 0.65. The existence of this minimum led to the decision to carry out an investigation of the relationship between C and ϵ, with the object of finding some method of evaluating the terms descriptive of the complex internal structure of the pad; it was conjectured that this might lead to a method of interpreting the electrokinetic experimental data. The experimentally observed C minimum at an ϵ value of $\sim$ 0.65 provided an invaluable test for the validity of theoretically derived expressions relating C to ϵ; any expression failing to predict minimum C at an ϵ value of $\sim$ 0.65 could be discarded as incorrect.

Assuming that the electrical conductance of a pad of fibers is due entirely to the liquid contained within the pores, of specific conductivity k, the total conductance of a cylindrical pad of length L and cross sectional area A is

$$\Omega = \frac{k}{L} A\epsilon \; f(\theta)_c \qquad \ldots \quad (48)$$

where $A\epsilon$ = the void cross sectional area of the pad.

The orientation factor $f(\theta)_c$ is included in the above equation in recognition of the fact that the lines of ionic transfer do not move through the pad in the direction of normal flow, but are oriented with respect to the axes of

the individual pores within the pad; the pore axes are inclined at a variety of different angles to the direction of normal flow. For the time being no attempt is made to evaluate $f(\theta)_c$; it will be considered to be constant, as was the analogous $\overline{\cos^2\theta}$ orientation factor by Goring and Mason (20, 21, 8).

By putting $kR = C$, equation 48 may be rearranged to give

$$Cf(\theta)_c = \frac{L}{A\epsilon} \qquad \ldots \quad (49)$$

By expressing the void fraction ϵ in terms of the external pad dimensions and the total volume of fiber in the pad V_o as

$$\epsilon = 1 - \frac{V_o}{LA} \qquad \ldots \quad (50)$$

and substituting into equation 49, the following expression is obtained, in which C is a function of the pad length L:

$$Cf(\theta)_c = \frac{L^2}{(LA - V_o)} \qquad \ldots \quad (51)$$

The theoretical void fraction of minimum C may be found by differentiating the right hand side of equation 51 with respect to L, and then equating to zero. This leads to

$$\frac{d}{dL}\left(\frac{L^2}{LA - V_o}\right) = \frac{L(LA - 2V_o)}{(LA - V_o)^2} = 0 \quad .$$

The significant solution of this equation is $V_o/LA = 0.5$, or $\epsilon = (1 - V_o/LA) = 0.5$; thus an extreme value of C is predicted at $\epsilon = 0.5$. This is in contradiction to the experimental data of Table XV, which show minimum C at an ϵ value of ~ 0.65.

It was first conjectured that the discrepancy between the theoretical and the experimental C minima might be explained by a significant electrical conduction taking place through the acetate rayon fiber, in contradiction to the previous assumption of negligible fiber conduction. This hypothesis was tested by deriving an equation relating C to the pad length for the case where significant electrical conduction takes place through the fibers, and differentiating as before to find the void fraction at which an extreme C value occurred. The equation was derived as follows.

The total conductance of a pad of fibers in contact with electrolyte of specific conductivity k and fiber specific conductivity k_f ($k > k_f$) consists of two terms. There is the conductance of the electrolyte

$$\Omega_e = \frac{kA\epsilon}{L} f(\theta)_c$$

and the conductance of the fiber structure

$$\Omega_f = \frac{k_f A}{L} (1 - \epsilon) f(\theta)_c$$

so that the total conductance of the pad is

$$\Omega = \Omega_e + \Omega_f = \frac{Af(\theta)_c}{L} \left(k_f(1 - \epsilon) + k\epsilon \right) .$$

A simplification can be effected by putting $k_f/k = \gamma$ ($\gamma < 1$), and substituting for ϵ from equation 50; this transforms the above equation to

$$\Omega = \frac{kA}{L} f(\theta)_c \left(1 - (1 - \gamma) \frac{V_o}{LA} \right)$$

or
$$Cf(\theta)_c = \frac{L^2}{LA - (1 - \gamma)V_o} \quad \ldots \quad (52).$$

This equation is of the same form as equation 51, with the constant V_o replaced by a different constant $(1 - \gamma)V_o$. Differentiating the right hand side of equation 52 with respect to L and equating to zero as before leads to

$$\frac{d}{dL} \left(\frac{L^2}{LA - (1 - \gamma)V_o} \right) = \frac{L(LA - 2(1 - \gamma)V_o)}{(LA - (1 - \gamma)V_o)^2} = 0$$

The significant solution of this equation is

$$\frac{V_o}{LA} = \frac{1}{2(1 - \gamma)} > 0.5 \quad \text{i.e.} \quad \epsilon = 1 - \frac{1}{2(1 - \gamma)} < 0.5$$

According to this equation an extreme C value occurs at ϵ values which fall increasingly below 0.5 as the specific

conductivity of the fiber increases. But the experimental data of Table XV show minimum C at an ϵ of $\sim$ 0.65; this represents a displacement in the opposite sense. It was therefore clear that the discrepancy between the experimental and theoretical C minima could not be attributed to electrical conduction occuring through the acetate rayon fiber.

In the foregoing analysis $f(\theta)_c$ was assumed constant at all pad concentrations. However, the correctness of this assumption is by no means certain. For the case of liquid flow through a bed of particles, Hawksley (55) assigned the orientation factor $\overline{\cos^2\theta}$ an average value of 2/3 over the ϵ range 0.8 to 0.4; he pointed out that $\overline{\cos^2\theta}$ must tend to unity with increasing void fraction, as the fluid streamlines became more and more parallel to the direction of macroscopic flow through the bed.

It is reasonable to suppose that the conductance orientation factor $f(\theta)_c$ also tends tounity with increasing pad void fraction. If this trend were significant over the range of void fractions covered by the experimental data of Table XV, minimum C might be expected to occur at a void fraction other than 0.5, the theoretical extreme for the case of constant $f(\theta)_c$. This hypothesis was tested by evaluating $f(\theta)_c$ for the acetate rayon pad of Table XV according to

$$f(\theta)_c = \frac{L}{CA\epsilon} \quad . \qquad \ldots \quad (49)$$

The results obtained appear in Table XVI, which shows the pad length L, C, ϵ, $f(\theta)_c$ and the ratio $\epsilon/f(\theta)_c$.

TABLE XVI

Calculation of $f(\theta)_c$ for Acetate Rayon Pad 16 in 10^{-2} M KCl solution

($A = 5.00$ cm.^{2})

L (cm.)	C (cm.$^{-1}$)	ϵ	$f(\theta)_c$	$\epsilon/f(\theta)_c$
8.860	2.84	0.817	0.762	1.07
7.605	2.615	0.788	0.738	1.065
6.750	2.525	0.760	0.702	1.08
6.010	2.44	0.731	0.672	1.09
5.330	2.355	0.696	0.650	1.07
4.910	2.355	0.670	0.623	1.07
4.615	2.34	0.650	0.607	1.07
4.350	2.39	0.628	0.580	1.08
4.150	2.40	0.609	0.568	1.07
3.930	2.44	0.588	0.545	1.08

It is immediately seen that the assumption of $f(\theta)_c$ = constant was incorrect; $f(\theta)_c$ increased steadily with increasing ϵ, thus showing the trend postulated by Hawksley (55). The ratio $\epsilon/f(\theta)_c$ was constant over the entire range of pad concentrations, averaging 1.075. This showed that $f(\theta)_c$ was a linear function of ϵ; the agreement between the two quantities was close enough to suggest that $f(\theta)_c$ was equal to ϵ, with the deviation of $\epsilon/f(\theta)_c$ from unity arising from experimental error.

This equality is seen to hold for the ideal limiting cases; at $\epsilon = 1$ there is no pad, and electrical conduction is in the direction of the axis of symmetry of the cell, i.e. $f(\theta)_c = 1$. At $\epsilon = 0$, assuming no electrical conduction takes place through the fibers, the resistance of the pad is infinite. Upon application of potential across the pad there is no flow of current; this is equivalent to saying that the lines of ionic transfer are at right angles to the axis of the pad, i.e. $f(\theta)_c = 0$.

A check of the validity of the hypothesis that

$$f(\theta)_c = \epsilon \qquad \ldots \quad (53)$$

was next carried out by setting $f(\theta)_c$ equal to ϵ in equation 49, which became

$$C = \frac{L}{A\epsilon^2} \quad . \qquad \ldots \quad (54)$$

Substituting for ϵ from equation 50, C was obtained as the function of L

$$C = \frac{AL^3}{(LA - V_o)^2} \qquad \ldots \quad (55)$$

As before, the void fraction for an extreme C was found by differentiating the right hand side of this equation with respect to L, and equating to zero. This gave

$$A. \frac{d}{dL}\left(\frac{L^3}{(LA - V_o)^2}\right) = A. \frac{(LA - 3V_o)(LA - V_o)}{(LA - V_o)^4} = 0$$

The significant solution of this equation is $V_o/LA = 1/3$, i.e. $\epsilon = 2/3$ at the extreme value of C. This was in agreement with the experimental data of Table XV, which showed minimum C at an ϵ of $\sim$ 0.65; the hypothesis that $f(\theta)_c$ equals ϵ was thus confirmed.

Conductance Equation

The equality between $f(\theta)_c$ and ϵ was further tested by rearranging equation 54 and taking the square root of both sides to give

$$\sqrt{L/C} = \sqrt{A}\,(1 - \alpha_c c) \qquad \ldots \quad (56)$$

According to this expression, a graphical plot of $\sqrt{L/C}$ versus the pad concentration c should be linear; extrapolation of the straight line to the co-ordinate axes should give correct values for α_c and $\sqrt{A}$, under conditions of negligible fiber conduction and surface conductance.

These experimental conditions are fulfilled when the conductance data are obtained in measurements on pads of slightly-swelling fibers in relatively concentrated electrolyte. Five of the pads measured in the high-compression cell fell into this category and were thus suitable for a test of the validity of equation 56; the conductance data for these pads appear in Figs. 24 - 25 as $\sqrt{L/C}$ versus c plots.

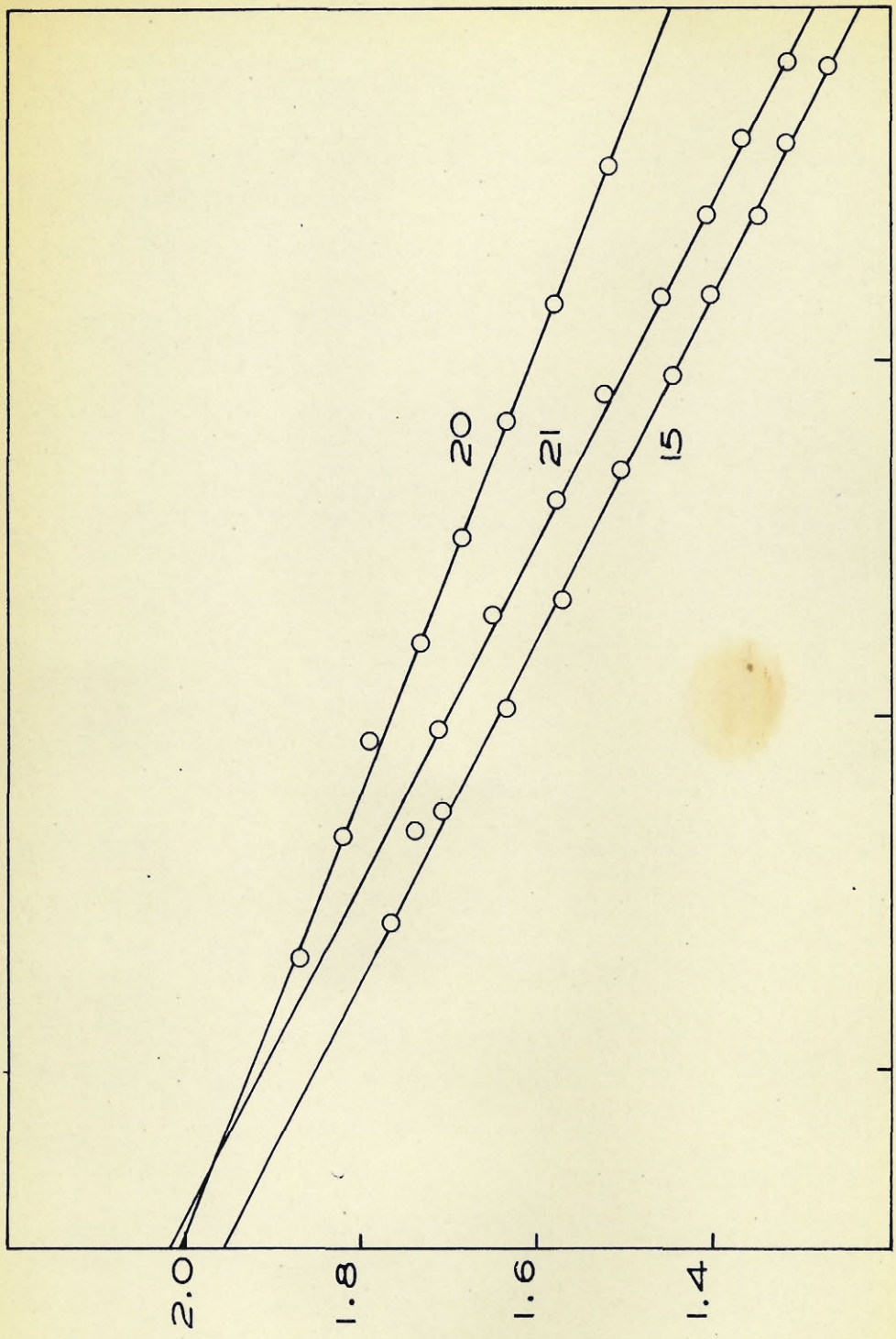

FIG. 24 $\sqrt{1/C}$ versus c plots for pads 15, 20, and 21

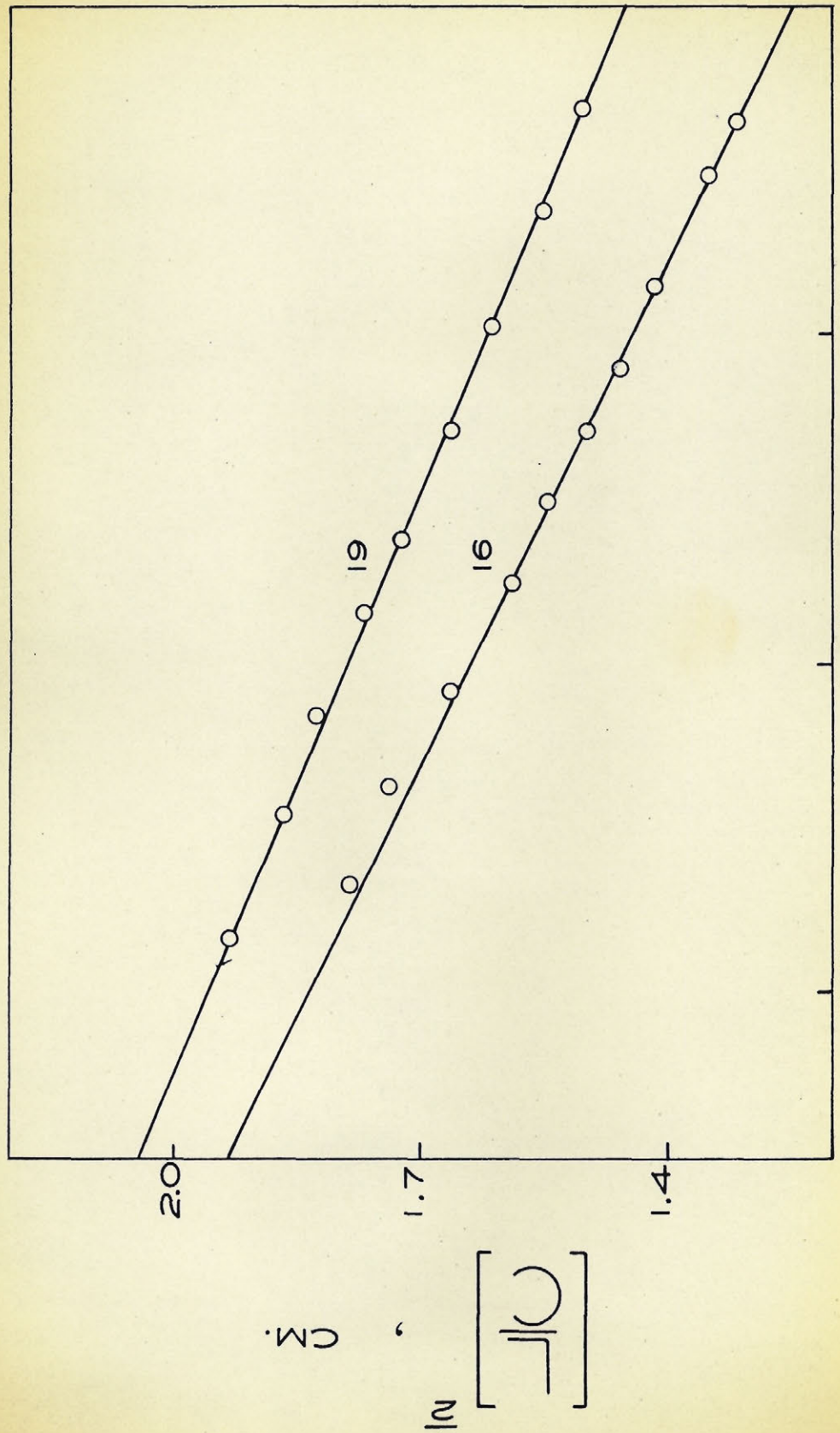

FIG. 25 $\sqrt{L/C}$ versus c plots for pads 16 and 19

It is seen that the plots were linear in all cases. The values of α_c and A calculated from the intercepts on the co-ordinate axes of the graph are listed in Table XVII; it is seen that excellent agreement is shown with the α_k values determined for the same pads from the concurrent permeability measurements. The A values, representing the effective area of the electrodes, ranged from 4.60 to 4.97 $cm.^2$, with an average A value of 4.75 $cm.^2$. This was 5% lower than the cell cross sectional area of 5.00 $cm.^2$; the discrepancy may arise from experimental errors in determining k, the specific conductivity of the electrolyte. It may also be relevant to remark that the area of each electrode is undoubtedly somewhat less than the cross sectional area of the cell, as there is a certain amount of play between the electrode and the cell wall .

However, the α_c and A values are sufficiently accurate to demonstrate the equality of $f(\theta)_c$ and ϵ for randomly sedimented cylindrical pads of fibers, under conditions of negligible surface and fiber conductance. The success of the demonstration is striking in view of the fact that the conductance data were completely incidental to the stream current measurements. There was no original intention of subjecting the conductance data to a separate analysis; the specific conductivity of the electrolyte k was measured solely as a check on the purity of the solution, and the pad resistance R was measured so that the observed stream current could be corrected for leak-back according to equation 44. The stream current data were entirely

TABLE XVII

Specific Volumes Obtained from Conductance and Permeability Measurements on Pads of slightly-swelling Fibers in Concentrated Electrolyte

Pad Number	Material	Electrolyte	α_c ($cm.^3 gm.^{-1}$)	α_k ($cm.^3 gm.^{-1}$)	A ($cm.^2$)
16	Acetate rayon	10^{-3}M KCl	0.94	0.93	4.60
15	Acetate rayon	10^{-2}M KCl	0.95	0.97	4.66
21	Nylon	3×10^{-5}M $ThCl_4$	0.94	0.98	4.97
20	Dacron	2×10^{-3}M KCl	0.74	0.74	4.70
19	Dacron	10^{-3}M KCl	0.77	0.75	4.90

independent of k, and the leak-back correction factor was usually less than 5%; thus no great degree of precision was considered necessary in the measurements, which were carried out with a small conductivity bridge whose accuracy was moderate at best.

Conductance Measurements from The Literature

While the equality between $f(\theta)_c$ and ϵ was demonstrated for cylindrical pads of randomly-sedimented fibers, there is experimental evidence that the relationship may be more widely applicable.

Archie (56), measuring the conductance of cylindrical

cores of porous rock and sand impregnated in normal NaCl solutions, found that his experimental data were described by the empirical expression

$$F = \epsilon^{-m} \qquad \ldots \quad (57)$$

where the value of m ranged from 1.3 to 2.0. In similar measurements Guyod (57) and others (58) observed m values from 1.3 to 3.0, with a most probable value of 2.0. Wyllie and Rose (58) remarked that Archie's equation was probably without theoretical significance.

In equation 57 the "formation factor" F is defined as the ratio of the specific conductivity of the liquid within the pores of the pad k and the specific conductivity k_m of the porous medium saturated with the electrolyte of specific conductivity k, i.e. $F = k/k_m$.

For a cylindrical bed of particles $k_m = L/AR$; equation 57 may therefore be expressed as

$$\frac{ARk}{L} = \epsilon^{-m} \qquad \text{which becomes} \qquad C = \frac{L}{A\epsilon^2}$$

for the case where m = 2. This expression is identical to equation 54, descriptive of conductance measurements on a cylindrical pad of fibers. The empirical equation of Archie (56) as interpreted by subsequent workers (57, 58) is thus additional experimental evidence of the equality of $f(\theta)_c$ and ϵ, and suggests that the equality holds for randomly formed statistically homogeneous beds of particles of arbitrary shape.

It is also of interest to note that Preston (59) employed conductance measurements for determining the external diameters of water swollen fibers. Model beds were formed for each fiber by threading a number of the fibers through a glass capillary tube containing M/2 electrolyte. This gave $f(\theta)_c = 1$; the ratio between the conductance of the capillary containing the fibers Ω_s and the capillary containing solution only Ω_o was

$$\frac{\Omega_s}{\Omega_o} = \left(\gamma(1 - \epsilon) + \epsilon\right) \qquad \ldots \quad (58)$$

where $\gamma = k_f/k < 1.0$, the ratio between the specific conductivities of the fiber and the electrolyte (cf. equation 52).

Equation 58 was used to find the diameter of fibers of regular cross section such as nylon and viscose rayon. The results obtained agreed with the value obtained from microscopic measurements of the fiber within experimental error.

This method is restricted to fibers of regular cross section which can be obtained as relatively lengthy strands; the experimental procedures are awkward. Equation 58 contains the quantity γ which must be evaluated independently for ϵ to be calculated; Preston (59) evaluated γ by determining ϵ from microscopic measurements of the water-swollen fiber. The result given by the conductivity method was therefore dependent upon the microscopic measurements, and does not represent an independent means of determining the fiber diameter, except for

the case of negligible k_f.

Stream Current Measurements

Attention was next directed to the interpretation of the stream current data. The stream current produced by flow of liquid through a channel of cross sectional area a and length l_c is

$$i = \frac{pD\zeta a}{4\pi\eta l_c} \quad . \qquad \ldots \quad (29)$$

Extending this equation to the case of a statistically homogeneous pad of length L and void cross sectional area $A\epsilon$, the stream current equation may be written

$$\frac{I\eta L}{pD} = \frac{\zeta A\epsilon}{4\pi} f(\theta)_\zeta \quad . \qquad \ldots \quad (59)$$

As in the case of the conductance equation 48, an orientation factor is included, in recognition of the fact that the lines of ionic transfer within the pad are oriented with respect to the pore axes. As with the conductance orientation factor $f(\theta)_c$, for the time being no attempt is made to evaluate the stream current orientation factor $f(\theta)_\zeta$.

It has been seen that Goring and Mason (20, 21, 8), deriving a stream current equation of the same form as that shown above, assumed $f(\theta)_\zeta$ to be a constant, assigning it the value of 0.5. However, it has been seen that this assumption is invalid; the Goring-Mason stream current equation is con-

tradicted by the experimental evidence.

If it be assumed that the stream current orientation factor $f(\theta)_\zeta$ is equal to the conductance orientation factor $f(\theta)_c$, which has been shown equal to ϵ, stream current equation 59 is transformed into

$$\frac{I\eta L}{pD} = \frac{A\zeta}{4\pi}\epsilon^2 \qquad \ldots \quad (60)$$

However, this equation cannot be correct. The substitution of

$$C = \frac{L}{A\epsilon^2} \qquad \ldots \quad (54)$$

into the Briggs stream current equation

$$I = \frac{pD\zeta}{4\pi\eta C} \qquad \ldots \quad (31)$$

also leads to the same result. Thus equation 60 is merely a restatement of the Briggs stream current equation in a different form; the Briggs equation has been seen to fail, leading to ζ-potential values which decrease with increasing pad concentration (Table XV).

By trial and error it was found that the stream current data obtained in the present investigation could be described by the empirical equation

$$\left(\frac{I\eta L}{pD}\right)^{0.4} = k_E(1 - \alpha_\zeta c) \qquad \ldots \quad (61)$$

in which k_E is a constant. The equation was valid within the same range of pad void fractions as the Kozeny (27) permeability equation, i.e., at $\epsilon < 0.80$.

The data obtained in the electro-osmotic measurements were thus described by

$$\left(\frac{F\eta L}{ED}\right)^{0.4} = k_E(1 - \alpha_\zeta c) \qquad \ldots \quad (62)$$

at $\epsilon < 0.80$; any argument depending upon the relationship between stream current and pad concentration can be applied equally well to the case of electro-osmotic flow.

This regularity in the experimental data suggested the following equation for the stream current generated by viscous flow through a porous diaphragm:

$$\frac{I\eta L}{pD} = \frac{A\zeta}{4\pi}\epsilon^{2.5} \qquad \ldots \quad (63)$$

which implies

$$f(\theta)_\zeta = \epsilon^{1.5} \qquad \ldots \quad (64)$$

This is in contrast with the result obtained in the conductance measurements, which led to

$$f(\theta)_c = \epsilon \qquad \ldots \quad (53)$$

Experimental evidence for the validity of the empirical equation 61 is presented in Figs. 26 - 29. All the stream current data from measurements in the high-compression cell, including the pads upon which concurrent stream and electro-osmotic measurements were carried out, appear as $(I\eta L/pD)^{0.4}$ versus c plots.

The α_ζ values obtained upon extrapolation of the straight lines to the concentration co-ordinate axis appear in Table XVIII. The α_k values obtained in the concurrent permeability measurements are also included; where available, α_c values from the conductance measurements also appear. ζ-potential values were also calculated for each pad according to stream current equation 63 in the alternative form

$$\left(\frac{I\eta L}{pD}\right)^{0.4} = \left(\frac{A\zeta}{4\pi}\right)^{0.4} (1 - \alpha_\zeta c) . \qquad \ldots \quad (65)$$

Since it was not possible to demonstrate the validity of this equation, the ζ-potentials thus calculated are denoted ζ', to indicate their empirical origin. It was assumed that the ζ' values constituted a measure of the charge density on the fiber, and could be used to compare the relative charge densities of different fibers.

Examination of Figs. 26 - 29 shows that the plots were generally linear at void fractions below 0.80. The deviations from linearity shown by the fast-draining pads at void fractions greater than 0.80 were slight; all exhibited the

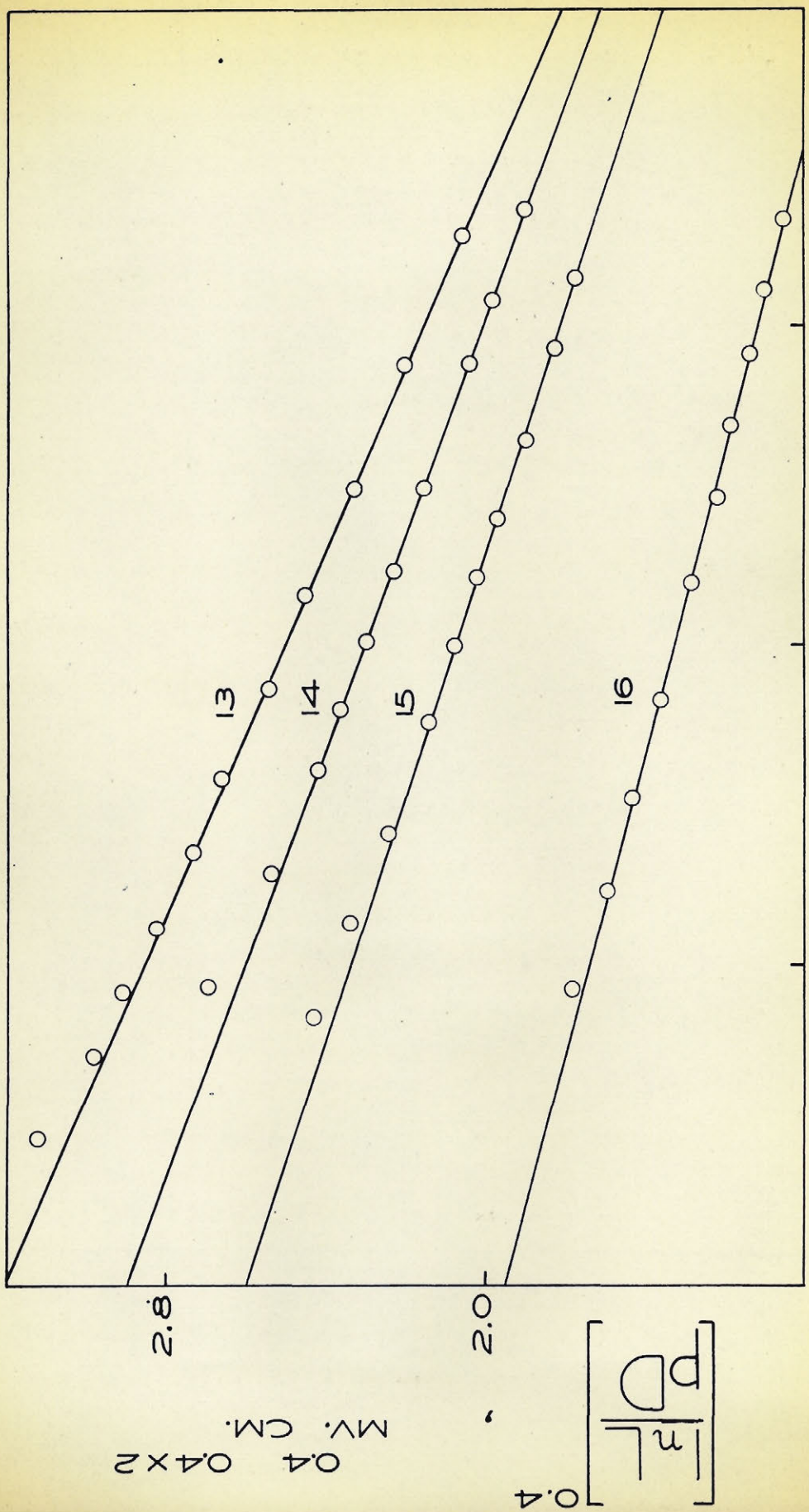

FIG. 26 $(\eta_L/\rho D)^{0.4}$ versus c plots for pads 13, 14, 15, and 16.

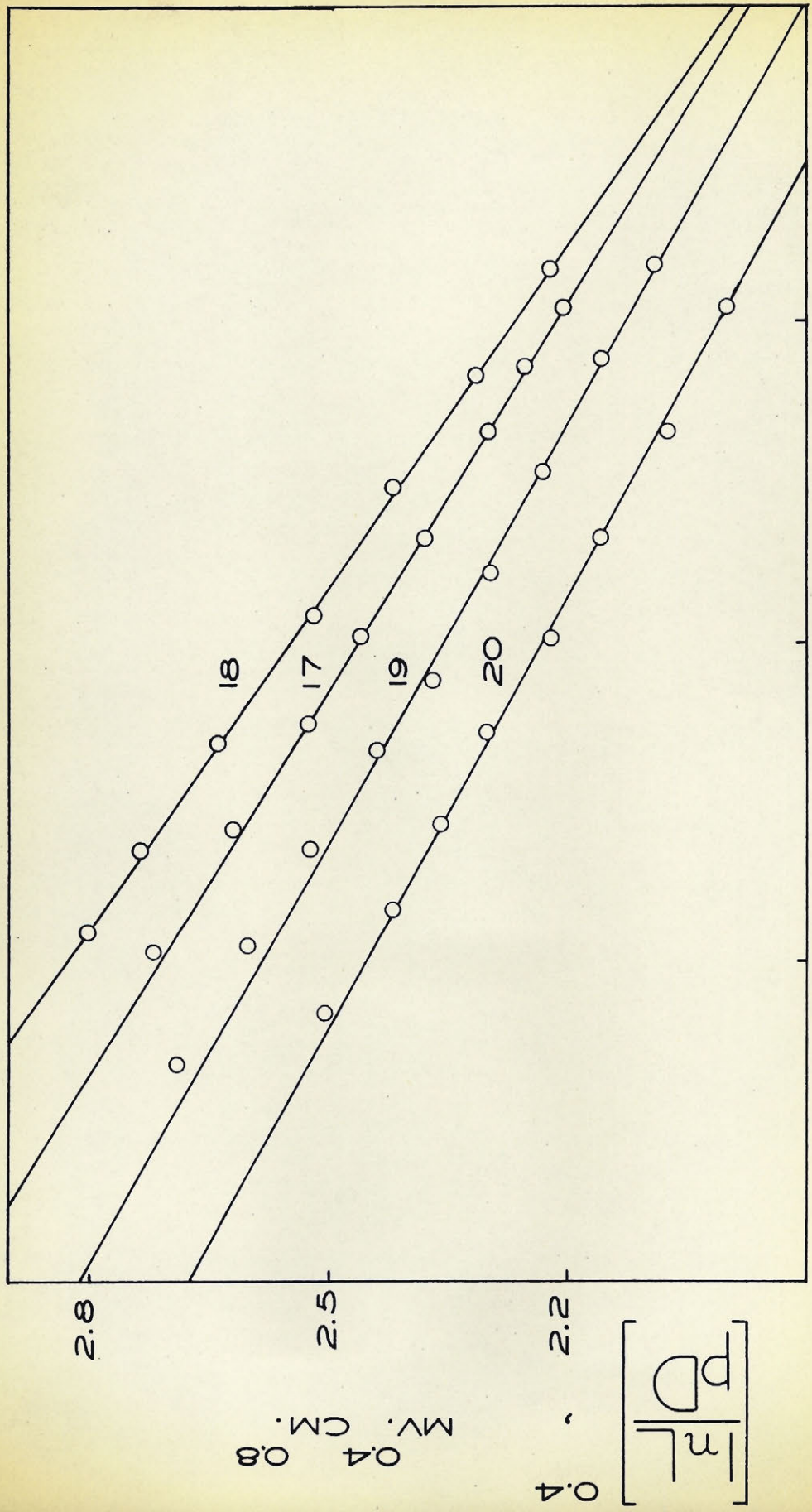

FIG. 27 $(\eta L/pD)^{0.4}$ versus c plots for pads 17, 18, 19, and 20.

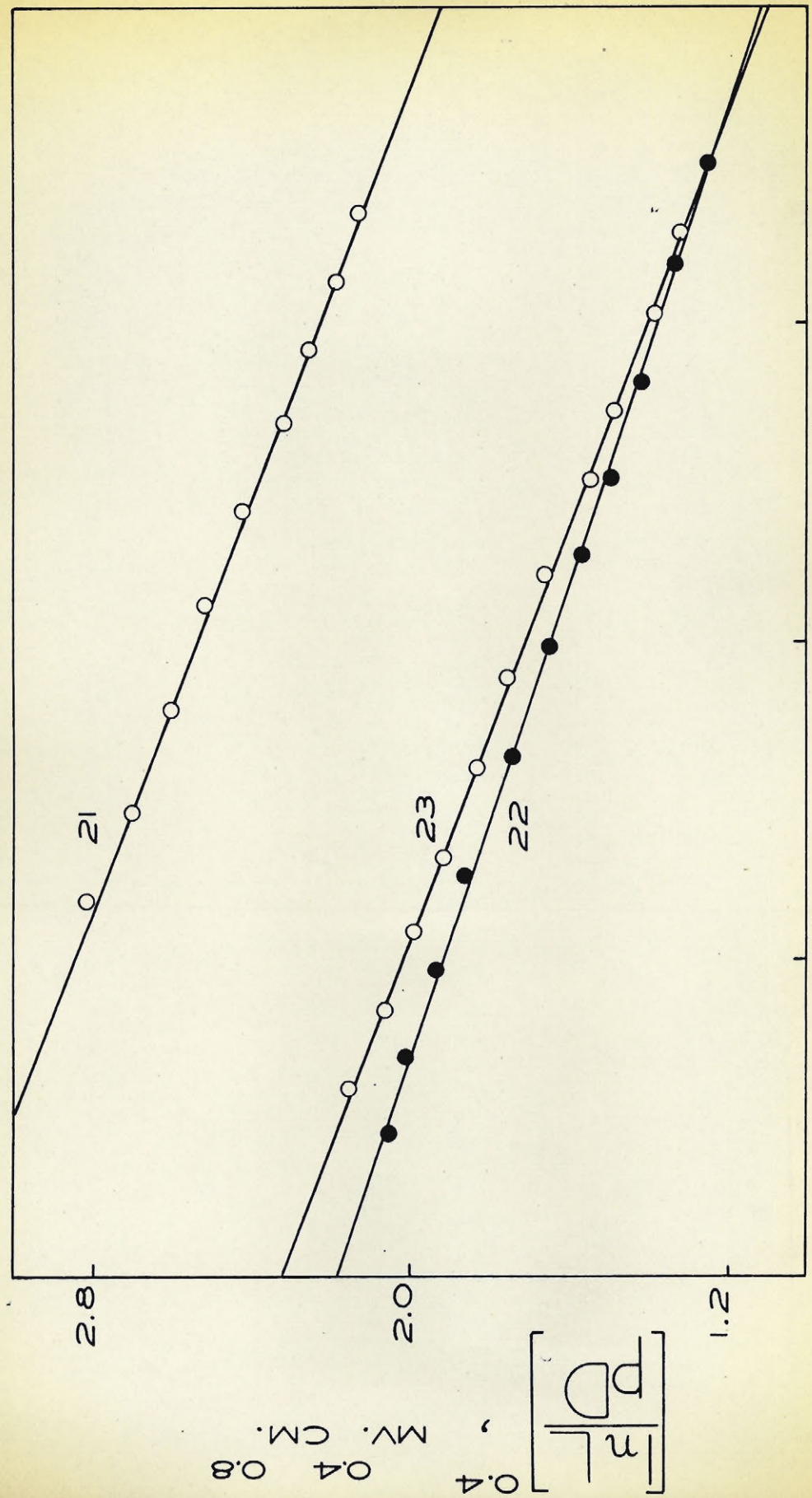

FIG. 28 $(\ln L/pD)^{0.4}$ versus c plots for pads 21, 22, and 23.

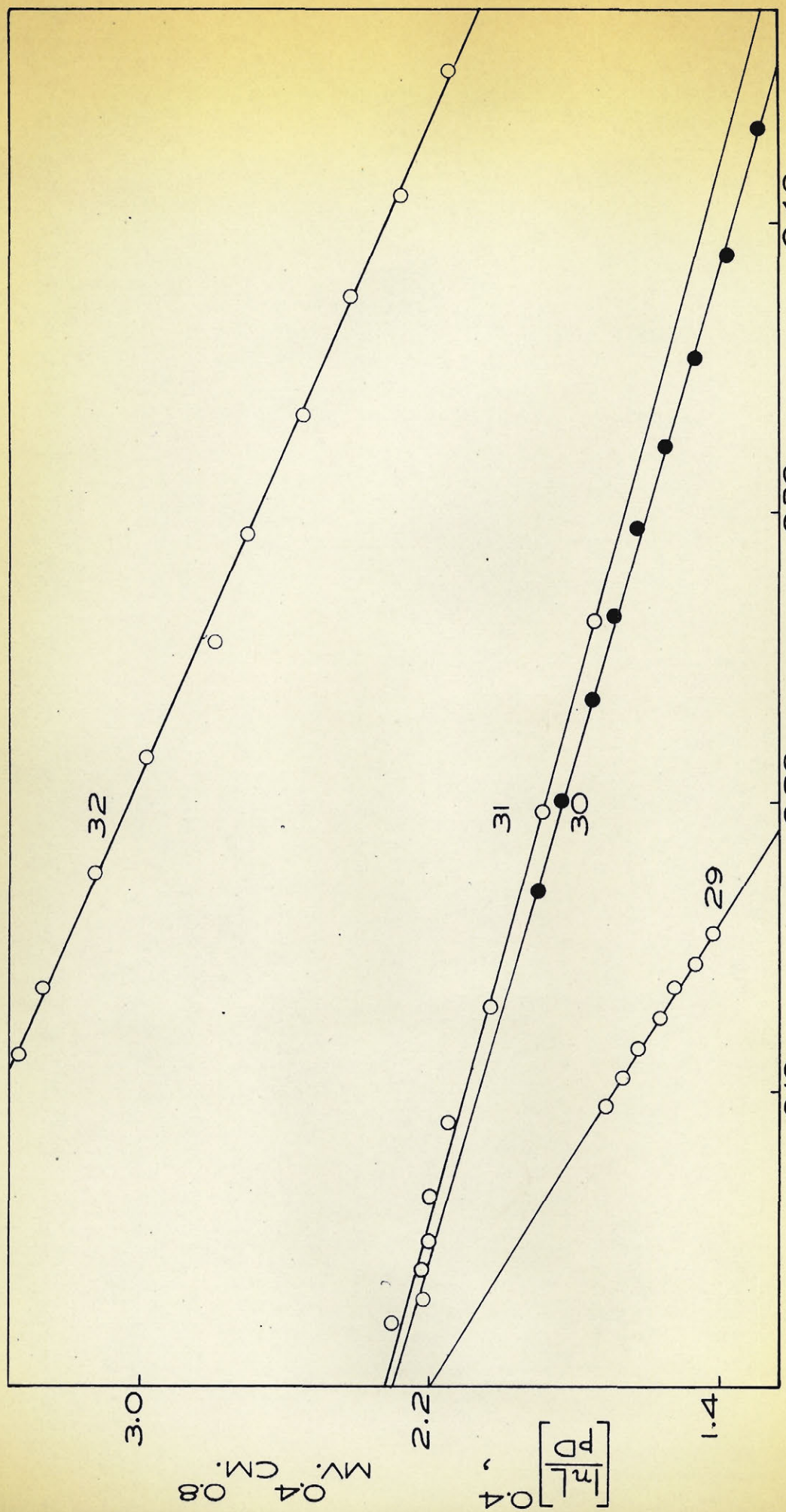

FIG. 29 $(\eta_{sp}/cT)^{0.4}$ versus c plots for pads 29, 30, 31, and 32.

TABLE XVIII

ζ' Values and Specific Volumes of Various Fibers Calculated from The Measurements of Stream Current, Permeability and Conductance in the High-Compression Cell

Pad Number	Material	Electrolyte	ζ' (mv.)	α_ζ ($cm.^3\ gm.^{-1}$)	α_k ($cm.^3\ gm.^{-1}$)	α_c ($cm.^3\ gm.^{-1}$)
13	Acetate rayon	2×10^{-5} M KCl	-59.6	0.99	1.00	....
14		2×10^{-4} M KCl	-45.7	0.93	0.95	....
15		10^{-3} M KCl	-35.5	0.94	0.97	0.94
16		10^{-2} M KCl	-17.2	0.97	0.93	0.95
32		2×10^{-5} M KCl	-66.5	0.93	0.92	....
17	Dacron	2×10^{-5} M KCl	-44.5	0.77	0.74	....
18		2×10^{-4} M KCl	-52.8	0.82	0.79	....
19		10^{-3} M KCl	-40.6	0.75	0.74	0.77
20		2×10^{-3} M KCl	-32.9	0.74	0.75	0.74
21	Nylon	3×10^{-5} M $ThCl_4$	+55.2	0.90	0.97	0.94
22	Surgical cotton	2×10^{-4} M KCl	-23.8	1.10	1.08	....
30	Surgical cotton	2×10^{-5} M KCl	-20.2	1.02	1.10	....
23	Viscose rayon	2×10^{-4} M KCl	-28.0	1.16	1.27	....
29	Sulphite pulp	2×10^{-5} M KCl	-18.1	2.34	2.86	....
31	0.5 micron Glass	2×10^{-5} M KCl	-20.7	0.94	....	....

same tendency, the $(I\eta L/pD)^{0.4}$ values rising increasingly above the straight line with decreasing pad concentration.

At the lower pad concentrations the fiber network is least rigid, and the rate of flow of liquid through the pad is greatest; this suggests that the deviations from linearity may be due to an elastic deformation of the pad structure during flow.

This suggestion is supported by an examination of the conductance data of Figs. 24 - 25, which show $\sqrt{L/C}$ versus c plots for five of the pads shown in Figs. 26 - 29. In determining $\sqrt{L/C}$ the pad resistance was always measured with the liquid resting in the pad; no consistent trend is shown in the few deviations from linearity which may be observed at the lower pad concentrations. This is in contrast to the $(I\eta L/pD)^{0.4}$ versus c plots for the same pads, which all showed deviations from linearity in the same sense.

An experiment designed to test the hypothesis that an elastic deformation of the pad may occur during flow is described in the final section of this thesis.

An examination of Table XVIII shows that there was generally good agreement between the α_ζ, α_k, and α_c values; however, the three methods of determining α can be compared more conveniently by a study of Table XIX, which lists the average α_ζ, α_k, and α_c values for each fiber, obtained from Table XVIII. Pad 31, 0.5 micron dia. glass, is omitted from

this table, as determinations of α_ζ and α_k failed; discussion of the results obtained with this pad is postponed.

For purposes of comparison, Table XIX also shows average α_k values as determined by Goring, Carroll, and Mason (20, 21, 8, 49, 50) from permeability measurements on pads of the same fibers measured in the present investigation. Water-swollen fiber specific volumes calculated by Carroll and Mason (49, 50) from measurements of the specific volume of the dry fiber in kerosene, corrected for the moisture regain at 100% relative humidity, also appear. A specific volume for Dacron, determined during the present investigation from displacement in water, is included. For each α value shown in Table XIX the number of experimental determinations making up the average is listed, where this information is available.

An examination of the average α values obtained in measurements with the high-compression cell shows that the deviation between α_ζ and α_k was less than 3% in every case where at least two pads of the fiber were measured, i.e. for acetate rayon, Dacron, and surgical cotton. For acetate rayon and Dacron, the deviation between α_c and the other two α values was less than 2%. In general, the α values for the three fibers showed good agreement with the reference α values.

For the cases where only one pad of the fiber was measured in the high-compression cell, i.e. viscose rayon, nylon, and sulphite pulp, a somewhat greater deviation was

TABLE XIX

Comparison of High-Compression Cell α Values with Independent α Determinations

Fiber	Results of Table XVIII: Average α Values Obtained in Stream Current, Permeability and Conductance Measurements in The High-Compression Cell			Average α Values from Permeability and Other Measurements: Carroll and Mason (49, 50)	
	α_ζ ($cm.^3\ gm.^{-1}$)	α_k ($cm.^3\ gm.^{-1}$)	α_c ($cm.^3\ gm.^{-1}$)	α_k ($cm.^3\ gm.^{-1}$)	α ($cm.^3\ gm.^{-1}$)
Acetate rayon	0.95 (5)	0.95 (5)	0.94 (2)	0.90 (2)	0.93 (2)
Viscose rayon	1.16 (1)	1.27 (1)	....	1.20 (2)	1.01 (2)
Nylon	0.90 (1)	0.97 (1)	0.94 (1)	0.98 (4)	0.98 (2)
Dacron	0.77 (4)	0.75 (4)	0.75 (2)	....	0.72 (2)[a]
Surgical cotton	1.06 (2)	1.09 (2)	....	~1.00 (?)	....
Sulphite pulp	2.34 (1)	2.86 (1)	....	2.45 (9)[b]	....

(a) Present investigation (b) Goring and Mason (20, 21, 8)

The figure in brackets after each α value indicates the number of experimental determinations making up the average.

shown between the different α values. For viscose rayon and nylon, α_ζ and α_k showed a deviation of $\sim$ 5%; the α_c value for nylon fell between the α_ζ and α_k values. For both viscose rayon and nylon, the α_k value determined in the present investigation showed good agreement with the α_k values determined by Carroll and Mason (49, 50) for these fibers.

The sulphite pulp pad showed the greatest discrepancy between the α values determined by the different methods; there was a deviation of 10% between the α_ζ and α_k. Goring and Mason (20, 21, 8) reported an average α_k value of 2.45 from a large number of permeability determinations on pads formed from the same sample of sulphite pulp used in the present investigation; this value shows good agreement with the α_ζ value of Table XVIII, and suggests that the α_k value of 2.86 reported for the single pad of sulphite pulp measured in the high-compression cell is erroneously high, due to experimental error.

It is of interest to point out a trend exhibited in the ζ' values for Dacron and surgical cotton; for both of these fibers, ζ' in 2 x 10^{-4} M KCl solution was greater than in 2 x 10^{-5} M KCl, indicating the existence of a maximum in the ζ-potential versus electrolytic concentration curve.

As was previously mentioned, some dispute exists as to the reality of such maxima, which cannot be explained on the basis of the simple Gouy-Chapman (2, 3) electrical double

layer theory, assuming a constant surface charge. Some workers have attributed the maxima to impurities in the electrolyte (6) or to surface conductance effects (14, 9). Other workers have pointed out that the maxima can be readily explained by assuming that adsorption of one ionic species occurs, in accordance with the Stern (4) theory of the electrical double layer, so that the charge density on the surface of the solid is a function of the concentration of the electrolyte (10, 11, 7).

In the present investigation acetate rayon showed a greater ζ' value in 2 x 10^{-5} M KCl than in 2 x 10^{-4} M KCl, thus exhibiting no evidence of a maximum in the ζ-potential versus electrolytic concentration curve. There are no grounds for supposing that surface conductance or impurities in the electrolyte should operate to produce spurious maxima for Dacron and surgical cotton, but not for acetate rayon; thus there is every reason to conclude that the observed maxima are real, in agreement with the conclusion of Goring and Mason (8), who observed similar maxima in their stream measurements on pads of cellulose.

The empirical stream current equation failed for the 0.5 micron dia. glass pad. The graphical plot gave an α_ζ value of 0.94, compared to the true specific volume of glass of $\sim$ 0.40. However, this failure was according to expectation. The $(I\eta L/pD)^{0.4}$ versus c plots for the other pads had exhibited deviations from linearity for $\epsilon > \sim 0.80$; it would be inconsistent

if the stream current data for the 0.5 micron dia. glass pad, determined over the ϵ range 0.99 to 0.90, gave a correct value for α_ζ.

The failure of the permeability method for the 0.5 micron diameter glass pad was also according to expectation. The flow measurements were carried out over the void fraction range 0.99 - 0.90; from their measurements on cylindrical pads of fibers, Carroll and Mason (49, 50) concluded that the Kozeny (27) permeability equation is only valid at void fractions below ~ 0.80. At void fractions above this upper limit there is a maximum in the $(Kc^2)^{1/3}$ versus c curve, after which there is a pronounced decrease of $(Kc^2)^{1/3}$ with decrease of c. This trend is clearly illustrated in Fig. 30, in which $I\eta L/pD$, $F\eta L/ED$, and $(Kc^2)^{1/3}$ versus c curves for the 0.5 micron dia. glass pad 31 are shown.

The foregoing discussion of the electrokinetic and permeability data for the 0.5 micron dia. glass pad serves to emphasize an experimental observation which may be of considerable theoretical significance: the valid range of pad void fractions of the empirical electrokinetic equations proposed in the present work coincides with the valid range of pad void fractions of the Kozeny (27) permeability equation.

Permeability Measurements

Equation 43, used throughout the present investigation to determine α_k, is a modified form of the Kozeny (27)

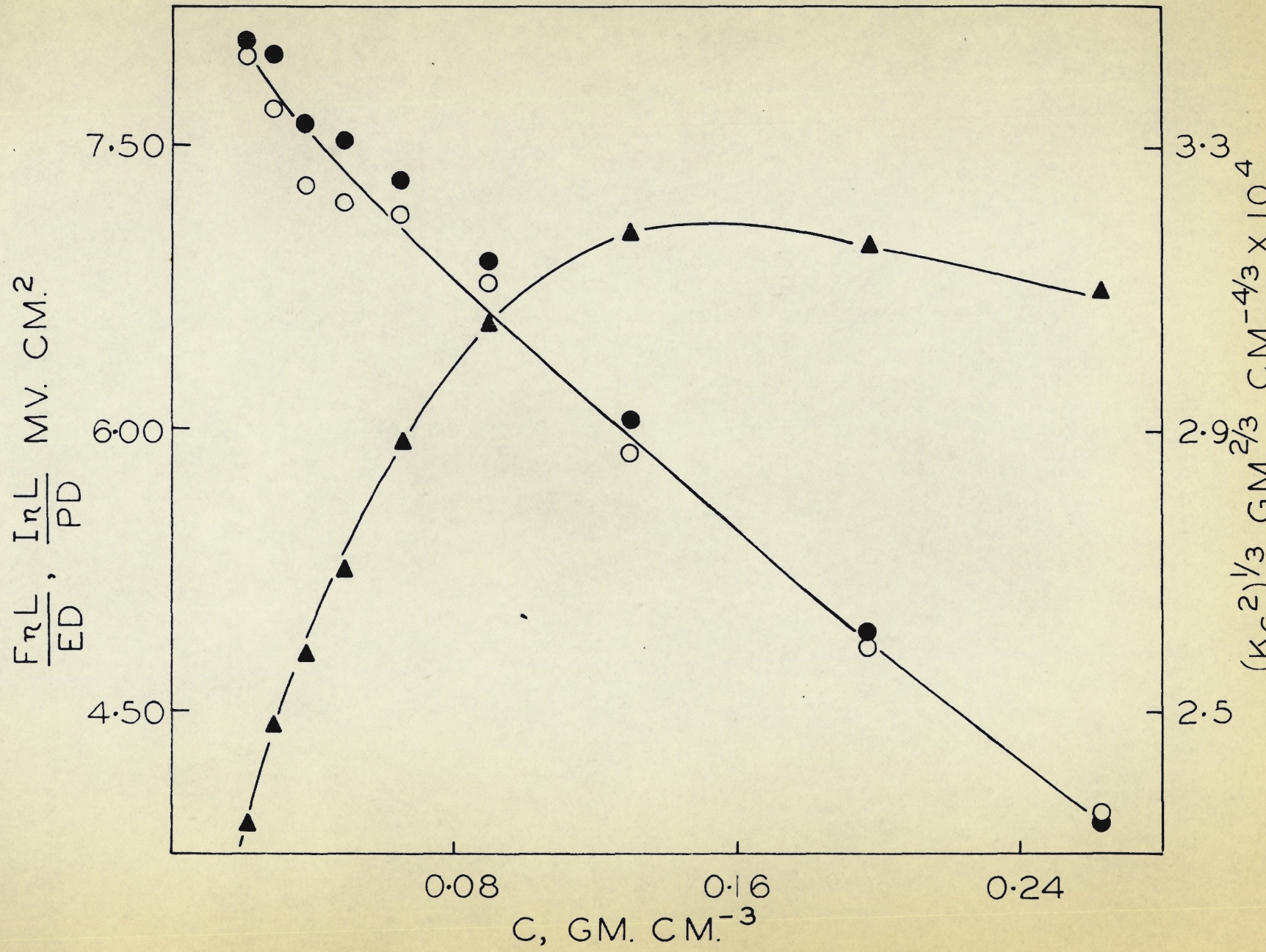

FIG. 30 $I\eta L/pD$, $F\eta L/ED$, and $(K_c^2)^{1/3}$ versus c plots for pad 31

permeability equation; it may be expressed in the alternative form

$$K = \frac{\epsilon^3}{k_1 S_o^2 (1 - \epsilon)^2} \quad \ldots (66)$$

where S_o = specific surface of pad material per unit volume of pad material

and k_1 = a combined orientation-shape factor.

In the present investigation k_1 was assigned a value of 5.55, after Fowler and Hertel (48).

Sullivan and Hertel (25, 47) introduced an orientation factor into equation 66. They pointed out that the liquid must follow a tortuous path in its flow through the pores of a complex porous diaphragm. If an individual streamline within the diaphragm makes an angle θ_L with the direction of normal flow, then the pressure gradient along the streamline is $\frac{p \cos \theta_L}{L}$ where p is the pressure across the diaphragm and L is the length of the diaphragm.

The actual velocity along the streamline must further be multiplied by $\cos \theta_L$ in order to obtain its component parallel to the axis of symmetry of the diaphragm. Thus the velocity of flow of any streamline in the normal direction of flow is $\cos^2\theta_L$ times what it would have been had not the streamline been inclined at an angle θ_L. The orientation factor $\overline{\cos^2\theta_L}$ for flow through the diaphragm as a whole was defined as the average $\cos^2\theta_L$ value of the liquid streamlines throughout the diaphragm.

In flow measurements on model beds of cotton and glass fibers, Sullivan and Hertel (25) demonstrated that the permeability coefficient K was directly proportional to $\overline{\cos^2\theta_L}$, all other terms in the Kozeny equation being held constant, for

the cases

1) fibers oriented in the direction of normal flow, i.e., the streamlines in the direction of normal flow, and $\overline{\cos^2\theta_L} = 1.0$; and

2) fibers oriented at right angles to the direction of flow, i.e., the streamlines at an angle of 45° to the direction of normal flow, and $\overline{\cos^2\theta_L} = 0.5$

On the basis of these measurements, and other measurements carried out on model beds of glass spheres (47), Sullivan and Hertel suggested that the orientation-shape factor for flow through porous beds may be expressed as $k_1 = k_2/\overline{\cos^2\theta_L}$, where k_2 is a shape factor having a value of approximately 3.0. This substitution transforms equation 66 into

$$K = \frac{\epsilon^3}{\frac{k_2 S_o^2}{\overline{\cos^2\theta_L}}(1-\epsilon)^2} \qquad \ldots \quad (67)$$

A large number of workers (44, 45, 46, 48, 49, 50) have demonstrated experimentally that K is directly proportional to $\epsilon^3/(1-\epsilon)^2$ over a considerable range of pad void fractions. Assuming that the shape factor k_2 and the effective surface S_o remain constant with changing void fraction, this indicates that $\overline{\cos^2\theta_L}$ is also a constant. Sullivan and Hertel (25) considered that $\overline{\cos^2\theta_L}$ was equal to about 0.5 for a porous bed consisting of randomly oriented cylindrical particles.

No conclusions as to the validity of this suggestion of constant $\overline{\cos^2\theta_L}$ could be formed from the flow data obtained in the present investigation. Sullivan and Hertel (25) concede that a positive knowledge of the appropriate shape factor k_2 is not available for beds composed of randomly oriented fibers; since the correct specific surfaces σ of the various fibers used in the present investigation were not known, it was not feasible to attempt a calculation of the combined shape-orientation factor k_1. It can only be remarked that the flow data of the present investigation confirm earlier observations that K is directly proportional to $\epsilon^3/(1 - \epsilon)^2$, which indicates that $k_1 S_o^2$ remains constant over the range of pad void fractions where the relationship is valid.

It may be remarked that $\overline{\cos^2\theta_L}$ values tending toward unity with increasing pad void fraction, as suggested by Hawksley (55), seem probable for the cylindrical pads of randomly sedimented fibers of the present investigation, by analogy with the trend shown by the orientation factors for stream current and electroosmosis $f(\theta)_\zeta$ and electrical conductance $f(\theta)_c$. However, the flow data of the present investigation offer no evidence in support of this suggestion.

Significance of $f(\theta)_\zeta$ and $f(\theta)_c$ Values

Analysis of the electrokinetic and conductance data of the present investigation, obtained in measurements on cylindrical pads composed of randomly sedimented fibers, led to

the conclusion that the orientation factor for stream current and electro-osmosis $f(\theta)_\zeta$ differed from the orientation factor for electrical current $f(\theta)_c$. Both orientation factors were functions of the pad void fraction, and could be evaluated by

$$f(\theta)_c = \epsilon \quad \ldots \quad (53)$$

and

$$f(\theta)_\zeta = \epsilon^{1.5} \quad \ldots \quad (64)$$

A consideration of equations 53 and 64 shows that $f(\theta)_c$ is always greater than $f(\theta)_\zeta$; this is clearly illustrated in Table XX, which shows the values of both orientation factors over the range of pad void fractions covered in the present investigation.

TABLE XX

$f(\theta)_c$ and $f(\theta)_\zeta$ with Changing ϵ

ϵ	$f(\theta)_c$	$f(\theta)_\zeta$
1.000	1.000	...
0.900	0.900	0.854
0.800	0.800	0.716
0.700	0.700	0.586
0.600	0.600	0.465
0.500	0.500	0.354

The data of Table XX may be interpreted as showing that

the average direction of transfer of electrical current through a pad of fibers is always more nearly parallel to the axis of symmetry of the pad than is the average direction of transfer of stream current or electro-osmotic flow, all other factors being equal.

This appears to be according to expectation; the flow of electrical current through a pad is essentially a linear transfer of electrical charges from one electrode to the other, which is interrupted and distorted by the interposition of solid non-conducting surfaces. With stream current and electro-osmotic flow, on the other hand, the appropriate driving potential must in general act along the planes of the solid surfaces in the pad, disposed at a variety of angles to the direction of normal flow. There is no primary underlying tendency for the movement to take place in the direction of normal flow, as there is in the case of the electrical current.

It is of interest to note that the data of Table XX are in qualitative agreement with the conclusions of Overbeek and Wijga (22), who demonstrated that the Briggs (19) method gave ζ-potential values which fell increasingly below the true ζ-potential as the importance of surface conductance increased. Since surface conductance decreases in importance with increasing pad void fraction, Overbeek and Wijga were in effect showing that $f(\theta)_c > f(\theta)_\zeta$, and that the values of the two orientation factors converged with increasing pad void fraction.

The observation of the present investigation that $f(\theta)_c$ and $f(\theta)_\zeta$ differ, and that both vary with the pad void fraction, contradicts the assumptions made by a number of workers in deriving electrokinetic and conductance equations for porous diaphragms of complex structure. Neale (5) and Goring and Mason (20, 21, 8) considered that $f(\theta)_\zeta$ was equal to the $\overline{\cos^2\theta_L}$ orientation factor of Sullivan and Hertel (25); Goring and Mason considered that $f(\theta)_c$ was also equivalent to $\overline{\cos^2\theta_L}$. This led to the incorrect assumption of constant $f(\theta)_\zeta$ with changing pad solid concentration. Neale put $f(\theta)_\zeta$ equal to 0.79, while Goring and Mason assigned $f(\theta)_\zeta$ a value of 0.5; this accounts for the failure of their stream current equations.

In the Briggs (19) method, no attempt was made to assign a numerical value to $f(\theta)_\zeta$. However, it was incorrectly assumed that $f(\theta)_\zeta$ and $f(\theta)_c$ were equivalent, and experimentally determined $f(\theta)_c$ values were substituted into the electrokinetic equations; this explains the failure of the Briggs method.

A solution of the exceedingly complex problem of deriving electrokinetic and conductance equations for the case of a porous diaphragm of complex structure is not attempted in the present work. However, the proposed methods of evaluating the orientation factor for electrical conductance $f(\theta)_c$ and the orientation factor for stream current and electro-osmosis $f(\theta)_\zeta$ should provide a useful test of the validity of any electrokinetic and conductance equations which may be derived on a theoretical basis.

APPENDIX A

THE LOW-FREQUENCY RESISTANCE DISPERSION EFFECT

Introduction

Reference has previously been made to a low-frequency resistance dispersion observed by Goring and Mason (8) for pads of sulphite pulp. The effect was first noticed when stream potential and stream current measurements were carried out on the same pad of sulphite pulp in 2 x 10^{-5} M KCl over a range of solid concentrations. The stream current function $I\eta L/pD$ should have been equal to the corresponding stream potential function $V\eta L/pDR$ by Ohm's Law; however, this equality was only shown when the d.-c. pad resistance R_o was inserted into the stream potential function. The 1000 c.p.s. a.-c. pad resistance R_{1000} was found to be 20 - 30% lower than R_o.

In the present investigation it was decided to confirm and extend these observations. This was done in the series of exploratory measurements described below.

Experimental

In studying the dispersion effect, measurements of stream current, stream potential, and pad impedance were carried out in the low-compression cell, using the reversible silver - silver chloride electrodes.

In the measurement of stream potential, the experimental procedures were similar to those already described for measurement of stream current, the vacuum tube voltmeter previously used by Goring and Mason (20, 21, 8) being substituted for the galvanometer.

In the impedance measurements, frequencies were generated by a Clough-Brengle oscillator of range 100 to 15,000 c.p.s. A well-shielded Jones bridge was used as balancing device, a cathode ray oscilloscope being used as detector. The pad resistance R_f and its equivalent shunt capacitance C_f were recorded at each frequency.

Measurements of d.-c. resistance were made at current densities of the same order of magnitude as the stream current, using a galvanometer as null detector. To correct for residual electrode polarization currents, the d.-c. measurements were made in both directions, and the mean value used.

Results

Measurements of stream potential and stream current were first carried out on the same pad of sulphite pulp in 10^{-4} M KCl solution over a range of pad concentrations. The d.-c. pad resistance R_o and the 1000 c.p.s. a.-c. pad resistance R_{1000} were measured at every pad concentration, and the R_o value used in calculating the stream potential function $V\eta L/pDR_o$. In Table A-I these quantities appear, along with the stream current function $I\eta L/pD$ and the ratio of the stream potential to

the stream current V/I.

TABLE A-I

Stream Current, Stream Potential, and Resistance Measurements on A Pad of Sulphite Pulp in 10^{-4} M KCl Solution

c gm. cm.$^{-3}$	R_{1000} ohms x 10^{-4}	R_o ohms x 10^{-4}	V/I ohms x 10^{-4}	$I\eta L/pD$ mv. cm.^{2}	$V\eta L/pDR_o$ mv. cm.^{2}
0.044	20.48	23.34	22.80	2.67	2.61
0.052	17.18	19.99	19.95	2.68	2.67
0.061	14.58	17.19	17.35	2.54	2.56
0.072	12.08	14.61	14.46	2.50	2.48
0.091	9.48	11.84	11.70	2.37	2.34
0.109	7.93	10.16	10.00	2.16	2.13
0.141	6.03	7.97	8.26	1.80	1.86

It is seen that the R_{1000} values were 15 - 30% lower than R_o; excellent agreement was shown between $I\eta L/pD$ and $V\eta L/pDR_o$, and between V/I and R_o. This result confirmed the original observations of Goring and Mason (8) upon sulphite pulp in 2 x 10^{-5} M. KCl.

The relationship between the resistance dispersion effect and the ζ-potential was next investigated. A number of 3-gram pads of sulphite pulp were formed, in contact with different electrolytic solutions. For each pad, stream current measurements were carried out at an electrode separation of approximately 5.0 cm., and the ζ-potential determined from the equation

$$\frac{I\eta L}{pD} = \frac{A\zeta}{4\pi} \epsilon^{2.5} \quad \ldots \quad (63)$$

In calculating ϵ from $(1 - \alpha_k c)$, α_k was assigned the value of 2.45, which was the average α_k value reported by Goring and Mason (20, 21, 8) in permeability measurements on a large number of pads of the same sample of sulphite pulp used in the present investigation.

For each pad, R_o, the a.-c. pad resistance R_f, and the equivalent shunt capacitance C_f, were measured at different frequencies in the range 100 - 15,000 c.p.s., at the electrode separation obtaining during the stream current measurements.

A "blank" run was carried out for each electrolyte, R_o, R_f and C_f being measured with no pad in the cell, the electrodes being separated by approximately 5.0 cm. This showed how much of the dispersion effect observed in the measurements on sulphite pulp in the same electrolyte could be attributed to the effect of the leads and apparatus.

The experimental data obtained in these measurements appear in Tables A-II and A-III. Table A-II shows, in detail, the results obtained in the impedance measurements with 10^{-4} M KCl as electrolyte; the ratio R_o/R_f is included as a rough indication of the extent of the dispersion effect.

Table A-III shows the experimental data for each of

TABLE A-II

Resistance Dispersion Effect for A Pad of Sulphite Pulp in 10^{-4} M KCl, and for 10^{-4} M KCl Solution only

Frequency c.p.s.	Sulphite Pulp c = 0.108 gm. cm.$^{-3}$ Electrode separation = 5.10 cm.			No pad Electrode separation = 5.04 cm.		
	R_f ohms x 10^{-3}	C_f µµf	R_o/R_f	R_f ohms x 10^{-3}	C_f µµf	R_o/R_f
0	64.5	....	1.00	52.1	....	1.00
100	53.65	1150	1.20	51.02	56	1.02
250	52.20	370	1.24	50.99	29.5	1.02
500	51.55	166	1.25	50.95	21.0	1.02
1000	51.07	78	1.26	50.90	16.3	1.02
2500	50.5	31	1.28	50.80	12.6	1.025
5000	50.05	18.3	1.29	50.60	10.2	1.03
10,000	49.55	16.2	1.30	50.30	8.1	1.035
15,000	49.20	14.0	1.31	50.10	6.7	1.04

the pads in the series, including the pad shown in Table A-II. The ratio R_o/R_f and C_f for frequencies of 100, 1000, 5000 and 15,000 c.p.s. show the extent of the resistance dispersion occurring in the pad; the same quantities are shown for the "blank" run with the same electrolyte. The ζ-potential, as calculated by equation 63 from the stream current measurements on the pad, also appears.

An examination of Table A-II shows that a marked resistance dispersion effect occurred in the pad of sulphite pulp

TABLE A-III

Resistance Dispersion Effect at Different ζ-Potentials on Pads of Sulphite Pulp

Electrolyte	Electrode Separation cm.	ζ' mv.	R_o x 10^{-3} ohms	$\frac{R_o}{R_{100}}$	C_{100} μμf	$\frac{R_o}{R_{1000}}$	C_{1000} μμf	$\frac{R_o}{R_{5000}}$	C_{5000} μμf	$\frac{R_o}{R_{15,000}}$	$C_{15,000}$ μμf
Pad No. 1											
2 x 10^{-5} M KCl	5.05	-12.8	149.3	1.25	174	1.28	43.5	1.32	16.5	1.35	13
Blank	5.02		133.1	....	...	1.03	17.0	1.04	14.0	1.06	9.5
Pad No. 2											
10^{-4} M KCl	5.10	-14.6	64.5	1.20	1150	1.26	78	1.29	18.3	1.31	14
Blank	5.04		52.1	1.02	56	1.02	16.3	1.03	10.2	1.04	6.7
Pad No. 3											
2 x 10^{-5} M $ThCl_4$	5.09	+ 2.8	90.4	....	...	1.07	28.5	1.09	16.2	1.11	7.0
Blank	4.96		58.5	1.02	42.5	1.02	21.4	1.03	11.2	1.05	6.5
Pad No. 4											
3.5 x 10^{-5} M $ThCl_4$	5.09	+12.5	62.8	1.03	143.5	1.04	32.5	1.05	17.0	1.07	11.4
Blank	5.04		39.1	1.02	39.5	1.02	15.5	1.03	6.5	1.04	3.1
Pad No. 5											
7 x 10^{-5} M $ThCl_4$	5.10	+16.2	34.6	1.03	143	1.03	36.3	1.04	20.5	1.05	15.9
Blank	5.06		18.6	1.03	157	1.03	31.0	1.03	16.0	1.04	11.5

in 10^{-4} M KCl solution, the R_o/R_f ratio varying from 1.20 at 100 c.p.s. to 1.31 at 15,000 c.p.s. Both R_f and C_f showed a decided decrease with increased frequency, the most pronounced change evidently occurring in the region between 0 and 100 c.p.s.

The "blank" run carried out in 10^{-4} M KCl solution showed comparatively little dispersion of resistance, demonstrating that the bulk of the effect observed in the measurements on sulphite pulp in 10^{-4} M KCl could be attributed to the physical properties of the swollen fiber.

The data of Table A-III show that a considerable resistance dispersion effect occurred in 2×10^{-5} M KCl as well as 10^{-4} M KCl. However, when the sign of the charge on the fiber was reversed by addition of thorium ions to the electrolyte, the resistance dispersion effect was sharply diminished; for the measurements in 7×10^{-5} M $ThCl_4$, resistance dispersion was negligible.

It is interesting to note that the stream current data in the KCl solutions indicated the existence of a maximum in the ζ-potential versus KCl concentration curve for sulphite pulp, as previously observed in the present investigation for pads of surgical cotton and Dacron fiber.

A series of measurements were next carried out to determine whether the resistance dispersion effect occurred in materials other than sulphite pulp. R_o and R_f were measured on pads of a number of different fibrous materials in

10^{-4} M KCl solution; Table A-IV shows R_o for each pad, and R_o/R_f for frequencies of 100, 1000 and 15,000 c.p.s. The data for sulphite pulp and the "blank" run which appear in Table A-IV were taken from Table A-II.

TABLE A-IV

Resistance Dispersion Effect for Miscellaneous Fibrous Materials in 10^{-4} M KCl Solution

Pad Material	Pad Weight (gm.)	L (cm.)	R_o (ohms)	R_o/R_{100}	R_o/R_{1000}	$R_o/R_{15,000}$
(10^{-4} M KCl)	....	5.04	52,100	1.02	1.02	1.04
Nylon	4.10	3.75	71,200	1.02	1.03	1.07
Asbestos	4.50	3.85	30,400	1.03	1.04	1.07
Glass wool	2.93	3.30	39,900	1.06	1.07	1.08
Acetate rayon	4.32	4.30	67,400	1.02	1.03	1.06
Wool	3.17	3.98	44,000	1.04	1.04	1.06
Surgical cotton	3.35	3.55	45,700	1.05	1.06	1.15
Silk	4.40	3.85	35,400	1.20	1.22	1.24
Viscose rayon	3.33	3.85	31,000	1.19	1.23	1.27
Sulphite pulp	2.82	5.10	64,500	1.20	1.26	1.31

Nylon, asbestos, glass wool, acetate rayon, and wool showed no significant effect. On the other hand, surgical cotton exhibited a marginal effect, while silk and viscose rayon showed a comparatively large R_o/R_f ratio, of the same order as that shown by sulphite pulp. As with sulphite pulp, the most marked decrease in resistance occurred in the region between 0 and 100 c.p.s.

Discussion

These results, while fragmentary, illustrate several interesting points:

1) When dispersion of the electrical resistance occurs, the effect is most marked at low frequencies, indeed in a region which is not normally covered in dispersion measurements. At the same time, an appreciable capacitive reactance is exhibited, the equivalent shunt capacitance increasing as the frequency is decreased. The systems are therefore roughly equivalent to a series resistance-capacitance network in parallel with a resistance, the latter corresponding to the measured d.-c. resistance.

2) Swelling is a necessary but not sufficient condition for the low frequency dispersion. Non-swelling asbestos and glass wool show no significant dispersion. Sulphite pulp, silk and viscose rayon, which undergo considerable swelling in water, show a pronounced dispersion, while wool and positively charged sulphite fibers do not. With cotton the effect if any is small; this accounts for the failure of Rabinov and Heymann (7) to detect dispersion in their resistance measurements on cotton pads at 60 and 1000 c.p.s.

The fact that the dispersion effect observed in pads of sulphite pulp in KCl solution was eliminated by the addition of thorium ions to the electrolyte, reversing the sign of the charge on the fiber, suggests that the effect can be explained by a surface mechanism; however, the dispersion effect cannot

be accounted for by the conventional theory of surface conductance. Rosenhead and Miller (60) in a rigorous theoretical analysis of the surface conductance in a conventional Gouy-Chapman diffuse layer showed that no appreciable dispersion should be observed below frequencies of 100,000 c.p.s.

Fricke and Curtis (61) have reported an analogous dispersion effect in aqueous suspensions of butter fat, latex, mineral oils, and kaolin over the frequency range 250 to 2,000,000 c.p.s., and conclude that it arises from a polarization phenomenon at the particle-liquid interface. It cannot be concluded whether a similar mechanism is operative here, or whether it arises from the restricted motion of adsorbed ions in the interior of swollen gels after the manner postulated by Murphy and Lowry (62) or whether it is a form of the Maxwell-Wagner dielectric relaxation effect (63).

A complete interpretation of the phenomenon is undoubtedly complex, but should provide a useful approach to the study of swelling phenomena in fibrous materials.

APPENDIX B

DISCREPANCIES OBSERVED IN THE ELECTRO-OSMOTIC FLOW MEASUREMENTS

In the present investigation the equivalence of electro-osmotic and stream current measurements was clearly demonstrated for cylindrical pads of cellulose and 0.5 micron dia. glass fiber. However, a number of minor discrepancies were observed in the electro-osmotic measurements, which may be summarized as follows:

1) The variation of ζ_E/ζ_s with bubble length, observed with the relatively permeable pad 24, 2.5 micron dia. glass fibers.

2) The decrease of ζ_E/ζ_s below unity where pad permeability was sufficiently high for the leak-back flow to be significant, particularly noticeable with acetate rayon pad 32 at the lower solid concentrations.

3) The decreasing values of $F\eta L/ED$ with decreasing E shown in Figs. 20 - 23, particularly noticeable with the more permeable pads.

While these data were insufficient for any conclusions to be reached, they suggested that the discrepancies were related to the pad permeability, as each was observed to occur in a relatively permeable pad.

It was decided to examine the electro-osmotic discrepancies more systematically, by measuring

1) the change of ζ_E/ζ_s with bubble length,

2) the change of $F\eta L/ED$ with E

on the same acetate rayon pad at three different pad solid concentrations. It was considered that the experimental data obtained in these measurements, which are listed in Tables B-I and B-II, would disclose any relationship between the electro-osmotic discrepancies and the pad permeability.

The experimental data of Table B-I indicated clearly that two of the electro-osmotic discrepancies occur together, and that both are related to the pad permeability. At the lowest pad concentration, where the pad was most permeable and leak-back flow consequently the greatest, ζ_E/ζ_s showed a marked change with changing bubble length, and fell 20 - 35% below the theoretical value of unity. At the intermediate pad concentration, where pad permeability and leak-back flow were much smaller, these discrepancies were considerably diminished, while at the highest pad concentration, where pad permeability was sufficiently small for leak-back flow to be almost negligible, the electro-osmotic discrepancies were absent. ζ_E/ζ_s was equal to unity within the experimental error for all bubble lengths.

It is suggested that the discrepancies in the electro-osmotic data of Table B-I can be explained by assuming that an incorrect value was assigned to the capillary permeabi-

TABLE B-I

Measurements of Electro-Osmotic Flow and Stream Current on A Pad of Acetate Rayon in 2×10^{-5} M KCl Solution, varying the Bubble Length at A Fixed E over A Range of Pad Concentrations

Pad Weight: 8.53 gm.

c gm. cm.$^{-3}$	Bubble Length (mm.)	Φ_p cm.^{3} x 10^8	Poiseuille Leak-Back Correction Factor	E volts	F_{obs} cm.^{3} sec.$^{-1}$ x 10^3	$F\eta L/ED$ mv. cm.^{2}	$I\eta L/pD$ mv. cm.^{2}	ζ_E/ζ_s
0.070	2.0	80.1	1.29	138.0	6.1	13.95	21.65	0.645
	2.4				7.8	17.90	21.60	0.830
	3.1				7.75	17.70	21.50	0.82
	3.8				7.60	17.45	21.65	0.805
	6.0				6.15	14.10	21.10	0.67
0.231	2.6	21.2	1.08	92.9	13.7	12.25	13.00	0.94
	3.1				13.7	12.15	13.00	0.935
	4.1				13.4	11.80	12.85	0.92
	6.0				13.1	11.60	12.90	0.90
0.437	2.7	5.05	1.019	138.0	21.6	6.35	6.35	1.00
	4.0				21.8	6.50	6.40	1.01
	8.5				21.8	6.45	6.40	1.01

TABLE B-II

Measurements of Electro-Osmotic Flow and Stream Current on a Pad of Acetate Rayon in 2 x 10^{-5} M KCl Solution at varying E over A Range of Pad Concentrations

Pad Weight: 8.53 gm.

c gm. cm.$^{-3}$	Bubble Length mm.	Φ_p cm.^{3} x 10^8	Poiseuille Leak-Back Correction Factor	E volts	F_{obs} cm.^{3} sec.$^{-1}$ x 10^3	$F\eta L/ED$ mv. cm.^{2}	$I\eta L/pD$ mv. cm.^{2}	Φ_c cm.^{3} x 10^8
0.070	3.0	80.1	1.29	138.2	8.1	18.45	21.55	157
				115.8	6.7	18.30		154
				92.3	5.28	18.10		149
				69.6	3.92	17.80		141
				48.0	2.64	17.40		133
				24.0	1.22	16.10		109
0.231	3.0	21.2	1.08	138.0	21.2	12.55	12.95	196
				115.6	17.4	12.35		171
				92.5	13.9	12.30		163
				69.8	10.3	12.10		144
				48.0	6.95	11.90		125
				24.1	3.36	11.40		96
0.437	2.7	5.05	1.019	138.3	21.7	6.35	6.40	...
				115.7	18.2	6.40		...
				92.6	14.3	6.27		...
				69.8	10.5	6.12		...
				48.0	6.95	5.90		...
				24.1	3.20	5.49		...

lity Φ_c in calculating the leak-back flow from

$$F = F_{obs}\left(1 + \frac{\Phi_p}{\Phi_c}\right) . \qquad \ldots \quad (45)$$

It will be recalled that difficulty was experienced in attempting to determine Φ_c from liquid flow measurements, and the quantity was finally evaluated by the Poiseuille equation 46, which gave $\Phi_c = 274 \times 10^{-8}$ cm.^{3}.

However, it is by no means certain that the Poiseuille equation is applicable when the flow takes place through a capillary containing an air bubble. If there were an additional resistance to flow due to the presence of the bubble, a true Φ_c value less than that given by the Poiseuille equation might be expected. If the bubble resistance to flow were assumed to increase as the length of the bubble increased, then the true Φ_c value would decrease as the length of the bubble was increased.

An analysis of the experimental data of Table B-I led to a result which was in qualitative agreement with this hypothesis. Assuming that conventional electrokinetic theory was applicable to these measurements, and that the discrepancy between $F\eta L/ED$ and $I\eta L/pD$ was solely due to the use of an incorrect Φ_c value in the correction of F_{obs} for leak-back, the true Φ_c values were calculated from the electrokinetic data at the lowest pad concentration as follows.

At a bubble length of 2.4 mm. the value of $F\eta L/ED$,

uncorrected for leak-back flow, is 17.90/1.29 = 13.90 mv. cm.^{2}. The corresponding stream current function $I\eta L/pD$ has a value of 21.60 mv. cm.^{2}. The true leak-back correction factor is that giving $I\eta L/pD = F\eta L/ED$, i.e. 1.555. The true value of Φ_c may therefore be calculated from

$$1.555 = \left(1 + \frac{\Phi_p}{\Phi_c}\right) = \left(1 + \frac{80.1 \times 10^{-8}}{\Phi_c}\right)$$

which gives $\Phi_c = 144 \times 10^{-8}$ cm.^{3}.

This method was used to calculate the true value of Φ_c for every bubble length employed in the measurements at the lowest pad concentration of Table B-I. The following results were obtained.

TABLE B-III

Φ_c as Calculated from The Electrokinetic Data of Table B-I at c = 0.070 gm. cm.$^{-3}$

Bubble Length (mm.)	Φ_c (cm.^{3} x 10^8)
2.0	80
2.4	144
3.1	141
3,8	132
6.0	86
Poiseuille value	274

In agreement with the hypothesis of bubble resistance to flow, the true Φ_c values were lower than the Poiseuille value, and decreased as the length of the bubble increased. The decreased value of Φ_c at a bubble length of 2.0 mm. is otherwise explained; the internal diameter of the capillary is 2.464 mm., which approximates the shortest bubble length to still maintain "contact" with the walls of the capillary (see Fig. B-1 (b)). At a bubble length of 2.0 mm., there is a visible gap between the bottom of the bubble and the capillary wall (see Fig. B-1 (a)). This permits flowing liquid to pass under the bubble, giving too low a value for F. Analytically, this is equivalent to lowering the apparent permeability of the capillary.

As a test of the validity of the foregoing analysis, the Φ_c value for a bubble length of 3 mm., estimated from Table B-III to be 142 x 10^{-8} $cm.^3$, was used in the leak-back correction of the electro-osmotic flow data for pad 32; with this pad, significant deviations of ζ_E/ζ_S from unity had been observed at the lower solid concentrations. The $F\eta L/ED$ values thus obtained were combined with the corresponding $I\eta L/pD$ value to give ζ_E/ζ_S equal to unity within experimental error over the entire range of solid concentrations; these data appear in Table XIV.

Thus it can be seen that two of the discrepancies observed in the electro-osmotic flow measurements--the variation of ζ_E/ζ_S with bubble length and the accompanying decrease of

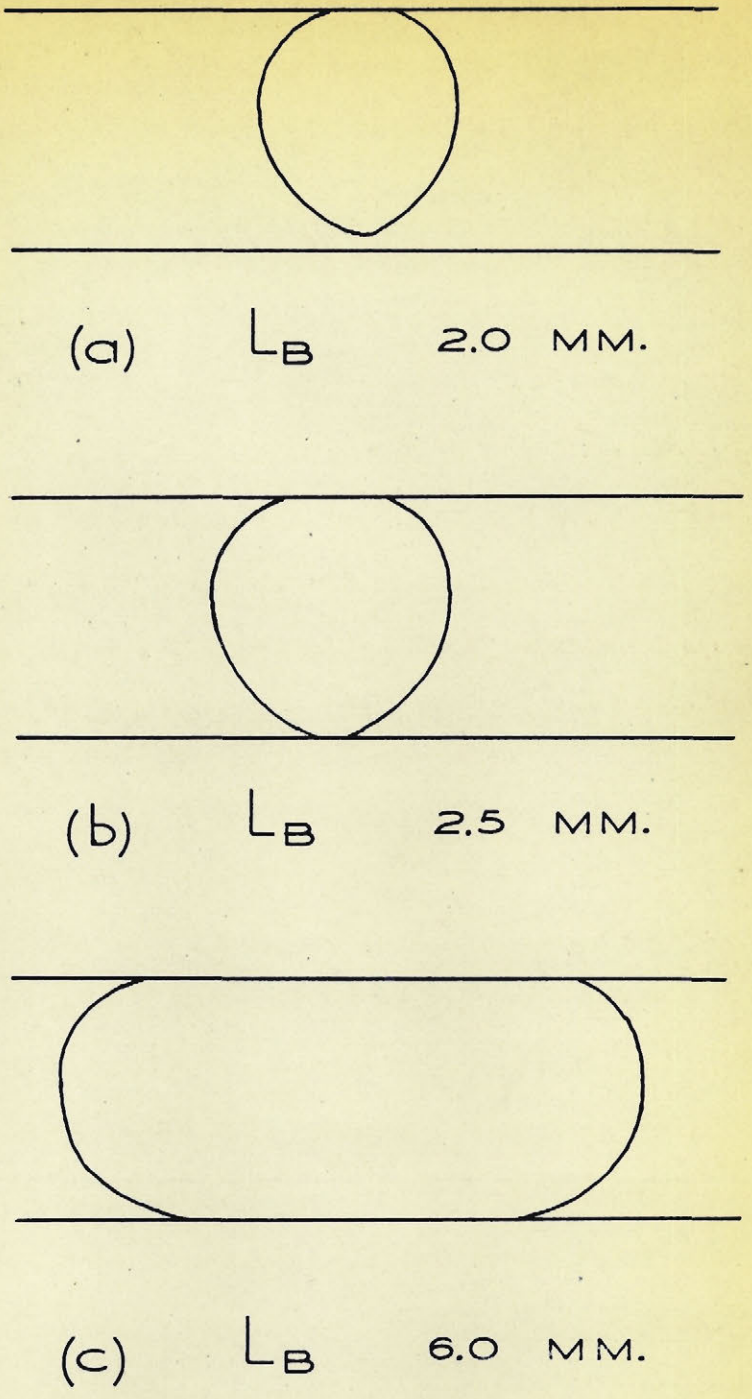

FIG. B-1 Bubble profiles at different bubble lengths.

ζ_E/ζ_s below the theoretical value of unity--can be accounted for qualitatively by assuming that the air bubble in the capillary resists flow, and that the resistance to flow increases as the bubble length increases.

The third of the discrepancies observed in the electro-osmotic measurements is exhibited in Table B-II. It is seen that in all cases $F\eta L/ED$ decreased with decreasing E, as previously observed in the data of Figs. 19 - 22. In contrast to the other electro-osmotic discrepancies, no relationship to the pad permeability was shown. The fractional decrease in $F\eta L/ED$ over the same voltage range was similar for all three pad concentrations, though the permeability values ranged from 5.05 to 80.1 x 10^{-8} cm.^{3}, with the Poiseuille leak-back correction to the observed electro-osmotic flow varying from 1.019 to 1.29.

Analytically, the effect was equivalent to an increase in Φ_c with increasing bubble velocity. This is illustrated in Table B-II, which lists Φ_c values calculated from the electrokinetic measurements at the low and intermediate pad concentrations using the method previously described. It should be noted that the Φ_c values at the intermediate pad concentrations are less reliable, as the value of $F\eta L/ED$ corrected according to the Poiseuille equation only falls below $I\eta L/pD$ by 3 - 12%. Thus a small error in the measurement of either quantity is greatly magnified in the calculation of Φ_c.

The marked increase of Φ_c with F_{obs} indicated that the treatment of the experimental data in the previous section was

oversimplified; the Φ_c values of Table B-III are only strictly accurate for the value of F_{obs} at which they were determined. However, judging from their successful application to the data of pad 32, the values are approximately correct. Table B-III indicates $\Phi_c = 142 \times 10^{-8}$ cm.^{3} for a bubble length of 3 mm., which appears to be a reasonable mean value, from an inspection of the Φ_c values of Table B-II.

Verification of Effect of Bubble upon Φ_c

To summarize the observations of the preceding pages, the discrepancies observed in the electro-osmotic flow measurements can be explained by assuming that the effect of the contained air bubble on the permeability of the capillary flowmeter is as follows:

1) Φ_c is reduced considerably below the Poiseuille value,
2) Φ_c increases with increasing bubble speed,
3) Φ_c decreases with increasing bubble length.

Before attempting to deduce a mechanism of bubble resistance to flow which would lead to the above effects, it was decided to confirm the reality of the effect of the bubble on Φ_c by means of an independent experiment. To this end a simple apparatus was constructed, which is described below.

A 100 ml. suction flask was fitted with a rubber stopper which was pierced by a glass tube which extended nearly to the bottom of the flask. The external end of the glass tube was connected by Tygon tubing to a capillary tube of about 2 mm.

internal diameter and 60 cm. length which was held rigidly at a slight angle to the horizontal, the open end of the capillary being uppermost.

A piece of rubber tubing was fastened to the sidearm of the suction flask, so that lung pressure could be used to push liquid from the flask into the inclined capillary. Upon release of pressure, the liquid in the capillary flowed back into the suction flask, and the time t for the meniscus to travel between two marked points on the capillary 41.5 cm. apart was recorded. The liquid was then blown up the capillary again, and a bubble introduced into the capillary by means of a hypodermic needle. Pressure was released, and the time t_b of descent over the same distance recorded. In the measurement of t_b the fixed points were shifted upward by the length of the bubble, so that the hydrostatic pressure during a run was the same for determinations of t_b and t.

Measurements were first carried out with the capillary at a fixed inclination. The time of descent t, with no bubble in the capillary, was measured, then the time t_b with bubbles of different length in the capillary. The results of these measurements appear in Table B-IV.

It is seen that t_b was always greater than t, and increased with the length of the bubble. This confirmed the hypothesis that an air bubble in a capillary resists flow, the resistance increasing with the bubble length, i.e. the true Φ_c

value is lower than the Poiseuille value, and the true Φ_c decreases with increasing bubble length.

TABLE B-IV

Time of Descent t of The Meniscus in The Capillary at A Fixed Inclination, without An Air Bubble, and Time of Descent t_b at The Same Inclination with Contained Air Bubbles of Different Lengths

Bubble Length (mm.)	t_b (secs.)	t (secs.)
5.0	22.9	18.1
8.0	30.3	18.1
14.5	50.4	18.1

Measurements of t_b and t were next carried out with the bubble length fixed at 7.5 mm., the inclination of the capillary being varied. The results obtained in these measurements, which appear in Table B-V, show that the ratio t/t_b increased markedly with decreasing t. Thus the resistance of the bubble to flow decreases with increasing bubble velocity, i.e. the Φ_c value increases with increasing bubble velocity, in confirmation of the trend shown by the Φ_c values calculated from the electrokinetic data of Table B-II.

TABLE B-V

Time of Descent t of The Meniscus in The Capillary without An Air Bubble, varying The Angle of Inclination of The Capillary, and The Time of Descent t_b of The Meniscus with A Contained Air Bubble of 7.5 mm. Length for Each Capillary Inclination

t (secs.)	t_b (secs.)	t/t_b
15.6	23.0	0.68
17.5	26.3	0.67
17.9	29.3	0.61
23.8	37.7	0.63
26.2	46.8	0.56
33.1	61.8	0.54
37.6	75.7	0.50
53.0	110.5	0.48
54.7	112.3	0.49
73.4	159	0.46

Discussion of Bubble Effects

An attempt was next made to account for the observed effect of the length and velocity of the contained air bubble from a theoretical basis. A method of treating the problem was suggested by the observations of Fairbrother and Stubbs (43), who carried out a study of the bubble flowmeter in which the apparent flow velocity u, as indicated by the observed rate of bubble motion, was compared with the true flow velocity u_t. It was found that u was always greater than u_t, the discrepancy increasing with increasing u. The effect

was attributed to the appreciable thickness Δx of the liquid layer separating the bubble from the capillary walls; it was suggested that this layer was left behind by the moving bubble and became part of the liquid behind the rear meniscus.

It is important to note that the effect upon the F_{obs} values reported in the present investigation due to this mechanism is within experimental error. Fairbrother and Stubbs (43) carried out their determinations of u and u_t at flow rates of 0.79 to 5.9 cm. sec.$^{-1}$, and found that the discrepancy between u and u_t varied from 1% to 3%. The highest flow rate recorded in the present investigation, using a capillary tube of similar i.d. to that employed by Fairbrother and Stubbs, was $\sim$ 0.5 cm. sec.$^{-1}$.

Assuming that the bubble moved along the capillary in plug-flow motion, separated from the walls of the capillary by a layer of liquid of thickness Δx, Fairbrother and Stubbs (43) deduced the empirical expression

$$\frac{u - u_t}{u} = \frac{2\,\Delta x}{R_c} = \sqrt{\frac{u\eta}{\sigma}} \qquad \ldots \quad (B\text{-}1)$$

where σ = the surface tension of the liquid in the capillary

and η = the viscosity.

The experimental data were found to be in accord with this expression, which shows Δx to be a function $\sqrt{u}$.

It is interesting to note that the existence of a liquid layer between a moving air bubble and the walls of a glass capillary has been confirmed by the conductance measurements of Marchessault and Mason (12) upon a capillary with a contained air bubble.

Accepting the mechanism of bubble motion postulated by Fairbrother and Stubbs (43), an equation may be derived which expresses the capillary permeability Φ_c as a function of u and bubble length as follows.

If it be assumed that there is a pressure drop Δp_b across the bubble, then there is a force $\Delta p_b \pi R_c^2$ causing the bubble to move in plug-type flow at a velocity u. Assuming that there is a layer of liquid of thickness Δx between the bubble and the walls of the capillary, then there is a velocity gradient $u/\Delta x$ across the liquid layer, and the frictional force opposing the bubble motion is $\eta \frac{u}{\Delta x} 2\pi R_c l_b$ where l_b is the length of bubble in contact with the capillary walls. Equating the two forces,

$$u = \frac{\Delta p_b \Delta x R_c}{2 \eta l_b} \quad . \qquad \ldots \text{(B-2)}$$

Where the observed flow through the capillary containing the bubble is Q volume units per unit time, then

$$Q = u\pi R_c^2 = \frac{\pi \Delta p_b \Delta x R_c^3}{2 \eta l_b} \quad , \qquad \ldots \text{(B-3)}$$

and the pressure necessary to cause bubble motion is

$$\Delta p_b = \frac{2\,\eta l_b Q}{\pi \Delta x R_c^3} \quad . \qquad \ldots \quad (B\text{-}4)$$

However, in addition to the resistance to flow of the bubble, which must be overcome by the application of a pressure Δp_b, there is the resistance to flow in the remainder of the capillary by-pass. If the permeability of the capillary by-pass without a contained air bubble is Φ_o, then the pressure Δp_o necessary to overcome the resistance to flow of the by-pass is

$$\Delta p_o = \frac{Q\eta}{\Phi_o} \qquad \ldots \quad (B\text{-}5)$$

The total pressure p required to overcome the resistance to flow of the by-pass when the capillary contains a bubble is therefore

$$p = \Delta p_b + \Delta p_o = Q\eta \left(\frac{2\,l_b}{\pi \Delta x R_c^3} + \frac{1}{\Phi_o} \right) \qquad \ldots \quad (B\text{-}6)$$

Substituting for Δx from equation B-1,

$$\Phi'_c = \left(\frac{Q\eta}{p} \right)_c = \frac{1}{\left(\frac{4\,l_b}{\pi R_c^4} \sqrt{\frac{\sigma}{u\eta}} + \frac{1}{\Phi_o} \right)} \qquad \ldots \quad (B\text{-}7)$$

This equation should give the true permeability of the capillary by-pass when a bubble is contained. It is seen that the expression is qualitatively correct; it indicates that Φ'_c should be less than the permeability of the capillary

by-pass without a contained air bubble Φ_o, and that Φ_c' should decrease with increasing bubble length and increase with increasing bubble velocity.

Equation B-7 was next tested by calculating Φ_c' from the electro-osmotic flow data of Tables B-I and B-II. In the calculations Φ_o was assigned the value given by the Poiseuille equation for the capillary, i.e. 274×10^{-8} cm.; the resistance to flow of the Tygon tubing and stop-cocks in the capillary by-pass was thus assumed to be negligible. At the relatively low flow velocities of the electro-osmotic runs, exit and entrance losses at the ends of the capillary were negligible. The results obtained appear in Table B-VI.

It is seen that agreement between the Φ_c values calculated by the two methods was generally good, thus validating the theoretical treatment proposed in the preceding pages.

It is important to note that there may be an experimental error in the Φ_c' values calculated by equation B-7. The quantity l_b represents the length of bubble separated by a distance Δx from the walls of the capillary; however, it was difficult to decide what fraction of the total length of the moving bubble was thus in "contact" with the walls, so the quantity l_b was set equal to the total bubble length. This approximation may yield spuriously low Φ_c' values at the lower bubble lengths, where the fraction of the bubble length in "contact" with the walls is lowest (Fig. B-1). Nearly all of the Φ_c' values of Table B-VI were calculated for bubble lengths suffi-

TABLE B-VI

Calculation of Φ_c from The Experimental Data of Tables B-I and B-II by Two Different Methods

c gm. cm.$^{-3}$	Bubble Length mm.	E volts	T °C.	F_{obs} cm.^{3} sec.$^{-1}$ x 10^3	Δx microns	Φ_c' cm.^{3} x 10^8	Φ_c cm.^{3} x 10^8
0.070	2.0	138.0	26.3	6.1	2.4	154	75
	2.4			7.8	2.7	151	144
	3.1			7.75	2.7	134	141
	3.8			7.60	2.7	119	132
	6.0			6.15	2.4	83	86
0.070	3.0	138.2	26.3	8.1	2.8	137	157
		115.8		6.7	2.5	130	154
		92.3		5.28	2.3	123	149
		69.6		3.92	1.9	112	141
		48.0		2.64	1.6	100	133
		24.0		1.22	1.1	77	109
0.231	3.0	138.0	25.0	21.2	4.6	170	196
		115.6		17.4	4.1	164	171
		92.5		13.9	3.7	156	163
		69.8		10.3	3.2	146	144
		48.0		6.95	2.6	133	125
		24.1		3.36	1.8	109	96

ciently low for this error to be noticeable; this may explain the fact that Φ_c' was generally lower than Φ_c.

Electro-Osmotic Pressure Measurements

As an additional experimental demonstration that the discrepancies in the electro-osmotic measurements were due to the effect of the bubble on Φ_c, it was decided to carry out measurements of stream current, electro-osmotic flow and electro-osmotic pressure on the same pad of acetate rayon in 2×10^{-5} M KCl solution. If the decrease of $F\eta L/ED$ at the lower E values were solely a bubble effect, there should be no parallel decrease in the corresponding electro-osmotic pressure function $P_E\Phi_p L/ED$.

The data obtained in these measurements appear in Table B-VII, which also lists the results obtained in the "depolarizing" electro-osmotic flow and electro-osmotic pressure runs, with the induced flow through the pad in the opposite direction to that of pad formation.

It is seen that $F\eta L/ED$ showed the usual decrease with decreasing E; in contrast, $P_E\Phi_p L/ED$ was constant within experimental error over the voltage range investigated. This confirmed the hypothesis that the decrease of $F\eta L/ED$ with decreasing E was a bubble effect; however, the electro-osmotic pressure function $P_E\Phi_p L/ED$ was observed to be about 10% larger than $I\eta L/pD$. This difference was in excess of the experimental error.

TABLE B-VII

Measurements of Stream Current, Electro-Osmotic Flow Rate and Electro-Osmotic Pressure on A Pad of Acetate Rayon in 2 x 10^{-5} M KCl Solution

($c = 0.458$ gm. cm.$^{-3}$ $\Phi_p = 3.87 \times 10^{-8}$ cm.^{3})

E volts	$F\eta L/ED$ mv. cm.^{2}		$P_E\Phi_p L/ED$ mv. cm.^{2}		$I\eta L/pD$ mv. cm.^{2}	P_E cm. H_2O
137.6	5.45	(5.45)	5.75	(5.35)	5.35	4.84
114.0	5.50	(5.60)	5.70	(5.10)	....	4.00
91.3	5.35	(5.30)	5.65	(5.05)	....	3.15
69.0	5.30	(5.20)	5.85	(4.85)	....	2.48
45.4	5.10	(5.05)	5.80	(4.75)	....	1.61
22.7	4.55	(4.20)	5.75	(4.10)	....	0.80

"Depolarizing" run, with flow in the reversed direction, is shown in brackets after the result obtained in the initial run.

Since only one set of electro-osmotic pressure measurements was carried out, it was not known whether this discrepancy was general; thus a cause for the discrepancy could not be assigned with certainty. However, the data of Table B-VII suggest that significant polarization may have taken place during the electro-osmotic pressure runs.

There is an important difference between electro-osmotic flow and electro-osmotic pressure measurements; in the former, the electrolyte within the pad is constantly being

replaced by a fresh supply. In the latter, there is little net transfer of liquid through the pad; for the most part, the electro-osmotic current flows through the electrolyte which was in the pores of the pad at the beginning of the run. Under these conditions, it would not be surprising if there were a greater polarizing tendency shown in measurements of electro-osmotic pressure, compared to measurements of electro-osmotic flow.

This suggestion is supported by the experimental data of Table B-VII, which showed that polarization was generally absent in the electro-osmotic flow measurements. Good agreement was shown between the initial and "depolarizing" electro-osmotic flow determinations, and the maximum $F\eta L/ED$ values agreed with $I\eta L/pD$ within experimental error.

The electro-osmotic pressure data, to the contrary, suggested that a significant polarization was taking place. In all cases there was a considerable discrepancy between the initial and the "depolarizing" run; the average $P_E\Phi_p L/ED$ value, while constant, exceeded $I\eta L/pD$ by an amount greater than the experimental error.

It may be noted that an anisotropy of the pad to flow, such that Φ_p was different with flow through the pad in opposite directions would also lead to $P_E\Phi_p L/ED$ values showing a distinct anisotropy. However, flow measurements on the acetate rayon pad used in the electro-osmotic pressure measurements

showed that Φ_p was identical within experimental error with the flow in opposite directions, thus showing that the results of Table B-VII could not be explained on this basis.

Description of New Type of Flowmeter

The scope of the electro-osmotic measurements carried out in the present investigation was restricted by the following limitations of the apparatus:

1) Electrode polarization effects became noticeable at electro-osmotic currents in excess of 0.5 ma.

2) Flow rates lower than $\sim 10^{-3}$ cm.^{3} sec.$^{-1}$ could not be measured accurately, due to the bubble sticking, or moving irregularly.

3) The variability of Φ_c imposed large and uncertain corrections to measurements carried out on relatively permeable pads.

Because of these factors, the measurements were generally carried out on pads of relatively low permeability in contact with 2×10^{-5} M KCl solution. At this low electrolytic concentration pad resistances were high; thus a relatively large potential could be applied across the pad at an electro-osmotic current less than 0.5 ma. The ζ-potential of the fiber in 2×10^{-5} M KCl solution was generally high enough so that an electro-osmotic flow rate in excess of 10^{-3} cm.^{3} sec.$^{-1}$ could be obtained.

However, at electrolytic concentrations greater than 2×10^{-5} M KCl, there is a decrease in pad resistance; thus the maximum potential which can be put across the pad at an electro-osmotic current less than 0.5 ma. decreases. This means that the maximum electro-osmotic flow rate obtainable also decreases. At electrolytic concentrations greater than 2×10^{-4} M another factor becomes important; the ζ-potential begins to decrease markedly, which decreases the maximum electro-osmotic flow rate obtainable still further. With the apparatus used in the present investigation, measurements would probably fail in $\sim 2 \times 10^{-4}$ M solution, the flow rates at an electro-osmotic current less than 0.5 ma. becoming too low for accurate measurement.

In order to increase the scope of the electro-osmotic flow measurements, the use of a new type of flowmeter is proposed. With this flowmeter, no air bubble is employed; Φ_c is constant under normal operating conditions, and the accurate measurement of much lower flow rates than those measured in the present investigation should be possible. In principle the flowmeter resembles a device which has been used by Archer, Kuzmak and Mason (64, 65) to measure flow rates as low as 2×10^{-5} cm.^{3} sec.$^{-1}$.

The flowmeter, which is depicted in Fig. B-2, consists of 2 pieces of capillary tubing of identical length and i.d. connected by means of a piece of glass tubing of $\sim$ 3/8" i.d. which is provided with a stop-cock. On either side of

the stop-cock there is a sidearm of $\sim$ 3/8" i.d.

When the flowmeter is in use, sidearms A and B may be fastened to opposite sides of the pad by means of Tygon tubing fastened to ground-glass taper joints (cf. Fig. 5). With stop-cock C open the flowmeter, which may be held in an adjustable cradle, is filled with sufficient electrolyte for a thread of liquid to extend along part of each capillary. The flowmeter is then levelled; after closing stop-cock C, a potential may be applied across the pad, and the electro-osmotic flow rate measured by means of the rate of movement of a meniscus in one of the capillaries.

The operating characteristics of the flowmeter should permit accurate measurements of electro-osmotic flow in solutions as concentrated as 10^{-3} or 10^{-2} M KCl, where the flow rates at an electro-osmotic current less than 0.5 ma. are extremely low. The resistance to flow Φ_c of the moving threads of liquid in the flowmeter can be accurately evaluated by the Poiseuille equation; it should therefore be possible to calculate the leak-back flow accurately for relatively permeable pads, and thus permit exact measurements of the electro-osmotic flow rate for such pads.

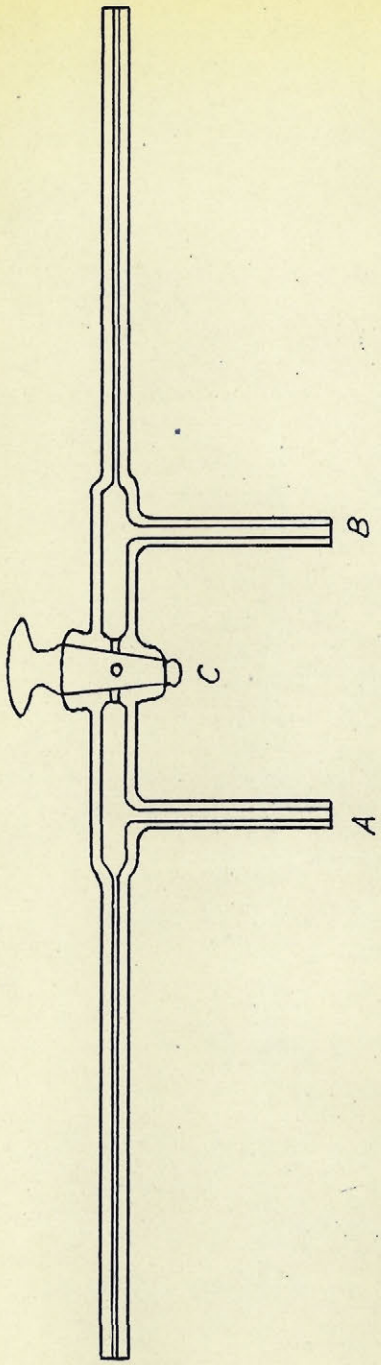

FIG. B-2 Proposed electro-osmotic flowmeter

APPENDIX C

COMPARISON OF STREAM AND ELECTRO-OSMOTIC MEASUREMENTS NEAR THE ISO-ELECTRIC POINT

As has been mentioned previously, there are indications that stream and electro-osmotic measurements on the same system of glass in contact with $ThCl_4$ solution fail to agree near the iso-electric point (40, 41, 33).

In order to determine whether this discrepancy was real, it was decided to repeat the measurements of Monoghan, Urban and White (40), who had compared stream potential and electro-osmotic flow measurements on a glass capillary in contact with $ThCl_4$ solutions over the concentration range 10^{-5} M to 10^{-7} M. They found that the iso-electric point was at $\sim 4 \times 10^{-7}$ M $ThCl_4$ according to the stream potential measurements, and at $\sim 3 \times 10^{-6}$ M $ThCl_4$ according to the electro-osmotic measurements.

Accordingly, a pad of 0.5 micron glass was formed in distilled water. Sorption equilibrium was attained with a $ThCl_4$ solution as previously described, i.e. the liquid in the cell was displaced by 500 ml. of the fresh electrolyte, then 100 ml. of electrolyte were run through the pad, this procedure being repeated three times in all. After the electrokinetic measurements had been carried out, sorption equilibrium was es-

tablished with another solution of $ThCl_4$ of different concentration in the same manner.

Superficially, the experimental results were in agreement with those of Monoghan, Urban, and White (40). The stream current measurements, which were normal in every respect, indicated that a reversal of sign of the charge on the fiber occurred at a concentration of about $\sim 3 \times 10^{-7}$ M $ThCl_4$, after which the charge was positive. According to the electro-osmotic measurements, the sign of the charge only became positive at an electrolytic concentration of $\sim 4 \times 10^{-6}$ M $ThCl_4$.

However, it is important to note that the electro-osmotic flow measurements showed distinctly anomalous behavior. For example, at a concentration of 10^{-7} M $ThCl_4$, where the stream current measurements indicated a small negative charge on the fiber, no electro-osmotic flow occurred upon application of potential across the pad at an electro-osmotic current of $\sim$ 0.6 ma. This was at first attributed to a sticking of the bubble, which sometimes occurred at low flow rates. The Tygon tubing of the capillary by-pass was therefore squeezed a few times, in order to free the bubble. However, no motion took place for 15 seconds, after which the bubble began to move in the direction indicative of a negative charge on the fiber. The periods for successive 0.1 ml. increments of flow were timed at 17, 13, 11 and 10.6 seconds, showing that acceleration was still occurring after 40 seconds of flow.

At a concentration of $\sim 1.6 \times 10^{-6}$ M $ThCl_4$, where

the stream current reading indicated a fairly large positive charge on the fiber, application of a potential across the pad at an electro-osmotic current of $\sim$ 0.9 ma led to an initial flow whose direction was indicative of a positive charge on the fiber. Then the bubble slowed down, stopped for 60 seconds, then reversed direction, as if the charge on the fiber were now negative.

The abnormality of these electro-osmotic runs is emphasized when comparison is made with the behavior shown in previous electro-osmotic measurements; in all cases, the bubble had started moving immediately upon application of potential and had attained its maximum constant speed within two seconds. Flow had never shown the slightest tendency to cease, or reverse in direction.

On the basis of this single series of runs it is impossible to say whether the unusual electro-osmotic behavior resulted from the fact that part of the "fixed" layer had been moved by electrostatic forces, as proposed by Monoghan, Urban, and White (40), or whether electrode polarization was taking place; the electro-osmotic currents were somewhat in excess of the usual operating limit of 0.5 ma., which supports the latter explanation.

It can only be concluded that the discrepancy between stream current and electro-osmotic measurements near the isoelectric point, observed in the present investigation, was due

to a failure of the electro-osmotic measurements in this region.

CONCLUSIONS

Suggestions for Further Work

1) A test of the validity of the ζ' values given by the empirical stream current equation by means of an independent determination of the ζ-potential of the particles comprising the pad, through electro-phoretic or sedimentation potential measurements.

2) Application of the conductance equation proposed in the present investigation to the measurement of specific volumes of highly-swollen fibers, either through

1) d.-c. pad resistance measurements

or 2) taking the specific conductivity of the fiber into account

or 3) measurements in electrolytic solutions of sufficient concentration for fiber conductivity to be negligible.

3) Measurements of electrical conductance on a pad of 0.5 micron dia. glass wool over a range of solid concentrations in contact with concentrated electrolyte, in order to determine the valid range of the empirical conductance equation. Comparison of the results obtained with the liquid resting in the pad, and flowing through the pad, might be a means of determining whether deformation of the pad structure occurs during flow at low pad void fractions.

4) Investigation into the relationship between stream current and surface conductance.

5) Comparison of stream current and electro-osmotic flow measurements in more concentrated solutions of electrolyte and near the iso-electric point, using the new type of flowmeter proposed in the present work.

Claims to Original Research

1) Excellent agreement was obtained between stream current and electro-osmotic flow measurements on cylindrical pads of cellulose and glass.

2) Some discrepancies in the electro-osmotic flow measurements were investigated, and shown to be due to the effect of the contained air bubble on the permeability of the capillary flowmeter. A theoretical explanation of the effect of the bubble was proposed.

3) A new type of flowmeter for the measurement of electro-osmotic flow rates was proposed.

4) Exploratory measurements of the low-frequency resistance dispersion effect were carried out.

5) The empirical relationship $\Omega = kA\epsilon^2/L$ was shown to exist between the electrical conductance and the void fraction of a cylindrical pad of randomly-sedimented slightly-swelling fibers under conditions of negligible fiber and surface conductance.

6) The empirical relationship $(I\eta L/pD)^{0.4} = k_E\epsilon$ was shown to exist between the stream current generated upon viscous flow through a pad of fibers and the pad void fraction. The relationship between electro-osmotic flow and pad void fraction was described by the analogous equation $(F\eta L/ED)^{0.4} = k_E\epsilon$.

7) The deficiencies of the various electrokinetic equations which have been proposed for the case of a porous diaphragm of complex internal structure were demonstrated.

BIBLIOGRAPHY

1. Helmholtz, H. Wied. Ann. 7: 337, 1879.
2. Gouy, L. J. Phys. 9: 457, 1910.
3. Chapman, D.L. Phil. Mag. 25: 475, 1913.
4. Stern, O. Z. Elektrochem. 30: 508, 1924.
5. Neale, S.M. Trans. Faraday Soc. 41: 473, 1946.
6. Neale, S.M. and Peters, R.H. Trans. Faraday Soc. 41: 478, 1946.
7. Rabinov, G. and Heymann, E. J. Phys. Chem. 47: 655, 1943.
8. Goring, D.A.I. and Mason, S.G. Can. J. Research, B, 28: 323, 1950.
9. Rutgers, A.J. Trans. Faraday Soc. 36: 69, 1940.
10. Abramson, H.A. Electrokinetic Phenomena. Chemical Catalog Co. Inc., U.S.A. 1934.
11. Abramson, H.A. J. Phys. Chem. 39: 749, 1935.
12. Marchessault, R.H. and Mason, S.G. Unpublished data.
13. Bull, H.B. and Gortner, R.A. J. Phys. Chem. 35: 456, 1931.
14. Bikerman, J.J. J. Phys. Chem. 46: 724, 1942.
15. Bikerman, J.J. Trans. Faraday Soc. 36: 154, 1940.
16. Buchanan, A.S. and Heymann, E. J. Colloid Sci. 4: 137, 1949.
17. Quincke, G. Pogg. Ann. 107: 1, 1859.
18. Smoluchowski, M. Krak. Anz. 182, 1903.
19. Briggs, D.R. J. Phys. Chem. 32: 641, 1928.
20. Goring, D.A.I. Ph.D. Thesis, McGill University, 1949.
21. Goring, D.A.I. and Mason, S.G. Can. J. Research, B, 28: 307, 1950.
22. Overbeek, J.T.G. and Wijga, P.W.O. Rec. Trav. Chim. 65: 556, 1946.

23. Buchanan, A.S. and Heymann, E. J. Colloid Sci. 4: 157, 1949.

24. Eversole, W.G. and Boardman, W.W. J. Phys. Chem. 46: 914, 1942.

25. Sullivan, R.R. and Hertel, K.L. Advances in Colloid Science, Vol. 1, p. 37. Interscience Publishers, New York, 1942.

26. Robertson, A.A. and Mason, S.G. Pulp and Paper Mag. Can. 50 (13): 103, 1949.

27. Kozeny, J. Sitzber. Akad. Wiss. Wien, Math. naturw. Klasse, (Abt. IIa) 136: 271, 1927.

28. Goring, D.A.I., Biefer, G.J. and Mason, S.G. Can. J. Research, B, 28: 339, 1950.

29. Ham, A.J. and Douglas, H.W. Trans. Faraday Soc. 38: 404, 1942.

30. Douglas, H.W. and Walker, R.A. Trans. Faraday Soc. 46: 559, 1950.

31. Ham, A.J. and Hodgson, W. Trans. Faraday Soc. 38: 217 1942.

32. Rutgers, A.J. and de Smet, M. Trans. Faraday Soc. 41: 758, 1945.

33. Rutgers, A.J. and de Smet, M. Trans. Faraday Soc. 43: 102, 1947.

34. Reuss, F.F. Memoires de la Societe des Naturalistes de Moscou 2: 327, 1809.

35. Wiedemann, G. Pogg. Ann. 87: 321, 1852.

36. Quincke, G. Pogg. Ann. 113: 513, 1861.

37. Coehn, A. and Raydt, V. Ann. Physik. 30: 777, 1909.

38. Saxen, U. Wied. Ann. 47: 46, 1892.

39. Wijga, P.W.O. Ph.D. Thesis, Utrecht, 1946.

40. Monoghan, B., White, H.L. and Urban, F. J. Phys. Chem. 39: 585, 1935.

41. Dubois, R. and Roberts, A.H. J. Phys. Chem. 40: 543, 1936.

42. Kanamaru, K. Chem. Abstracts 25: 3895, 1931.
Cellulose Ind. (Tokyo) 7: 3, 29, 1931.

43. Fairbrother, F. and Stubbs, A.E. J. Chem. Soc. p. 527, 1935.

44. Carman, P.C. Trans. Inst. Chem. Engrs. (London) 15: 150 1937.

45. Carman, P.C. J. Soc. Chem. Ind. 57: T 225, 1938.

46. Carman, P.C. J. Soc. Chem. Ind. 58: 1, 1939.

47. Sullivan, R.R. and Hertel, K.L. J. App. Phys. 11: 761, 1940.

48. Fowler, J.L. and Hertel, K.L. J. App. Phys. 11: 496, 1940.

49. Carroll M.N. Ph.D. Thesis, McGill University, 1951.

50. Carroll, M.N. and Mason, S.G. Unpublished data.

51. Darcy, H.P.G. Les Fontaines Publiques de la Ville de Dijon. Victor Dalmont, Paris, 1856.

52. Fairbrother, F. and Balkin, M. J. Chem. Soc. p. 389, 1931.

53. Mark, H. Chem. Rev. 26: 169, 1940.

54. Campbell, W.B. The Cellulose-Water Relationship in Paper-Making. Dept. Interior, Forest Service, Bull. 84, Ottawa, 1933.

55. Hawksley, P.G.W. Some Aspects of Fluid Flow, p. 114. Edward Arnold and Co., London, 1951.

56. Archie, G.E. Trans. Amer. Inst. Mining and Metallurgical Eng. (Petroleum Division) 146: 54, 1942.

57. Guyod, H. Oil Weekly, 115: 38, 1944.

58. Wyllie, M.R.J. and Rose, W. TP 2852 J. Pet. Tech. 2: 105, 1950.

59. Preston, J.M. Trans. Faraday Soc. 42B: 131, 1946.

60. Rosenhead, L. and Miller, J.C.P. Proc. Roy. Soc. (London) A 163: 298, 1937.

61. Fricke, H. and Curtis, H.J. J. Phys. Chem. 41: 729, 1937.

62. Murphy, E.J. and Lowry, H.A. J. Phys. Chem. 34: 598, 1930.

63. Schneider, W.C., Carter, W.C., Magat, M. and Smyth, C.P. J. Am. Chem. Soc. 67: 959, 1945.

64. Kuzmak, J.M. and Mason, S.G. Unpublished data.

65. Archer, W.L. Ph.D. Thesis, McGill University, 1950.